Identification of small molecule inhibitors of Mcm2-7 replicative helicase, and structural determination of mutants affecting the Mcm2/5 gate

by

Nicholas Edward Simon

Bachelor of Science, Michigan State University, 2007

Submitted to the Graduate Faculty of the

Kenneth P. Dietrich School of Arts and Sciences

in partial fulfillment

of the requirements for the degree of

Doctor of Philosophy

University of Pittsburgh

2014

UNIVERSITY OF PITTSBURGH

Dietrich School of Arts and Sciences

This thesis was presented

by

Nicholas Edward Simon

It was defended on

March 7th, 2014

and approved by

Jeffrey Brodsky, PhD, Professor, Biological Sciences

James Conway, PhD, Associate Professor, Structural Biology

Linda Jen-Jacobson, PhD, Professor Emeritus, Biological Sciences

Andrew VanDemark, PhD, Assistant Professor, Biological Sciences

Dissertation Advisor: Anthony Schwacha, PhD, Associate Professor, Biological Sciences

Identification of small molecule inhibitors of the Mcm2-7 replicative helicase, and structural determination of mutants affecting the Mcm2/5 gate

Nicholas E. Simon, PhD

University of Pittsburgh, 2014

The replication of the eukaryotic genome is a highly regulated process requiring the coordinated efforts of several enzymes to ensure that multiple chromosomes are efficiently replicated once, and only once, per cell cycle. This coordination is largely achieved by loading and activating the eukaryotic replicative helicase, the molecular motor that separates duplex DNA, at different points in the cell cycle. Consistent with this central role in DNA replication's regulation, the eukaryotic helicase, Mcm2-7, is unique among known helicases in that it is composed of six unique and essential subunits. Prior work has indicated that only a subset of these subunits are required for helicase activity, suggesting a regulatory role for the remainder. It has been posited that two of the subunits, Mcm2 and Mcm5, form an ATP dependent 'gate' involved in loading and/or activating the complex. The presence of this gate has been shown biochemically and structurally, but its physiological role remains speculatory. My dissertation research has focused on two areas. The first has been the identification and characterization of quinolone-based inhibitors, with the goal of finding compounds that selectively inhibit the subunits that make up the 'gate.' I have found that the fluoroquinolone ciprofloxacin and related compounds are selective for the Mcm2-7 helicase over other helicases and inhibit the complex in both *in vitro* DNA unwinding assays and in tissue culture. The second area of research has been determining

the structure of regulatory mutants we predict have aberrant gate function with transmission electron microscopy and single particle image averaging. I have shown that the regulatory mutant *mcm5bob1* biases the complex toward a closed state, potentially allowing for the premature loading of replication factors. I have also demonstrated that a mutation in the Walker B AAA+ ATPase active site motif in the active site between Mcm2 and Mcm6 changes the size of the Mcm2/5 gate, indicating a role for this active site in the regulation of Mcm2-7 topology.

TABLE OF CONTENTS

LIST OF TABLES

LIST OF FIGURES

PREFACE

There are many people I need to thank who helped me along this journey.

First and foremost, I need to thank my advisor, Anthony Schwacha. Tony's creative thinking, unwavering support, and dogged determination were invaluable in helping me drive through some of the more difficult aspects of this project. We've gone through some rough patches as a lab, and his leadership and concern for his subordinates has been a lesson more valuable than any ATPase assay. I also need to thank our collaborator, James Conway, for being our Sherpa as we've navigated the unfamiliar realm of structural biology.

I also need to thank past and present members of the Schwacha lab, especially Matthew Bochman, Emily Tsai, Sriram Vijayraghavan. I've learned so much from all of you, and I'm truly lucky to count you all as colleagues and friends.

Special thanks to the members of my thesis committee, Drs Brodsky, Conway, Jen-Jacobson, and VanDemark, for their guidance and advice over the years in committee meetings.

Various people contributed technical and experimental help to different parts of this project. Tom Harper and Alexander Mahkov taught me how to operate electron microscopes and were always willing to answer my questions about sample preparation. Undergraduates Rebecca Theophanous and Eva Bugos contributed to fluoroquinolone project, and I'm sure are on their way to great things.

I’d like to thank Pitt’s Department of Biological Sciences for providing a great environment to be graduate student, and for encouraging great science and the ability to communicate it effectively. Special thanks in particular to the office staff, especially Cathy Barr for her extreme patience in reminding me to sign up for classes every semester.

Finally I need to thank my family and friends. My friends, thank you for being my support group and making Pittsburgh a great place to live. Finally, my parents, Edward and Patricia, and my sisters Kim and Jill for their love and support over the years.

1.0 INTRODUCTION

"Decades later, DNA and genes captured the spotlight from enzymes; but in my theater, enzymes kept the leading role. DNA and RNA provide the script, but enzymes do the acting. For the cell, DNA is the construction manual, and RNA transcribes it into readable form, but the proteins, particularly the enzymes, carry out all the cellular functions and give the organism its shape"

-Arthur Kornberg, *For the Love of Enzymes: The Odyssey of a Biochemist*

1.1 EUKARYOTIC DNA REPLICATION

The faithful replication of the eukaryotic genome is one of the most technically impressive feats in all of biology. In a highly regulated series of events, the largest macromolecules in nature are duplicated and segregated with incredible fidelity. Several enzymes contribute to active replication (Figure 1). Helicases unwind the double stranded DNA to form a single strand template. Single-stranded binding proteins bind and stabilize the release of single-stranded DNA (ssDNA). Topoisomerases relieve torsional strain generated in the DNA substrate by the migrating replisome. Various polymerases are involved in the creation of RNA primers and the subsequent extension of nascent DNA along the leading and lagging

strands. Care must be taken to not only faithfully duplicate the genome, but also ensure that each daughter cell receives a single copy of the complete genome.

In eukaryotes, this is complicated by the presence of multiple, large chromosomes. Unlike in prokaryotes, multiple origins of replication are required in order to replicate all of the chromosomes in an efficient manner. This introduces an inherent problem: if the origins of replication load their replication machinery and begin replication (henceforth referred to as 'licensing' and 'firing' respectively) *ad hoc*, there exists a high likelihood that some origins may reinitiate and refire before a round of replication has finished. This has severe consequences for genome integrity, evidenced by the observation that unregulated origin firing has been shown to cause re-replication, leading to accumulation of ssDNA, head to head fork collisions, fork stalling or collapse, accumulation of aberrant DNA structures, and genome instability (reviewed in (Hook et al. 2007)).

To avoid re-replication problems, eukaryotes employ a two-stage regulatory system for licensing and firing replication machinery. In the first step, components of the replisome are loaded onto chromatin, but remain catalytically inactive. The factors responsible for loading this machinery are then inactivated or removed from the nucleus, and only then is DNA replication initiated. This temporal separation of loading and activation events is what ensures that each round of licensing and firing happens once per cell cycle.

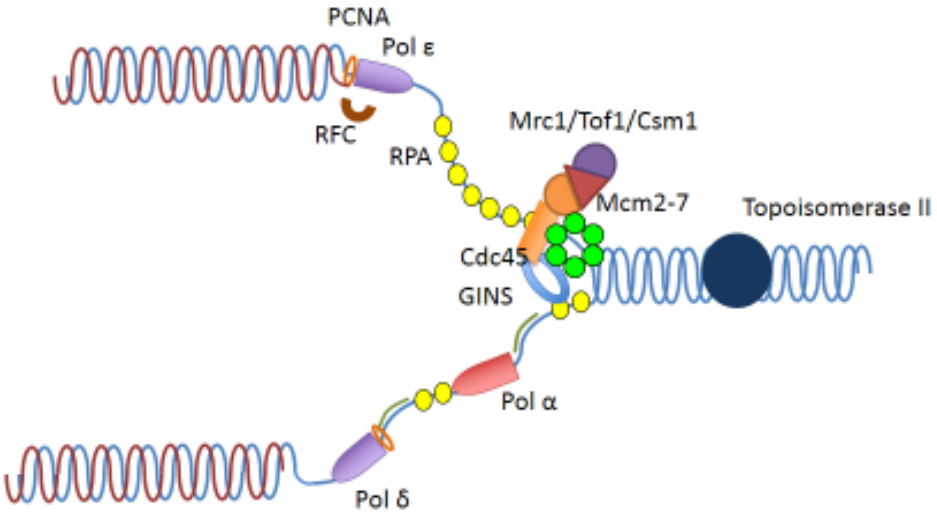

Figure 1: The Eukaryotic Replication Fork

Overview of the proteins involved in eukaryotic replication. Shown are the polymerases (pol α, δ, and ε), the single stranded binding protein (RPA), the replicative topoisomerase Topo II, clamp loader (RFC), processivity factor (PCNA), the components of replicative helicase (Cdc45, GINS, and the Mcm2-7)

A key player in this regulation is the eukaryotic replicative helicase, the molecular motor that unwinds double-stranded DNA (dsDNA) into a single-stranded DNA template for the rest of the DNA replication machinery. Although many factors are involved in origin licensing and firing, the replicative helicase is the only component found in both licensed origins and actively unwinding forks, making its activation the key regulatory event for the cell's entry into S-phase (Bell and Dutta 2002).

Consistent with this central importance in DNA replication, the eukaryotic replicative helicase, known to be the Mcm2-7 complex, is the most complicated helicase known. Like other replicative helicases it is a hexameric toroid, however unlike other helicases it is uniquely formed of 6 distinct and essential subunits, numbered 2-7, rather than six copies of a single protein like other well studied replicative helicases such as E1

and SV40 large T antigen. This unique subunit architecture has long been assumed to be a consequence of the multiple steps of the cell cycle it coordinates and the multitude of proteins it must interact with. Biochemical differences between subunits (Schwacha and Bell 2001; Bochman and Schwacha 2007; Bochman et al. 2008; Bochman and Schwacha 2008) have been proposed to be indicative of Mcm2-7's multiple roles in the cell cycle.

1.1.1 Discovery and initial characterization of the Mcm Complex

The name of the Mcm proteins derives from a screen designed to find mutants defective in plasmid (minichromosome) retention (Maine et al. 1984). In this screen, Maine *et al.* took advantage of the well-defined **A**utonomous **R**eplicating **S**equence in yeast, which are sequences that designate origins of replication, and constructed plasmids containing a centromere sequence and either a single or multiple ARSs. The resulting 40 mutants representing 16 complementation groups were accordingly named **M**ini**c**hromosome **M**aintenance (*MCM*) genes, and were divided into two classes: those in which plasmid retention could be rescued with multiple ARSs, posited to be involved in replication initiation, and those that were defective for plasmid segregation regardless of the ARS sequence, deemed general segregation mutants.

Among the proposed initiation mutants where the genes *MCM2, MCM3,* and *MCM5*, all of which code for members of the Mcm helicase. Other notable, non-helicase mutants were in *MCM1,* which codes for a transcription factor that drives the expression of the Mcm complex (Jarvis et al. 1989; Passmore et al. 1989), and *MCM10* (originally *MCM4*, see below), another DNA replication factor (Merchant et al. 1997). *MCM4, MCM5* and *MCM7* were originally isolated as *CDC54, CDC46* and *CDC47* in an earlier screen for

cold-sensitive cell cycle division mutants (Moir et al. 1982). This screen is also notable for isolating the CMG complex member *CDC45*. The last member of the complex, *MCM6*, was not identified until ten years later when it was isolated as the missegration mutant *mis5* in a screen done in the fission yeast *Schizosaccharomyces pombe* (Takahashi et al. 1994). In 1996 it was established that the six proteins worked in concert, were homologous, and thus far found in all eukaryotes. It was proposed for clarity's sake that the nomenclature be standardized and the genes were all assigned consecutive MCM designations, 2 through 7, and the original *MCM4*, *MCM6*, and *MCM7* were renamed *MCM10*, *MCM11*, and *MCM12* (Chong et al. 1996).

1.1.2 The different Mcm subunits have diverse functions

Mcm2-7, like several other hexameric helicases, is a member of the **A**TPase **a**ssociated with cellular **a**ctivities superfamily (AAA+). This family of proteins has been extensively reviewed (Erzberger and Berger 2006) however, the salient features of the superfamily as they apply to the Mcms will be discussed here. Like other typical members of this superfamily, the ATPase active sites are formed *in trans* between neighboring subunits. Canonical Walker A, Walker B motifs (Walker et al. 1982) and sensor I (Guenther et al. 1997) motifs are contributed by one subunit, and the arginine finger (Wittinghofer et al. 1997) and sensor II (Guenther et al. 1997) motifs are contributed by the neighboring subunit (Figure 2).

This architecture necessitates oligomerization of subunits to form a functional active site. The eukaryotic Mcm complex also has the additional constraint of having 6

different subunits, resulting in six unique pairs forming six active sites, assuming only one oligomeric state exists *in vivo.* Consistent with this assumption, pairwise combinations of Mcm proteins able to dimerize provided a putative subunit order (Davey et al. 2003; Bochman et al. 2008), which was subsequently confirmed via electron microscopy of tagged subunits (Costa et al. 2011; Fernandez-Cid et al. 2013; Sun et al. 2013). Notably, hexamer-sized complexes containing only Mcm4, 6, and 7 have been shown by multiple groups to have *in vitro* helicase activity (Ishimi 1997; Lee and Hurwitz 2000; Kaplan et al. 2003; Bochman and Schwacha 2007). More recently hexamers containing only Mcm4 and Mcm7 (Kanter et al. 2008) and, curiously, hexamers of Mcm6 alone from pea plants (Tran et al. 2010), have been shown to have *in vitro* helicase activity, indicating that other, presumed non-canonical, active site pairings can form functional ATPases, but to date it has not been shown if these have physiological relevance.

The observation that only a subset of the Mcm proteins are necessary for DNA unwinding runs contrary to many hexameric helicase activity models (Patel and Picha 2000). Quite the contrary, the presence of Mcm2, 3, and 5 actually prevents helicase activity of the Mcm2-7 hexamer except under specific assay conditions (Bochman and Schwacha 2008). This raises an obvious question: what do the remaining subunits do?

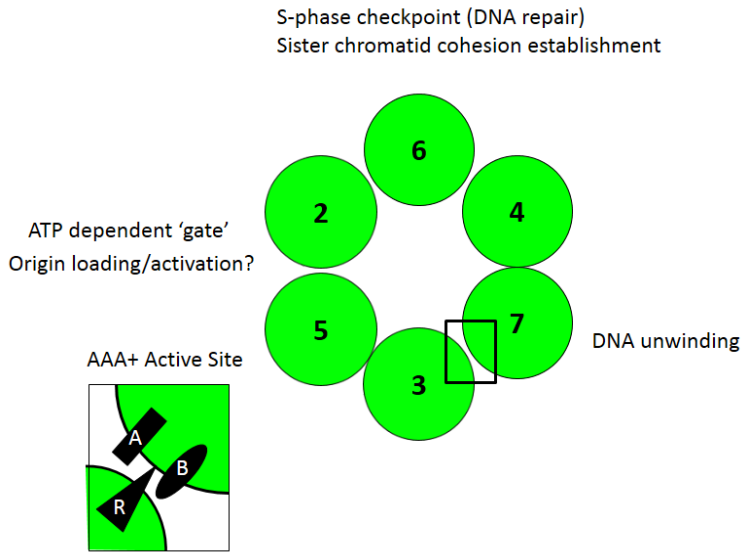

Figure 2: Location and functions of active sites in the Mcm2-7 complex

Schematic representation of the Mcm subunits as proposed by (Davey et al. 2003) and (Bochman et al. 2008), confirmed by (Costa et al. 2011) and (Speck et al. 2005), with proposed functions associated with the 2/5, 3/7 (Bochman and Schwacha 2008), and 6/2 active sites (E. Tsai and S. Vijayraghavan, in preparation). Inset: Cartoon representation of the 3/7 AAA+ active site. Mcm7 provides canonical Walker A (A) and Walker B (B) motifs, while Mcm3 contributes the Arginine Finger (R) motif *in trans.*

Walker A mutations in any of the subunits results in lethality in yeast (Bochman et al. 2008), indicating that each of these active sites performs an essential function not compensated for by the other five. Addressing this question has been the subject of a great deal of Mcm biochemistry that supports the hypothesis that these different subunits serve different functions. The strongest evidence of this is the fact that subcomplexes of Mcm467 have *in vitro* helicase activity, but the addition of Mcm2, 3, and 5 abolish helicase activity unless the reaction is supplemented with large anions (Bochman and Schwacha 2008). Additionally, the Mcm4/7 and 7/3 active sites contribute to the majority of bulk ATP hydrolysis in solution (Schwacha and Bell 2001). These data suggested that active sites

formed by Mcm4, 6, and 7 are primarily responsible for DNA unwinding. Since the additional subunits make helicase activity conditionally dependent on reaction conditions, it was thought that they may be negatively regulating the activity of the complex.

Biochemical comparison of the Mcm2-7 and Mcm467 complexes provided the first evidence that this might be the case, first showing that Mcm2-7 binding kinetics for ssDNA was slower than that of Mcm467, but were increased to equivalent rates after ATP preincubation (Bochman and Schwacha 2007). This was later demonstrated by the fact that Mcm2-7, unlike Mcm467, is capable of binding circular DNA substrates. These differences were reliant on the ATPase active site assumed to form between Mcm2 and Mcm5. Notably, unlike the other subunit pairs, these two subunits do not dimerize without crosslinking (Davey et al. 2003), suggesting the existence of an ATP dependent gate between Mcm2 and Mcm5 (Bochman and Schwacha 2008), later confirmed by electron microscopy (Costa et al. 2011).

Is this gate relevant physiologically? All published work regarding its existence to date has been done in biochemical or structural studies, and most mutants that cause aberrant gate states biochemically are lethal. However, one can speculate roles for such a discontinuity at various points in the cell cycle, such as loading of the complex onto DNA and during the transition from G1-phase to S-phase (Figure 3)

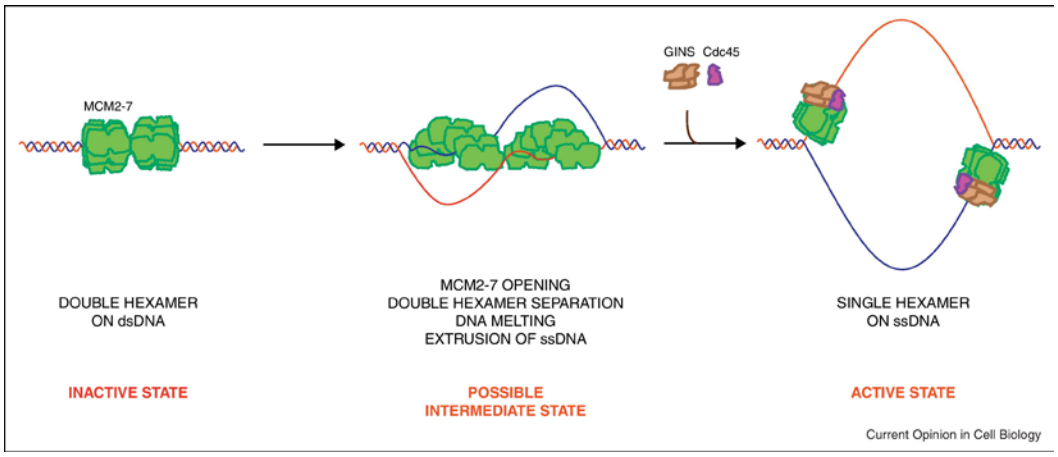

Figure 3: Proposed conformational changes of Mcm2-7 during the cell cycle

After loading, the Mcm2-7 complex transitions from dsDNA bound form to a ssDNA bound form. Reproduced from (Boos et al. 2012) with the permission of Elsevier

1.1.2.1 Loading of the helicase at origins of replication

Beginning in late mitosis, origins of replication are first bound by the six-protein **O**rigin **R**ecognition **C**omplex in an ATP-dependent matter (Bell and Stillman 1992). The loading factors Cdt1 and Cdc6 then load Mcm2-7 at ORC-bound sites and collectively these components make up the licensed Pre-replication complex (Pre-RC). Since Mcm complexes are assembled as hexamers before entry into the nucleus (Nguyen et al. 2000), there must be some method for opening the toroid so it can be loaded onto DNA. One can speculate a role for the 2/5 gate during the loading phase, as the open state, in which the complex has no helicase activity (Bochman and Schwacha 2008), would be conducive to loading the complex onto DNA. In disagreement with this hypothesis is the recent OCCM structure (Sun et al. 2013), in which the Mcms, in complex with ORC and Cdt1, are bound around DNA but do not show a prominent 2/5 gate reported by other groups. One possible explanation for this discrepancy is in the purification of these complexes, as the OCCM

structure involves a high salt wash in which loosely bound proteins are washed off DNA, which may bias the system towards complexes that have securely closed around DNA.

1.1.2.2 Initiation

Unlike prokaryotes, eukaryotes possess numerous origins of replication, which necessitates a method for coordinating the start of DNA replication between these sites to prevent relicensing and refiring of Pre-RCs once DNA replication has commenced. This is achieved through an irreversible initiation step required to activate the helicase.

The actual trigger for the start of initiation remains cryptic, but it is known that in *S. cerevisiae* one of the first events is the phosphorylation of Pre-RC components by the regulatory kinases Cyclin-Dependent Kinase (CDK) and DBF4-Dependent kinase (DDK)(Labib 2010). The essential substrates of CDK for initiation are Sld2 and Sld3, which when phosphorylated interact with Dbp11 (Zegerman and Diffley 2007). Dpb11 in turn recruits CDC45 and GINS to Mcm2-7 for assembly of the CMG complex (Takayama et al. 2003). At this time, extensive remodeling of the DNA and proteins at the origin occurs. The Mcm complex shifts from a dsDNA-bound state to a ssDNA-bound state, and the release of origin ssDNA displaces SLD3, allowing for GINS to take its place (Bruck et al. 2011; Bruck and Kaplan 2011b; Bruck and Kaplan 2011a). DDK phosphorylates multiple members of the Mcm complex, and can be bypassed entirely with a P83L mutation in Mcm5 (*mcm5bob1)*(Hardy et al. 1997). Notably, this mutation is predicted to cause a conformational change in the complex (Fletcher et al. 2003), and is a likely candidate for a mutation that disrupts normal Mcm gate function (discussed in detail below).

1.1.2.3 The S-phase checkpoint and termination.

Unpublished data from our lab implicates the Mcm6/2 active site in the replication checkpoint (E Tsai, and S. Vijayraghavan, in preparation). Furthermore, it has been observed that CDC45 has ssDNA binding capabilities that are important for fork stalling during replication stress (Bruck and Kaplan 2013). Given that conformational changes involving the gate control Mcm2-7's *in vitro* helicase activity, one can speculate that ATPase activity at the 6/2 active site and/or CDC45 dissociation open the complex to stall replication fork progression when the replisome encounters DNA damage.

Finally, it's conceivable that the 2/5 gate may play a role in termination. The details of termination in eukaryotes are poorly studied, but the gate could be necessary to remove the Mcms from chromatin at the end of S-phase.

Numerous hypotheses can and have been made about the functional roles the gate may play *in vivo.* The following sections will discuss two promising tools for dissecting gate function and the role they've played thus far in understanding helicase function: small molecule helicase inhibitors and structures of different Mcm helicases.

1.2 PROBING MOLECULAR FUNCTION OF HELICASES WITH SMALL MOLECULE INHIBITORS

As discussed above, the heterohexameric nature of the Mcm2-7 complex makes it unique among replicative helicases in that the six members of the hexamer are different proteins. From an experimental standpoint, this allows for selective inactivation of a single subunit of the helicase. Indeed, this strategy has been use to great effect in biochemical studies of

the Mcm complex (Schwacha and Bell 2001; Bochman and Schwacha 2007; Bochman et al. 2008; Bochman and Schwacha 2008; Bochman and Schwacha 2010).

While these studies have been illuminative in identifying subunits that primarily contribute to DNA unwinding, it is becoming clear that, unlike their prokaryotic counterparts, the Mcms do much more than unwind dsDNA, and are involved in the coordination of several regulatory events. These aspects are less amenable to biochemical examination, and ideally could be studied through genetic manipulations. However, like most replication proteins, all of the Mcm proteins are essential (Labib et al. 2000). Furthermore, most mutations made in the conserved AAA+ ATPase active sites are lethal (Bochman et al. 2008).

Small molecule inhibitors provide a useful alternative to traditional genetic techniques. They offer the ability to inactivate a protein with precise timing without relying on mutants. The lack of genetic manipulations required simplifies assay design, is conducive to high throughput analysis, and allows for the stoppage of proteins in systems less amenable molecular cloning, such as *Xenopus laevis* extracts. Indeed, small molecules such as HU and Nocodozole have had long histories in the DNA replication field. Beyond the laboratory, inhibitors of DNA replication machinery have potential for therapeutic use, as cancer cells undergo rounds of DNA replication at a faster rate than normal cells.

To date, bacterial and eukaryotic topoisomerases have both been used as clinical targets. Bacterial topoisomerase (DNA gyrase) inhibitors are the target of several classes of antibiotics, such as the quinolones (and associated derivatives) and aminocoumarins, both of which are widely used clinically. In humans, Topo I and Topo II are both validated cancer targets. Topo I inhibitors such as camptothecin are used clinically, and there are a

wide variety of Topo II inhibitors, including etopside, anthracyclines, and mitoxantrone used in the treatment of cancer (reviewed in (Pogorelcnik et al. 2013)).

By comparison, helicases are a relatively underutilized therapeutic target, especially in light of their pervasiveness among biological processes. The most successful strategies for inhibiting helicases have been found in the search for antiviral compounds, specifically targeting the SF1 helicase UL5 from *Herpesviridae* family of viruses (Shadrick et al. 2013).

1.2.1 Identifying helicase inhibitors

The primary difficulty in identifying new helicase inhibitors lies in the fact that DNA unwinding involves the interaction of the helicase, ATP, and double stranded DNA. The ternary nature of the reaction is highly susceptible to false positives, and is particularly vulnerable to compounds that non-specifically interact with DNA. A variety of experimental strategies have been developed to circumvent this problem, including creative substrate design, counterscreening, structure-based rational design, and alternative readouts to DNA unwinding.

1.2.1.1 Bacterial Replicative Helicase inhibitors

The prokaryotic helicase DnaB has been the target of several inhibitor studies, however most of these studies assayed compounds against the DnaB helicase from benign laboratory *E. coli*, and resulted in the identification of few compounds and/or compounds of low potency (Earnshaw et al. 1999; Earnshaw and Pope 2001; Zhang et al. 2002; Griep et al. 2007). However, these initial studies have led to the development of high throughput

assays, which has resulted in the identification of compounds with much greater therapeutic promise. Mckay *et al*. utilized the assay developed by Zhang *et al.* (Zhang et al. 2002) to screen over 230,000 compounds against the DnaB from *Pseudomonas aeruginosa,* identifying triaminotriazines with low micromolar inhibition (McKay et al. 2006).

More recently, Aiello *et al.* performed a fluorescent helicase assay based screen against the DnaB helicases from *Bacillus antracis* and *Staphylococcus aureus,* screening over 186,000 compounds and identifying 160 which inhibited helicase activity. Eighteen of these remained after counterscreening eliminated false positives (Aiello et al. 2009). Of these, the coumarin-based compounds exhibited the highest potency and selectivity against bacterial cells with low general cytotoxicity. The same FRET-based method was later used in the identification of benzobisthiazole derivatives with nanomolar potency, shown to be acting competitively with the DNA substrate (Li et al. 2013).

1.2.1.2 Viral Helicase inhibitors

The helicase/primase complex UL5 from the *Herpesviridae* (HSV) is the most successful example of a helicase drug target to date, with multiple compounds that inhibit the complex used as antivirals clinically. Many of the high throughput techniques used to identify helicase inhibitors were first developed in HSV (reviewed in (Shadrick et al. 2013)).

The other class of viral helicases widely studied come from polyomavirsuses and papillomavirsuses. The viral replication factor large T-antigen (TAg) has recently been the focus of multiple high throughput screens, with the hope of developing treatments for polyoma virus infection in immunocompromised individuals. Given that TAg from SV40

is a well-studied AAA+ hexameric replicative helicase, strategies and compounds from these studies may be applicable to finding inhibitors of the Mcm complex. SV40 inhibitor studies have largely focused on inhibiting ATPase activity (Wright et al. 2009; Seguin et al. 2012)

Why has there been such greater success in developing treatments targeting viral helicases as opposed to bacterial helicases? It has been posited that one reason may be viral helicases, in addition to their DNA unwinding function, coordinate other regulatory events as well (Shadrick et al. 2013). Indeed, large T antigen exemplifies this particularly well, as the various domains of the complex have been tied to a large number of different cellular processes. This multifunctional nature of viral helicases makes them indispensable to a variety of viral functions, rather than just bulk replication. This not only increases potency of small molecule inhibitors, as more cellular systems are impacted, but also lowers the likelihood of second site suppressor mutations occurring, since multiple processes are compromised.

This coordination of disparate regulatory events is also seen in the Mcm2-7 complex, discussed above, which may make it an attractive target for inhibitor studies.

1.2.2 Inhibitors of the Eukaryotic Replicative helicase

In contrast to their prokaryotic and viral counterparts, no high throughput screens have been performed on Mcm2-7. One reason for this is largely practical: it is difficult to purify Mcm2-7 and the CMG complex in amounts large enough to perform these screens, and *in vitro* helicase activity has not been demonstrable for the whole complex until

recently. However, there have been individual compounds identified that disrupt the complex's activity and expression. The compound heliquinomycin was first identified as an inhibitor of *in vitro* replication in cell extract systems (Chino et al. 1996), and was later shown to inhibit the DNA unwinding properties of a Mcm467 (Ishimi et al. 2009). In cell culture, heliquinomycin has been shown to selectively decrease the proliferation of cancer cells overexpressing Mcm7 (Toyokawa et al. 2011).

A second compound, Widdrol, was observed to have antiproliferative activity against human colon adenocarcinoma HT29 cells (Kwon et al. 2010). Interestingly, this effect appeared to be due to a downregulation of Mcm gene expression as a downstream consequence of DNA damage. While not a direct effect, it does further validate the use of compounds that reduce Mcm availability or activity as chemotherapeutic agents.

1.3 STRUCTURAL INSIGHTS INTO MCM2-7'S FUNCTION

Structural biological studies of the Mcm complex fall into two broad categories. The first is high resolution studies of X-ray crystallography structures of Mcm subunits and complexes isolated from Archaeal organisms. These studies are useful in they show us atomic resolution of the complex, but have limited applicability to eukaryotes as they are not highly conserved with eukaryotic Mcms outside the C-terminal domain containing the AAA+ active site and helicase motifs, and there are fundamental differences in archaeal DNA replication, which only have one Mcm protein and lack accessory factors necessary in eukaryotes like GINS and CDC45.

The second category is low-resolution structures determined with electron microscopy techniques. This includes 3-dimensional reconstructions of dodecamers of the archaeal mcm complex, and hexamers of the eukaryotic Mcm2-7 as well as larger complexes (CMG and OCCM) from single particle image averaging of electron microscopy images. These recent structures have proved invaluable in confirming predicted protein interactions.

Table 1 List of published Mcm structural papers

Organism	Resolution	Notes	Ref.
S. pombe	N/A	Rotary shadowing of complexes isolated from cell extracts	(Adachi et al. 1997)
Human	N/A	2D EM of individual Mcm467 hexamers	(Sato et al. 2000)
M. thermautotrophicus	3 Å	Crystal structure of N-terminal fragment, packs as a dodecamer	(Fletcher et al. 2003)
M. thermautotrophicus	25 Å	Single particle reconstruction of dodecamer, open and closed rings observed	(Gomez-Llorente et al. 2005)
M. thermautotrophicus	24 Å	3D reconstruction of dodecamer	(Costa et al. 2006a)
M. thermautotrophicus	N/A	2D analysis of MtMCM with various ligands, evidence of both double and single hexamers/heptamers	(Costa et al. 2006b)
M. thermautotrophicus	25 Å	DNA bound to outside of single hexamer	(Costa et al. 2008)
S. sulfolobus	2.8 Å	Crystal structure of an N-terminal fragment, packs as a hexamer	(Liu et al. 2008)
S. sulfolobus	4.35 Å	Crystal structure of near full length Mcm monomer	(Brewster et al. 2008)
M. kandleri	1.9 Å	Full length crystal structure of a nonfunctional Mcm homologue	(Bae et al. 2009)
D. melanogaster	28,32,35Å	EM single particle reconstruction of CMG complex, and closed and open Mcm hexamers	(Costa et al. 2011)
Human	N/A	NMR structure of the C-terminus of Mcm6 bound to Cdt1	(Liu et al. 2012)
E. cuniculi	24 Å	Mcm from a minimalist eukaryote. Forms an open hexamer even in the presence of ATP	(Lyubimov et al. 2012)
S. cerevisiae	14 Å	CryoEM structure of OCCM complex containing Mcm2-7	(Fernandez-Cid et al. 2013)

The earliest electron microscopy analyses of Mcm2-7 (Adachi et al. 1997) and 467 (Sato et al. 2000) were our first indication that the Mcm complex forms a toroid, which

when combined with the knowledge that the complex elutes off gel filtration columns at approximately 600 kDa yielded the initial evidence that the eukaryotic Mcms are hexameric helicases.

1.3.1 Archaeal Structural Studies

It wasn't until the crystal structure of the N-terminal portion of the *Methanothermobacter. thermautotrophicus* archaeal Mcm that we had physical confirmation that the Mcm proteins can form hexameric toroids. Although this initial structure lacked the C-terminal (and much more highly conserved) helicase domain, it still demonstrated the toroid had a positively charged central channel sufficiently large to accommodate DNA, and also demonstrated that the archaeal Mcm hexamers are able to pack against each other at the N-terminus, forming a dodecamer with oppositely facing complexes. This raised the possibility that the functional form of the Mcm complex may be a double hexamer at one or more stages of the cell cycle. This possibility was supported by electron microscopy single particle reconstructions of the full length *M. thermautotrophicus* Mcm complex (Gomez-Llorente et al. 2005; Costa et al. 2006a), which showed the full length protein forming a dodecamer. Conversely, a crystal structure of the equivalent N-terminal portion of the archaeal Mcm from *S. sulfolobus* packs as a hexamer. Given the high degree of variability of the N-terminal region of the Mcms, even within archaea, it remains unclear how applicable these structures are to the eukaryotic Mcm complex.

Later crystallographic analyses of the full length *S. sulfolobus* and *M. kandleri* Mcms provided the first views of the Mcm helicase domain. Several features distinguish the Mcms among other helicases.

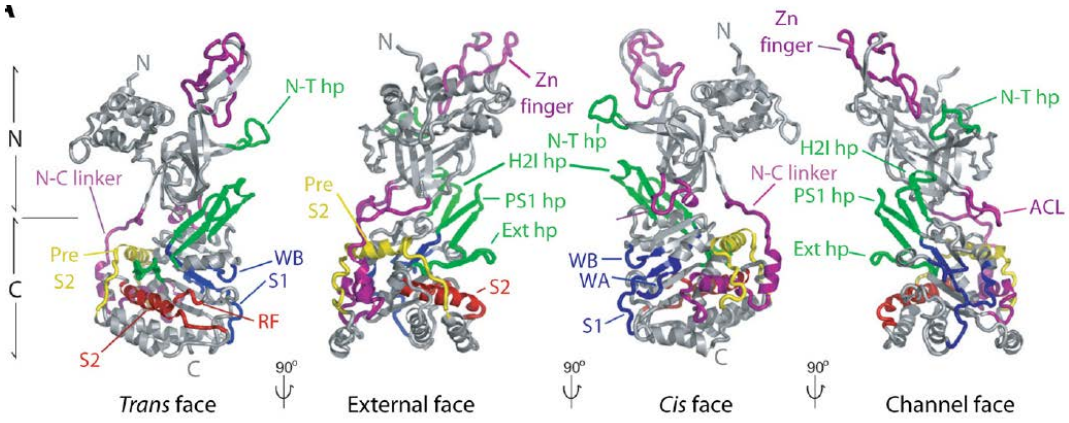

Figure 4: Mcm structural motifs in *S. sulfolobus*

Adapted from (Bochman and Schwacha 2009) with the permissions granted by the American Society of Microbiology. PreS2: Presensor 2, S2: Sensor2, N-T hp: N-terminal hairpin, WB: Walker B motif, RF: Arginine Finger motif, Zn Finger: Zinc Finger, H2I hp: Helix-2-insert hairpin, PS1 hp: Presensor 1 hairpin, Ext hp: External Hairpin, WA: Walker A motif, S1: Sensor 1, ACL: allosteric control loop.

Figure 4 depicts the near full length structure with notable motifs highlighted in color. Absent is the Winged Helix domain, which is disordered and not visible. Many of these motifs have been analyzed for their role in the complex's helicase activity. As expected (McGeoch et al. 2005), and consistent with other AAA+ ATPases (Erzberger and Berger 2006) Walker A and B motifs are present on the *cis* side of the intersubunit active interface, along with the Sensor 1 motif, while the *trans* side of the monomer contributes the arginine finger and Sensor 2 motifs. The *trans* acting Sensor 2 motif is a feature unique to the Mcms, as it functions *in cis* in other AAA+ proteins. This difference is a result of the Presensor 2 insertion found in the Mcm helicase clade (Erzberger and Berger 2006).

Several β fingers depicted in the structure have been shown to be important for DNA binding and helicase activity of archaeal Mcm complexes and have been proposed to be in physical contact with the DNA substrate. In the N-terminus, the N-terminal hairpin

extends into the central channel, and has been shown to be important for the complex's ssDNA binding capabilities (McGeoch et al. 2005).

In the C-terminus two additional hairpins extend into the central channel. The first is the Presensor 1 insert, found to be moderately important for ssDNA binding, but is essential for archaeal helicase activity (McGeoch et al. 2005). The second is Helix 2 insert, which is the unique and defining feature of the Mcm helicase superfamily, and has been shown to be essential for coupling ATPase activity to DNA unwinding (Jenkinson and Chong 2006).

One remaining hairpin lies near a conserved side channel (per pair of monomers) in the *S. sulfolobus* structure. While a biological role for this side channel has not yet been demonstrated, the external hairpin is involved in DNA binding (Brewster et al. 2008)

All of these structural motifs are conserved in the eukaryotic Mcms to varying extents, however, evidence suggests that, like the active sites motifs, they are not all functionally equivalent. An example of this is the Presensor 1 and 2 motifs of Mcm3. Sequence alignment of the Mcm proteins show that Mcm3 alone has an extensive insertion within the Presensor 2 motif that is conserved across multiple species (Bochman and Schwacha 2009) and represents one of the few areas of sequence divergence in the AAA+ domain among the six Mcm proteins. Functional differences are also seen in the Presensor 1 motif, as only the presensor 1 motif from Mcm3 is essential for viability and helicase function (Lam et al. 2013).

1.3.2 Eukaryotic Structural Studies

Structural analyses of the full eukaryotic Mcm2-7 complex have to date been limited to electron microscopy reconstructions. The first 3D model of the eukaryotic replicative helicase was reported by Costa *et al.*, in a comprehensive analysis of the *Drosophila melanogaster* Mcm2-7 complex (Costa et al. 2011). As expected, the complex forms a hexameric toroid, with a central channel large enough to bind ssDNA. Furthermore, they confirmed the subunit order predicted from biochemical studies (see Figure 2) through the use of MBP fusion tags.

Most importantly, the 3D structure confirmed many of the mechanistic predictions made by prior biochemical DNA binding studies (Figure 5). The apo form of the complex appears to exist in an equilibrium between two discrete states. The first is a right handed spiral ‘lockwasher’ with an open gap between Mcm2 and Mcm5, and second a planar notched form.

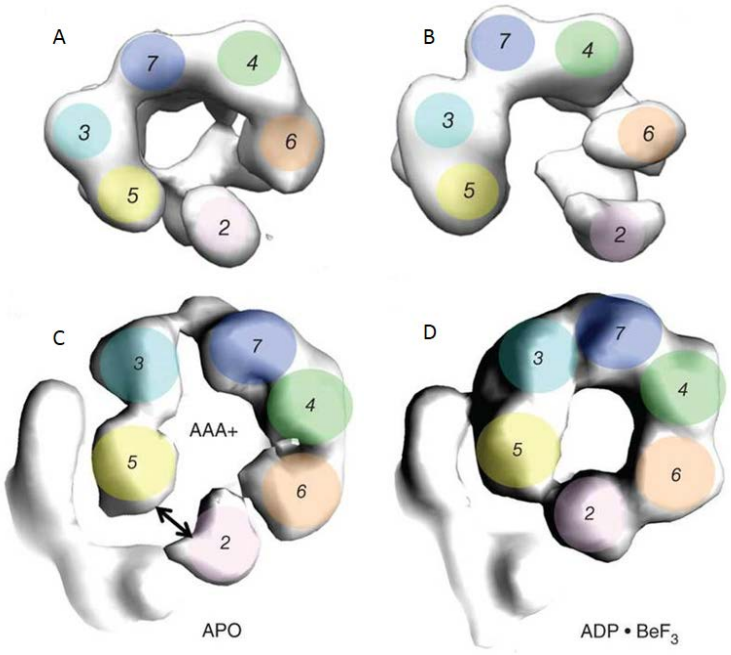

Figure 5: Conformational states of the *Drosophila* Mcm complex

Panels A and B: The *Drosophila* Mcm2-7 complex exists two discrete states, a planar notched form and a right handed lockwasher form. C) Addition of Cdc45 and GINS forms the CMG complex, which restricts the Mcms into the planar notched state D) Addition of ADP·BeF_3 tightens the ring in the CMG complex, as shown by the narrowing of the space between Mcm2 and Mcm5. Adapted from (Costa et al. 2011) with the permission of Nature Publishing Group.

It had previously been determined that the functional form of the replicative helicase requires the accessory factors Cdc45 and GINS (Moyer et al. 2006; Ilves et al. 2010), forming an 11-protein CMG complex. Interestingly, it appears that the binding of these factors and a non-hydrolysable analogue serve to close the ring, supporting the hypothesis that gate closure is how the Mcms are activated.

While the CMG complex represents the biochemically active state of the Mcm complex, a recent structure of a Pre-RC intermediate, the ORC-Cdc6-Cdt1-Mcm2-7 (OCCM) complex was recently isolated from yeast and its structure determined with cryo-EM (Sun et al. 2013). Key differences arise when comparing this structure with that of the CMG complex (Figure 6).

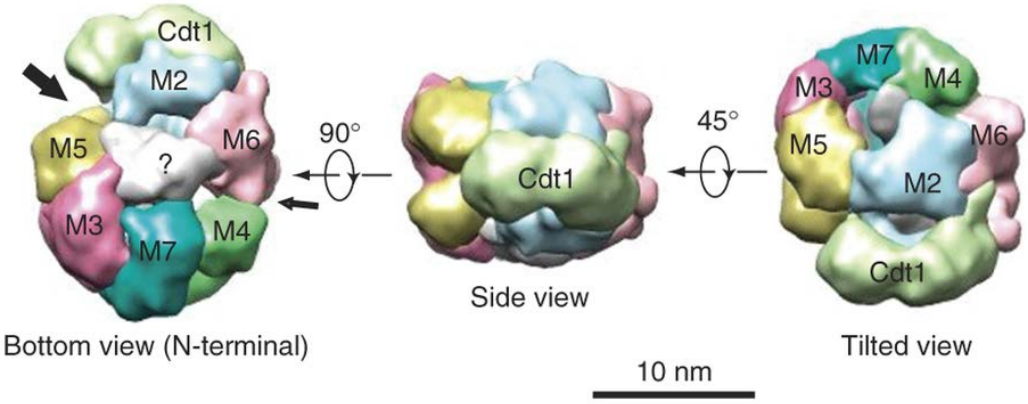

Figure 6: *S. cerevisiae* Mcm2-7 in the OCCM complex

Shown are the Mcm2-7 and Cdt1 components of the OCCM complex, (ORC and Cdc6 not pictured). The (?) designates unexpected positive density determined to be co-purifying DNA. Adapted from (Sun et al. 2013) with the permission of Nature Publishing Group.

Sun *et al. (Sun et al. 2013)* found that the subunit order of the *S. cerevisiae* Mcm complex was consistent with what was seen in the *D. melanogaster* structure and predicted biochemically. Of note is the state of the Mcm2/5 active site, which lacks the large discontinuity seen in the Costa *et al.* structure (Costa et al. 2011). Unexpectedly, the 4/6 active site seems to have a slight discontinuity. The implications of these discrepancies will be discussed below.

1.3.2.1 Double VS Single hexamer

A long standing question has been whether the functional state of the Mcm complex is a single or double hexamer. Given the observation that *M. thermautotrophicus* assembles as a double hexamer in crystal and EM structures, and the observation of double hexamers of the eukaryotic Mcms bound at origins (Evrin et al. 2009; Remus et al. 2009; Gambus et al. 2011), several models were originally proposed which suggested that the active unwinding complex could either split as two hexamers from a single origin, or stay together and function as a dodecamer (Brewster and Chen 2010)., However, recent single molecule studies have confirmed that the functional form of the eukaryotic Mcm complex during S-phase is a single hexamer (as part of the CMG complex) operating by the steric exclusion model (Yardimci et al. 2010; Fu et al. 2011; Yardimci et al. 2012) while the loaded form (as part of the Pre-RC complex) is a double hexamer (Remus et al. 2009).

1.3.2.2 The Mcm Gate: Discrepancies between species and structures

The recent structures of Mcm2-7 in *D. melanogaster* (Costa et al. 2011), *S. cerevisiae* (Sun et al. 2013), and *E. cuniculi* (Lyubimov et al. 2012) display a slight discrepancy with the previous literature. While they all indicate a role for gate dynamics, they do not quite conform to the ATP-dependence and activity states that have been shown biochemically (Bochman and Schwacha 2008). The *D. melanogaster* Mcm2-7 appears to be dynamically shifting between open and notch states, and requires CDC45, GINS, and ATP for full closure. Costa *et al* report a minor shift in the apo structure's propensity for the notched form in the presence of non-hydrolysable ATP analogues (Costa et al. 2011), but not to the degree predicted from *S. cerevisiae* DNA binding data (Bochman and Schwacha 2007; Bochman and Schwacha 2008). *E. cuniculi* also has a visible gate in the presence of ATP

analogues. Conversely, the preRC intermediate OCCM structure isolated from G1 extracts shows the gate to be nearly closed, despite the fact that Mcm2-7 should be biochemically inactive at this stage of the cell cycle.

What is the reason for these differences? One obvious possibility is species specific differences. Neither *D. melanogaster* nor *E. cuniculi* Mcm2-7 have been shown to have *in vitro* helicase activity alone. It has been assumed that proper assay conditions have not yet been discerned for these species as they have in *S. cerevisiae* (Bochman and Schwacha 2008), but alternatively this could indicate fundamental biochemical differences in the complex in different organisms.

Another explanation is that the regulation of the complex via the Mcm2/5 gate is more complicated than simply an 'open and shut case' and the gate opens and closes at multiple points in the cell cycle depending on Mcm2-7's binding partners.

Finally, we must also consider differences in purification protocol. Sun *et al.* included a high salt wash step, which is expected to dislodge any loosely bound Mcms (Sun et al. 2013). It's conceivable that this step enriched their purification for Mcms found in the closed state bound to DNA.

1.4 THESIS OVERVIEW

The goal of my dissertation research has been to understand the role the Mcm2/5 gate plays in Mcm2-7's function as the replicative helicase. Toward this end I have operated under the central hypothesis that disrupting the gate should have functional consequences, as well

as the reverse hypothesis that some of the previously characterized functionally deficient Mcm mutants have aberrant gate function. To test these hypotheses I investigated two independent, but complementary, specific aims.

The first has been the identification and characterization of small molecule inhibitors of the Mcm2-7 complex. The second has been the structural characterization of the *S. cerevisiae* Mcm2-7 apo structure and Mcm mutants predicted to disrupt the Mcm2/5 gate.

1.4.1 Specific Aim 1: Identification and characterization of small molecule inhibitors of Mcm2-7

The goal of this study was to address the possibility of finding an inhibitor specific to the regulatory active sites of Mcm2-7, which we reasoned could be identified by assaying for compounds that inhibit Mcm2-7 but not Mcm467 or Large T-antigen. The fluoroquinolone ciprofloxacin had been shown to be a likely starting candidate, and I assayed a variety of related fluoroquinolone and other structurally related compounds for greater selectivity and/or potency. After identifying promising candidates, I characterized their effects on ATPase activity, DNA intercalation, and assessed their effects on cells *in vitro*, ultimately identifying a ciprofloxacin resistant allele of Mcm4.

1.4.2 Specific Aim 2: Structural characterization of mutants effecting the Mcm 2/5 'gate'

Evidence for the Mcm2/5 gate has now been presented biochemically and structurally, but without a phenotype to attribute to the gate's malfunction, its role in the cell cycle remains largely speculatory. Furthermore, there are discrepancies between the biochemical and structural literature regarding conditions that contribute to gate opening and closure, possibly due to species differences. To address these issues, I used single particle reconstruction to solve the structure of the *S. cerivisiae* in the apo state, along with mutants predicted to be open or closed based on DNA binding assays, and regulatory mutant, *mcm5bob1,* which bypasses the need for the regulatory kinase DDK for entry into S-phase. My findings show agreement between the biochemical and structural data for the state of the gate in *S. cerevisiae,* and support a role for the gate in S-phase entry.

2.0 MATERIALS AND METHODS

2.1 DNA OLIGONUCLEOTIDES, CHEMICALS, ANTIBODIES, AND OTHER REAGENTS

Oligonucleotides were all purchased from IDT. pUC19 DNA was purchased from New England Biolabs.

Radiolabeled ATP was purchased from either MP Biomedical or Perkin Elmer Life Sciences. Nucleotides were purchased from GE Healthcare. All chemicals purchased for use in buffers and assays were of the highest available purity.

Stock solutions of putative inhibitors were made in anhydrous DMSO at either 13 mM (MAL2-11B (Wright et al. 2008)) or 100 mM (N-ethoxy-carbonyl-2-ethoxy-1,2-dyhydroquinolone (EEDQ; Aldrich), N,N'-dicyclohexylcarbodiimide (DCCD; Sigma), pyridoxal 5'-phosphate (PP; Fluka), phenylglyoxal (PG; Aldrich), 4-chloro-7-nitrobenzofurazan (Nbf; Fluka), ofloxacin (Sigma) and ciprofloxacin (Fluka, > 98% pure by HPLC)). N-ethylmaleimide (NEM, USB) was made as a 1M stock in absolute ethanol. These stock solutions were stored at -20°C and were stable for at least several months. All compounds were completely soluble at the final assay concentrations except as noted.

For initial small molecule inhibitor screening, a collection of 144 compounds was obtained from the Drug Discovery Center (DDC, University of Cincinnati, Cincinnati, OH) (Appendix). For follow-up experiments on selected inhibitors (Table 2), neat samples of

each inhibitor were obtained from DDC or ChemBridge (compounds 924384 and 271327 correspond to ChemBridge 7473736 and 5281925, respectively) and stored as 100 mM stock solutions in DMSO. The purity of these compounds was either established by the manufacturer or was determined by the DDC using mass spectrometry and HPLC analysis and found to be >90-100% in all cases (Table 2).

2.2 BUFFERS

The following list is organized as follows:

Name of the buffer *Description of buffer's purpose* Buffer recipe

1. Binding Buffer: *Used in ssDNA binding assays and for dilution of samples prior to electron microscopy*. 25 mM potassium-HEPES, pH7.4, 50mM KCl, 10mM MgOAc, 50 µM ZnOAc, 100 µM EDTA (pH 8.0), 10% glycerol, 0.02% NP-40, 1mM DTT
2. 2X Helicase Buffer *Used in helicase and ATPase assays*: 40 mM Tris-HCl pH 7.5, 20mM MgOAc, 40% glycerol, 200 µM EDTA 10mM DTT
3. 10X Stop load buffer: *Loading dye used in quenching helicase assays an subsequent electrophoresis.* 0.25% Bromophenol Blue, 0.25% Xylene Cyanol, 1% SDS, 100mM EDTA (pH 8.0), 25% Ficoll type 400.
4. Tris/Borate/EDTA Buffer (TBE) *Native PAGE.* 90 mM Tris base, 90 mM borate, 2mM EDTA, adjust pH to 8.0

5. Tris Buffered Saline+Tween 20 (TBST), 10X stock *Western Blotting*. 50 mM Tris, 150 mM Nacl, 0.05% Tween
6. Topoisomerase Buffer *For assaying DNA intercalation with topoisomerase II* 50 mM Tris-HCl (pH 8), 1 mM EDTA, 1 mM DTT, 20% glycerol, and 50 mM NaCl.

2.3 PROTEIN PURIFICATION

Hexameric *S. cerevisiae* Mcm2-7 and Mcm467 complexes were expressed in baculovirus-infected insect cells, and purified using affinity, gel filtration, and ion exchange chromatography as described (Bochman and Schwacha 2007; Bochman et al. 2008)Gel filtration and Western blot analysis indicates that the complexes contain equimolar amounts either all three (*i.e.*, Mcm467) or all six (*i.e.*, Mcm2-7) of the indicated Mcm subunits. The Simian Virus 40 large tumor antigen (TAg) was purified as previously described (Cantalupo et al. 1999). Additional helicases were generously provided by colleagues: the SsoMcm complex (M. Trakselis, University of Pittsburgh, Pittsburgh, PA); Srs2 (E. Antony, Washington University School of Medicine, St. Louis, MO); T7 gp4 (S. Patel, University of Medicine and Dentistry of New Jersey, Piscataway, NJ); DnaB (K. Marians (Sloan-Kettering, New York, NY); and T4 gp41 (S. Benkovic, Pennsylvania State University, University Park, PA).

2.4 METHODS

2.4.1 *In vitro* Helicase Assay

Helicase assays were performed as described previously, (Bochman and Schwacha 2007; Bochman and Schwacha 2008), except when inhibitors were used in which case the incubation time was increased from 30 minutes to one hour. Synthetic replication forks were prepared by annealing oligos 233 and 235 (IDT (Coralville, IA), oligo 233 5’ $(T)_{40}$GGTTGGCCGATCAAGTGCCCAGTCACGACGTTGTAAAACGAGCCC; oligo 235 5' CACTCGGGCTCGTTTTACAACGTCGTGACTGGGCACTTGATCGG-CCAACC$(T)_{40}$) and then filling in the recessed 3’-end with [a^{32}P]dATP and unlabeled dNTPs using Klenow Fragment. Briefly, reactions (6 µL) were performed in 1x helicase assay buffer (20 mM Tris HCl (pH 7.5), 10 mM MgOAc, 20% glycerol, 100 µM EDTA, and 5 mM DTT) and contained a final concentration of 1 nM fork substrate, 5 mM ATP, 40 mM creatine phosphate, 16.5 mg/mL creatine kinase, 33 µg/mL BSA. Reactions containing Mcm2-7 and Mcm467 were supplemented with 200 mM potassium glutamate. Reactions containing SsoMcm were incubated at 65°C, those containing T4 gp41 were incubated for 30 min at 37^{o}C, and all other reactions were incubated at 37°C for 1 h. The products were separated by 10% native PAGE, the resulting gels dried, and the radioactivity quantified using a Fuji FLA-5100 phosphoimager. Irrespective of the protein used, all helicase assays contained equal molar protein concentrations (100 nM, assuming in all cases that the active helicase form is hexameric).

2.4.2 DNA Binding assay

Single stranded DNA binding assays were performed as described (Bochman and Schwacha 2007). The single stranded DNA substrate was a mixed 50mer probe, oligo 826 TGTCTAATCCCGAAAGGCCCTGCCACTGAAATCAACACCTAAAGCATTGA, radiolabeled at the 5' end with T4 polynucleotide kinase (New England Biolabs) and (γ^{32}P) ATP. Standard reactions contained 4nM unlabeled oligonucleotide 826 spiked with a small amount of labelled probe, 120 nM Mcm hexamers, 5mM ATPγS, and 5mM β-glycerophospate in binding buffer. Reactions were incubated for 30 minute at 30 degrees C.

Double filter binding with nitrocellulose and DEAE filters was performed as described (Wong and Lohman 1993). Prepared filters were stacked on a GE healthcare FH 225V Filter Manifold and washed with 500 µL of binding buffer. Reactions were spotted on the filter stack, washed with an additional 500 µL of binding buffer, then the radioactive counts on DEAE and nitrocellulose filters were measured separately by scintillation counting. Percent DNA bound was calculated as the number of radioactive counts on the nitrocellulose filter divided by the total counts on both filters.

2.4.3 Steady State ATPase assay

Steady-state ATP hydrolysis was assayed as published (Schwacha and Bell 2001). In short, reactions were set up essentially as in the helicase assay, with minor exceptions. A non-radiolabeled DNA fork was used, helicase concentration was 100 nM (hexamer) the total ATP concentration was 500 µM and included ~0.5 µCi of [a^{32}P]ATP, and the ATP

regeneration system was omitted. Reactions were incubated for 1 h at 37°C and stopped by the addition of SDS. ATP was separated from ADP by PEI thin layer chromatography, and the ratio of ATP:ADP was quantified with a Fuji FLA-5100 phosphoimager. Based upon our prior work (Schwacha and Bell 2001), conditions were established to ensure that the results shown are within the linear range of the assay

2.4.4 Topoisomerase Assays

Topoisomerase assays were adapted from (Jones-Held 1992). Reactions (10 µL) contained were carried out in topoisomerase buffer and containing pUC19 (50 ng; NEB) was incubated at 37°C for 2.5 h with 4 units of Wheat Germ Topoisomerase I (Promega). Inhibitors were added at the indicated concentrations at either t=0 or t=90 min as described in the figure legends. Following incubation, topoisomers were separated via gel electrophoresis on a 1.0% agarose gel for 2 h at 8 V/cm in TAE buffer. After electrophoresis, the gel was stained with ethidium bromide and imaged with a Fuji LAS-3000. In all of the above assays, dilutions of the test compound were made with Milli-Q H_2O and DMSO such that the final concentration of DMSO in the biochemical assays was 1% (v/v), and the reported activity was normalized to solvent controls.

2.4.5 Yeast Growth inhibition assay

S. cerevisiae growth inhibition was quantified using an established 96-well plate assay (Simon et al. 2000). Two isogenic W303 testers strains were used (construction details available upon request): UPY675 (*matA, ade2-1, ura3-1, his3-11,15, trp1-1, leu2-3,112,*

can1-100, bar1::hisG, Derg6:: kanMX) and UPY1056 (isogenic to UPY675 but containing *mcm4chaos3*). Overnight yeast cultures were grown in YPD, diluted to 0.05 OD_{600}, grown to an OD_{600} of 0.1-0.15, aliquoted into a 96-well plate, and then treated with inhibitor titrations. Inhibitors were first diluted in pure DMSO, then added to wells to a final volume of 100 µL containing 2% DMSO. Plates were grown without shaking at 30ºC for 24 h. Optical density was quantified at 0 and 24 h with a Bio-tek EL800 Universal Microplate reader. Percent relative growth was determined by calculating the change in optical density over 24 h at each concentration relative to a 2% DMSO control.

2.4.6 Yeast membrane permeabilization assay

Due to the difficulty of doing genetics with Δ*erg6* strains, some replication mutants were tested using an assay adapted from (Pannunzio et al. 2004), which renders wild type yeast permeable to small molecules when grown in the presence of sodium dodecyl sulfate (SDS) and L-proline instead of ammonium sulfate as the nitrogen source. Strains were grown overnight in synthetic media with appropriate amino acids, 0.17% yeast nitrogenous base, 0.1% L-proline, and 2% glucose. The following day the cultures would be diluted to 0.15 OD in fresh media containing 0.003% SDS and allowed to recover for 3 hours before challenging with inhibitors.

2.4.7 Graphing and statistical analysis

Inhibition and the corresponding 95% confidence intervals (CIs) from both the helicase assays and growth inhibition assays were plotted using GraphPad Prism Version 5.0f for

Macintosh. The inhibitor concentrations were converted to Log_{10}, and then nonlinear regression was used to fit the data points with a sigmoidal dose-response curve using the following equation:

$$y = y_{min} + \left(\frac{y_{max} - y_{min}}{1 + 10^{(LogIC_{50} - x) - HillSlope}} \right)$$

where y_{min} is the minimum helicase activity, y_{max} is the maximum helicase activity, IC_{50} is the effective concentration of inhibitor that decreased helicase activity by 50%, and the Hill Slope describes the steepness of the curve. In all cases, the equation was constrained by subtracting the baseline from the data and normalizing all values to helicase activity in the absence of inhibitor. Thus, ymin and ymax were 0 and 100%, respectively. The software was also used to calculate the 95% CIs, the quality of the fit (i.e., R2), and to determine the extra sum-of-squares F test to calculate P values to compare the $LogIC_{50}$ values between curves. Differences in values were considered statistically significant when $P < 0.05$.

2.4.8 Electron Microscopy Sample Preparation

Purified Mcm proteins were diluted to approximately 50ng/µL in binding buffer. A 10 µL drop of dilute protein was spotted onto a piece of Parafilm and was adsorbed for 30-60 s to a glow-discharged (Quorum Emitech K100X Glow Discharger) carbon coated grid (Formvar backed 400-mesh carbon, Ted Pella 1702-F) held with fine tip tweezers. The excess liquid was gently wicked onto a piece of Whatman paper, and the grid was transferred to a 100 µL drop of 1.5% uranyl acetate for 30 s. The excess liquid was once again wicked away and the grid was allowed to air dry.

Certain protein preparations had a tendency to lay on the grid in a preferred orientation, leading to an overrepresentation of certain views. In these cases, additional views of the complex were obtained by increasing the glycerol concentration of the dilution buffer (binding buffer) to 20%. Under these buffer conditions a 70 kelvin cryo holder was use to protect the sample from damage during imaging.

Images taken for optimizing staining conditions were taken on a FEI Morgagni microscope operating at 80kv at the listed magnifications. Images were taken with an Advanced Microscopy Techniques XR-60 digital camera.

Images for model building were taken on a Tecnai TF20 transmission electron microscope operating at 200kv, at nominally 29000X magnification in low dose mode. Images collection was done in Digital Micrograph with a Gatan Ultrascan 4000 CCD camera with a post column magnification of 1.4 and CCD elements of 15 µm dimensions. The effective pixel size was 3.7 Å.

2.4.9 EMAN Single Particle 3D reconstruction.

All final model building was done using the EMAN2 image processing suite (http://blake.bcm.edu/emanwiki/EMAN2) (Tang et al. 2007) Version 2.07. For all steps command strings were built using the e2projectmanager interface, and parameters and arguments referred in this section based on how they are organized in the interface for each module.

2.4.9.1 Particle Import and CTF tuning

Raw image files were initially CTF corrected and imported into EMAN2 with e2eval.py. For this step, the parameters for voltage, area/pixel, and spherical aberration from the microscope used to collect data were specified (200kV, 3.7, and 2 respectively for the Tecnai TF20). Amplitude contrast was set to 0.7 and a box size of 512 pixels was used for the initial CTF tuning. Initial CTF tuning was performed by roughly adjusting the defocus parameter so that the graph of the contour transfer function aligned with the phase of the power spectrum. Micrographs were imported without contrast inversion.

Particles were collected semi automatically using the swarm function in e2boxer.py. The box size used was the nearest 'good box size' that was roughly 1.5 the width of the Mcm complex (100 angstroms). This generally was 168, depending on which version of EMAN2 was used for particle picking.

CTF tuning was done on the selected particles with e2ctf.py with the default parameters, except the amplitude contrast was increased to 70 as is appropriate for negative stain. After generating a structure factor, particles were CTF tuned again, manually corrected, then exported as phase flipped particles.

At this stage particles were analyzed on a micrograph by micrograph basis, and poor particles (those poorly centered, too small, or too close to other particles) were rejected for particle set building. Particle sets of varying sizes were assembled, generally smaller sets (less than 10,000 particles) were used for reference free class averaging and initial model building, and larger sets (20,000-40,000 particles) where used for further model refinement. In cases where high glycerol conditions were used to increase representative views of the complex, the smaller particle set would contain roughly equal numbers of particles collected under 'high glycerol' and standard conditions.

2.4.9.2 Reference free class averaging

Reference free class averages were constructed in e2refine2D.py by generating an appropriate amount of classes depending on particle set size and the thresholding level (generally 50%), such that approximately 10-20 particles were generated per class average, typically resulting in 300-500 classes. Generally, the only parameters adjusted when optimizing reference free class averages where the total number of particles in the particle set, the number of class averages, and the thresholding level.

For the refine2d parameter options, typically fast seeding was used when generating a greater than 100 class averages, and normalized projection vectors were not used unless a marked improvement in class averages were seen with its usage. Eight iterations were done during each refinement. The number of alignment references (naliref) and the number of MSA basis projection vectors (nbasisfp) where each set to the default value of 5.

Under simmx options, the shrink factor was set to a value of 3 and an oversampling to a value of 2. The comparator (simcmp) used to align the images was the cross correlation coefficient (ccc) and the aligner used prior to comparing the images (simalign) was rotate_translate_flip. Finally, the aligner along with construction arguments (simaligncmp) was the cross correlation coefficient (ccc). Second stage alignment was not used in reference free class averaging.

For class averaging options, the level of thresholding was varied to experimentally to see what resulted in optimal classes. Initially, the default level of 0.85 would be used and lowered on subsequent refinements, with optimal results generally obtained with a level of 0.5. For each refinement, five iterations were performed. For class normalization (classnormproc) ‘normalize.edgemean’ was used. The class averager used was ‘mean,’

class comparator (classcmp) used was ‘ccc,’ the class aligner (classalign) was ‘rotate_translate_flip’, and the first stage comparator used was ‘ccc.’

Once optimal reference free class averages were defined, 20-30 selected class averages representing different views of the Mcm toroid were saved as a .hdf image stack.

2.4.9.3 3D modeling

The selected class averages were used to generate a roughly toroidal initial model with e2initialmodel.py, as determined by Z-slices through the generated volume. Eight iterations and ten tries were performed for each round of modeling, with C1 symmetry (no symmetry) applied.

Refinement of the initial model was done in e2refine.py against the phase flipped particle set. Once conditions were established that lead to convergence on a solution, refinement was done iteratively until successive iterations failed to improve the model. Options used in e2refine.py varied as model building progressed.

Under ‘e2refine options’ the area per pixel for all refinements was 3.6 angstroms, the particle mass was 600 kDa (estimated mass of the Mcm2-7 complex). The number of iterations and parallel processors were varied depending on available computational capabilities.

For ‘e2refine model options’ the best previously generated model (either an initial model or a model from a previous refinement) was used as the refinement seed. Auto Mask 3D was used in all refinements, with the default parameters (threshold=0.8, radius=30, mask dilations=5, Gaussian dilations=5, NMax=30).

Under ‘e2project options’ the projecter used was ‘standard’, the orientation generation argument (orientgen) used was EMAN, with the parameters delta=5.0:inc_mirror=0:perturb=1 and model was assigned the C1 symmetry group.

For ‘e2simmx options,’ a shrink factor of 3 was used for early refinements, and reduced to 1 when refining higher quality models to obtain higher resolution. When shrinking was used, a shrink factor of 2 was applied to the two stage similarity matrix. The simmx comparator (simcmp) used was Fourier Ring Correlation (frc) with the parameters zeromask=1:snrweight=1. The simmx aligner (simalign) used was rotate_translate_flip, and the comparator used by the first stage aligner (simaligncmp) was ccc. The number of classes a particle could contribute was restricted to 1 (sep=1).

Several options were varied under ‘classaverage options,’ depending on the quality of the seed map and the particle set. Class iteration was set to 5 for initial model refinements, then reduced to 1 when improving resolution. The class averaging threshold was varied similar to the reference free class averaging step. The normalization processor for class averaging (classnormproc) was ‘normalize.edgemean.' The classaverager used was ‘mean.’ The comparator used to compute similarity scores (classcmp) was ‘frc’ with options zeromask=1:snrweight=1. For multiple iterations, the class average aligner (classalign) was rotate_translate_flip. The comparator used by the first stage aligner (classaligncmp) was ccc. For speed purposes, second stage alignments generally were not used unless the referenced class averages generated were poor, in which case the second stage aligner was set to ‘refine’ with the comparator ‘dot.’

Under ‘e23dmake’ options, the only parameter that was varied between refinements was the m3dkeep parameter, which is the fraction of 3d slices kept during modeling, and was varied from 0.3 to 0.85. The number of iterations was held constant at 2. The

reconstructor used was fourier, and the ‘pad’ parameter was the ‘good box size’ (defined in the EMAN2 supporting documentation) that was closest to 125% the size of the boxsize used to pick particles, generally 196. No post processing arguments were used within e2refine.py

2.4.9.4 Resolution, filtering, and final map generation.

Resolution was calculated using the FSC method using the 0.5 criterion using e2eotest.py. This was achieved by running the e2eotest.py command string with identical arguments used to generate the model (see 2.4.8.3), with two additional arguments: path=refineXX, where XX is the number of refinement resolution is being estimated for, and iter=X, which specifies the iteration within that refinement. Most maps refined to final resolution of approximately 25 angstroms

Molecular graphics of EM maps were generated in UCSF Chimera (Pettersen et al. 2004). For all structures, a low pass Gaussian filter was applied and the isosurface threshold was adjusted such to equivalent mass specific volumes, assuming a protein specific density of 1.35gm/cm^3.

3.0 CIPROFLOXACIN AND RELATED COMPOUNDS ARE INHIBITORS OF THE MCM2-7 COMPLEX

The contents of this chapter, with some additions and modifications, come from (Simon et al. 2013), per our retained copyright. Nicholas Simon conducted this work with the following exceptions: Matthew Bochman performed the initial experiments summarized in Figure 7. Sandlin Seguin purified the SV40 Large T antigen (TAg) and performed the human cell culture experiment under the direction of Jeffrey Brodsky. William Seibel assembled and provided the small molecule library and verified the purity of individual compounds. Anthony Schwacha supervised the conduct of the experiments of Nicholas Simon and Matthew Bochman.

3.1 SUMMARY

Most currently available small molecule inhibitors of DNA replication lack enzymatic specificity, resulting in deleterious side effects during use in cancer chemotherapy and limited experimental usefulness as mechanistic tools to study DNA replication. Toward development of targeted replication inhibitors, we have focused on Mcm2-7, a highly conserved helicase and key regulatory component of eukaryotic DNA replication. Unexpectedly we found that the fluoroquinolone antibiotic ciprofloxacin preferentially

inhibits Mcm2-7. Ciprofloxacin blocks the DNA helicase activity of Mcm2-7 at concentrations that have little effect on other tested helicases and prevents the proliferation of both yeast and human cells at concentrations similar to those that inhibit DNA unwinding. Moreover, a previously characterized mcm mutant (mcm4chaos3) exhibits increased ciprofloxacin resistance. To identify more potent Mcm2-7 inhibitors, we screened molecules that are structurally related to ciprofloxacin and identified several that compromise the Mcm2-7 helicase activity at lower concentrations. Our results indicate that ciprofloxacin targets Mcm2-7 in vitro, and support the feasibility of developing specific quinolone-based inhibitors of Mcm2-7 for therapeutic and experimental applications.

3.2 INTRODUCTION

As cancer cells demonstrate uncontrolled proliferation relative to most non-cancer cells, DNA replication has traditionally been an important target for cancer chemotherapy. Such therapeutics are frequently nonspecific and mutagenic, as they either chemically modify the DNA to block replication fork progression or trap deleterious topoisomerase II/DNA double strand break intermediates (Hurley 2002). Not surprisingly, these therapies have multiple toxic side effects (reviewed in (Zhou and Bartek 2004)). Newer topoisomerase inhibitors, which inhibit the catalytic activity of the enzyme rather than trapping the toxic protein-DNA intermediate, show therapeutic promise (Nitiss 2009), suggesting that compounds that specifically inhibit DNA replication enzymatic activity may be better suited as therapeutic agents. Moreover, enzyme inhibitors have had a long and important history in biochemical research, and their use has been an essential avenue

to obtain critical mechanistic insight (e.g., the F1 ATPase (Vignais and Lunardi 1985)). As eukaryotic DNA replication is a complex process that is poorly understood at a mechanistic level, the development of targeted small molecule inhibitors of specific replication factors would be of significant research utility.

One potential therapeutic target is the Mcm2-7 eukaryotic replicative helicase, a molecular motor that unwinds duplex DNA to generate ssDNA templates for replication. Unlike other replicative helicases, the toroidal Mcm2-7 complex is formed from six distinct and essential subunits, numbered Mcm2 through Mcm7 (Bochman and Schwacha 2009). Each subunit is an AAA^+ ATPase, and the unique heterohexameric composition of this helicase is conserved throughout eukaryotic evolution (reviewed in (Bochman and Schwacha 2009)). Consistent with its vital function during DNA replication, Mcm2-7 is a key target of regulation, as its loading is a carefully controlled and limiting feature of replication initiation, while its cell cycle-dependent activation is a limiting feature of elongation (Bell and Dutta 2002). The importance of its regulation is demonstrated by the observations that both specific mutations in Mcm2-7 (Kawabata et al. 2011) and over expression of its subunits (Honeycutt et al. 2006) cause cancer or contribute to tumorigenesis. Despite the potential of helicases as disease targets, few specific small molecule inhibitors of these enzymes have been identified (Crute et al. 2002; Ali et al. 2007; Wright et al. 2008; Tani et al. 2009). To date, one compound, heliquinomycin, has been identified that inhibits a non-physiological Mcm subcomplex (Mcm467) (Ishimi et al. 2009) and decreases the proliferation of cancer cells *in vitro* (Toyokawa et al. 2011), further suggesting that Mcm inhibitors may have therapeutic value.

Following examination of amino acid modifiers and small molecule ATPase inhibitors (Vignais and Lunardi 1985; Ali et al. 2007; Wright et al. 2008), we found that

the commercially available fluoroquinolone antibiotic ciprofloxacin preferentially inhibits the *in vitro* helicase activity of the *Saccharomyces cerevisiae* Mcm2-7 complex. Ciprofloxacin also appears to target Mcm2-7 in cell culture, as it blocks proliferation of both yeast and human cells at concentrations that inhibit the purified enzyme, and a previously studied cancer-causing mutation in Mcm4 confers ciprofloxacin resistance (Shima et al. 2007). Additional inhibitors of greater potency were identified among compounds structurally related to ciprofloxacin. Several of these agents exhibited increased selectivity toward Mcm2-7, while others had varying specificities against a range of unrelated helicases. These data suggest that (fluoro)quinolone-based compounds may provide a general scaffold for future development of helicase inhibitors with targeted specificity

3.3 FLUOROQUINOLONES BLOCK MCM HELICASE ACTIVITY

A variety of amino acid modifiers were initially tested. These chemical probes covalently modify carboxyl groups (carbodiimide derivatives EEDQ and DCCD), guanidyl groups (PG), amino groups (PP), phenol groups (Nbf), and thiol groups (NEM) and have been previously used to study the ATPase active sites in the F1-ATPase (reviewed in (Vignais and Lunardi 1985)). Although most of these amino acid modifiers inhibited all three helicases, DCCD had no effect (Figure 7A, treatment 3), and PG (Figure 7A, treatment 5) preferentially inhibited Mcm2-7 and Mcm467, suggesting the unique role of one or more accessible arginines in the Mcm complexes, possibly the external β-hairpin, a motif which is lacking in SV40 TAg and contains a conserved arginine (see Figure 2 in (Bochman and Schwacha 2009)).

The effects of several previously identified helicase inhibitors were also examined. The pyrimidinone-peptoid hybrid molecule MAL2-11b and the fluoroquinolones ofloxacin and ciprofloxacin have been previously reported to inhibit various TAg-mediated activities (Ali et al. 2007; Wright et al. 2008). MAL2-11b inhibited all three helicases to a similar extent at 1 mM (Figure 7A, treatment 8), but little or no inhibition of TAg helicase activity was observed with 1 mM ciprofloxacin or ofloxacin (Figure 7A, treatments 9 and 10; however inhibition was observed at higher concentrations, see below). In contrast, 1 mM ciprofloxacin inhibited the helicase activity of both Mcm2-7 and Mcm467 (Figure 7A, treatment 10).

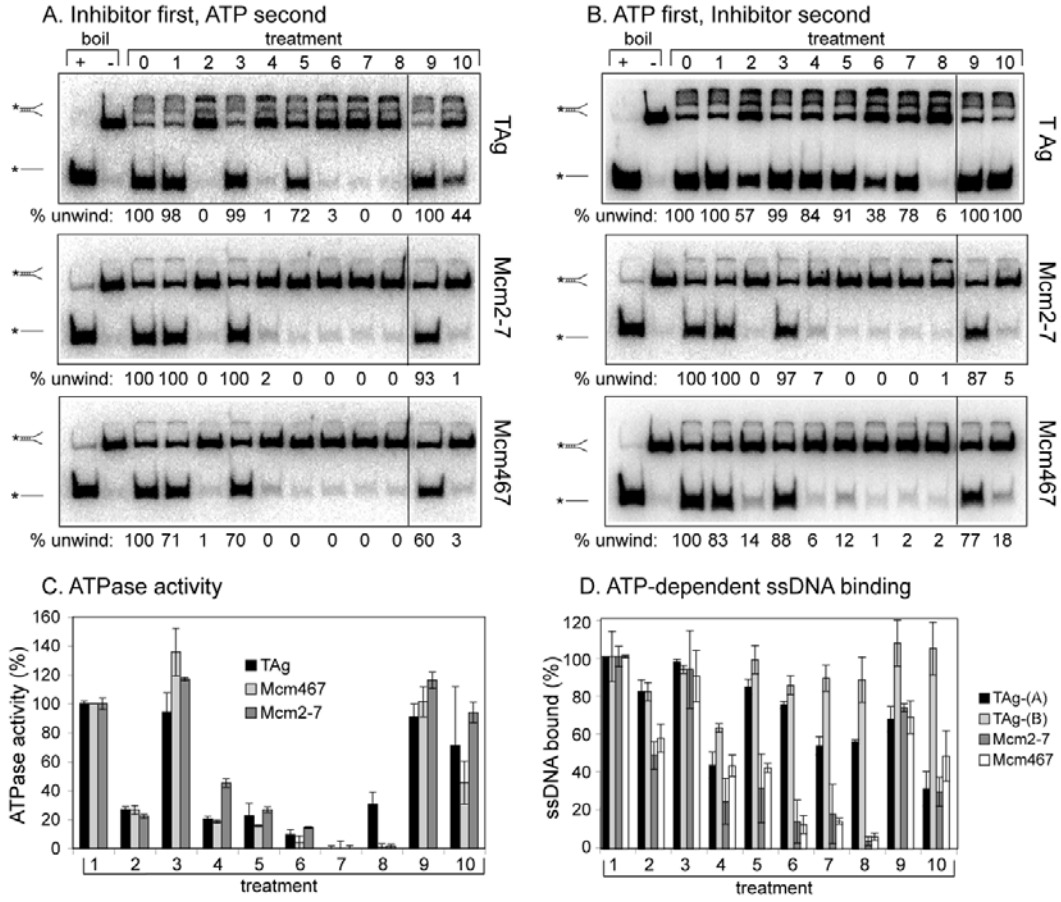

Figure 7: Identification of Mcm2-7 inhibitors

A) Inhibition of helicase activity. Helicase assays were conducted as described in the Materials and Methods chapter, The indicated proteins (TAg, Mcm2-7, Mcm467), at 100 nM concentration, were preincubated with the indicated small molecules (treatments 2-10) for 20 min at 37°C prior to addition of ATP and the DNA substrate. For each panel: +, boiled DNA fork; -, intact fork; 0, reconstituted helicase assay without small molecule; 1, standard assay containing 1% DMSO. Treatments 2-10 are reconstituted helicase assays additionally containing 1 mM of the following compounds: 2, EEDQ; 3, DCCD; 4, PP; 5, PG; 6, Nbf; 7, NEM; 8, MAL2-11b; 9, ofloxacin; and 10, ciprofloxacin. B) With SV-40 T-antigen, prior ATP preincubation protects from inhibition. This experiment was identical to A), except that the indicated helicase was preincubated with 5 mM ATP for 20 min at 37°C prior to addition of inhibitor and DNA substrate. The discontinuities in these gel images, denoted by a vertical line between treatments 8 and 9, indicates the location where an irrelevant treatment in the assay was electronically removed. C) The small molecules have

variable effects on ssDNA binding. Filter binding assays were conducted as described in Materials and Methods using 150 nM of the indicated helicase. For TAg-(A), Mcm2-7 and Mcm467, the indicated helicase was incubated with the small molecule prior to ATP addition as in A); for TAg-(B), TAg was preincubated with ATP prior to small molecule addition as in B). D) Small molecule inhibition of helicase ATPase activity. ATPase activity was assayed as described in Materials and Methods using 100 nM final helicase concentration. The treatment numbering in C) and D) are identical to those in A). The data in Figure 7C represent the average of ≥2 experiments, and the error bars represent the range or standard deviation, as appropriate. The data in Figure 7D represent the average of ≥3 experiments, and the error bars represent the standard deviations.

Because TAg subunits oligomerize only in the presence of ATP (Gai et al. 2004), and ATP preincubation likely causes a conformational change in Mcm2-7 (Bochman and Schwacha 2007; Bochman and Schwacha 2008), we also tested the effects of the potential inhibitors after the proteins were preincubated with ATP (Figure 7B). Although this treatment had essentially no effect on either Mcm complex, it completely or partially protected TAg from all modifiers except Nbf (Figure 7B, treatment 6) and MAL2-11b (Figure 7B, treatment 8), suggesting that at least one effect of the other inhibitors may be to block TAg oligomerization.

Because helicase activity depends upon ATP hydrolysis and ssDNA binding, the effects of the chemical modifiers and small molecules on both activities were examined. Using previously established steady-state ATP hydrolysis (Schwacha and Bell 2001) and ssDNA filter binding (Bochman and Schwacha 2007) assays, the effect of the same panel of small molecules on each of the three helicases was examined. With the exception of DCCD and ofloxacin, which failed to inhibit helicase activity, most of the remaining

treatments severely inhibited the ATPase activities of all three helicases (Figure 7C). These data suggest that the inhibition of DNA unwinding is mediated by compromised function of one or several ATPase active sites. However, these small molecules caused a less severe and variable decrease in TAg ssDNA binding regardless of the order of ATP addition. Conversely, Nbf, NEM, and MAL2-11b did inhibit Mcm2-7 and Mcm467 ssDNA binding (Figure 7D, treatments 6-8). Ciprofloxacin stands in sharp contrast: Even though it completely inhibited Mcm helicase activity, it had only modest effects on ATP hydrolysis and ssDNA binding of the three helicases (Figure 7C and D, treatment 10). Collectively, these results suggest that ciprofloxacin inhibits a step or steps specifically required for DNA unwinding, possibly through selective inhibition of the Mcm regulatory subunits.

3.4 CIPROFLOXACIN SHOWS SELECTIVITY FOR MCM2-7

We quantified the IC_{50} values of ofloxacin and ciprofloxacin on Mcm2-7, Mcm467, and TAg helicase activity. We found that very high concentrations of ofloxacin inhibited both Mcm2-7 and Mcm467 with similar IC_{50}s (Figure 8A): 4.17 mM (95% CI = 3.31-5.26 mM) and 5.29 mM (95% CI = 4.92-5.69 mM), respectively while the apparent IC_{50} of ofloxacin for TAg was much higher (>20 mM; Figure 8A). In contrast naladixic acid, the parent quinolone compound for both ciprofloxacin and ofloxacin, had essentially no effect on the activities of the three helicases at any concentration tested (data not shown).

Interestingly, ciprofloxacin inhibited Mcm2-7 at an approximately 3-fold lower concentration than Mcm467 (Mcm2-7 IC_{50}=632 µM, 95% CI=552-723 µM; Mcm467 IC_{50}=1.89 mM, 95% CI=1.24-2.87 mM, respectively; Figure 8B) and at an approximately

6-fold lower concentration than TAg (IC_{50}=4 mM, 95% CI=2.91-5.53 mM). This selectivity of ciprofloxacin for Mcm2-7 relative to TAg supports the proposal that Mcm-specific inhibitors may be found. In addition, the selectivity of ciprofloxacin for Mcm2-7 relative to Mcm467 supports the proposal that active site-specific inhibitors of the Mcm complex can be identified.

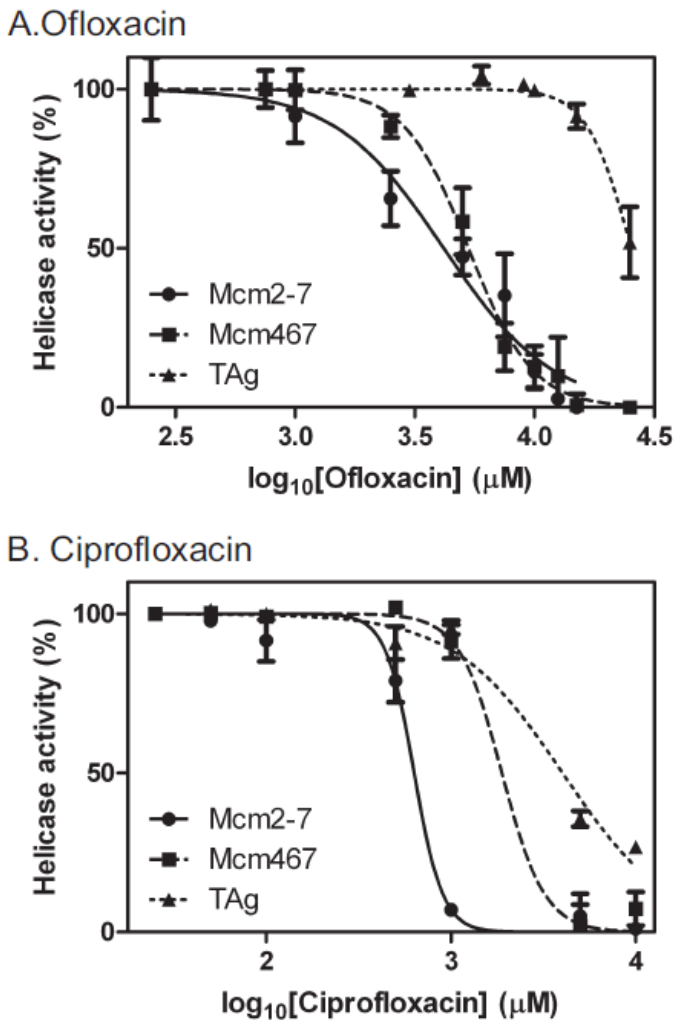

Figure 8: Two fluoroquinolones show preference for the Mcm helicases

The inhibitor effects of either ofloxacin A) or ciprofloxacin B) were tested on the DNA unwinding activity; the indicated helicases were all used at a final concentration of 100 nM following preincubation with inhibitor. The results were quantified and converted to % activity relative to the respective activity in the absence of inhibitor. All reactions contained 1% solvent (DMSO).

3.5 A LIBRARY SCREEN OF SMALL MOLECULE INHIBITORS

We reasoned that other (fluoro)quinolone derivatives might show enhanced Mcm2-7 specificity at potentially lower inhibitor concentrations. As the fluoroquinolones are used as antibiotics (reviewed in (Collin et al. 2011)), prior drug discovery efforts have resulted in the synthesis of chemically diverse libraries modeled on key elements found in the basic fluoroquinolone scaffold. Therefore, we investigated a 144-compound chemical library that contained either (fluoro)quinolone derivatives or molecules with various substructures found in ciprofloxacin and other marketed quinolones.

This library of 144 compounds was initially screened for inhibition of Mcm2-7, Mcm467, and TAg helicase activity at a final concentration of 1 mM (see Appendix for chemical structures and a complete list of results). Of the compounds tested, 27 reproducibly inhibited at least one of the three helicases to ≥90%. Both (fluoro)quinolone and triaminotriazine-like inhibitors were identified. Although a wide range of results were obtained, two general conclusions emerged from the data 1) Few molecules exhibited robust inhibition of TAg, and those that did (*e.g.*, 924384, 125248, and 486369) also inhibited Mcm2-7 and Mcm467; and 2) many molecules demonstrated at least partial inhibition of Mcm2-7 with little or no inhibition of TAg. Interestingly, although some of the inhibitors appeared to inhibit both Mcm2-7 and Mcm467, the relative strength of this inhibition varied. One agent appeared to act like ciprofloxacin and preferentially inhibited Mcm2-7 (314850), while others appear to preferentially inhibit Mcm467 (*e.g.*, 502432 and 502423).

3.6 SELECT LIBRARY COMPOUNDS DISPLAY GREATER POTENCY AND SELECTIVITY THAN CIPROFLOXACIN

In addition to ciprofloxacin, seven representative compounds from among those described above were chosen for additional study based either upon potency, selectivity, reproducibility, dose-dependent effect, and/or availability. Figure 9 summarizes their effects on the DNA unwinding activity of TAg, Mcm2-7, and Mcm467, again at a final concentration of 1 mM. To provide a quantitative measure of inhibitor affinity and selectivity, fresh samples of known purity (>90%) were obtained for each of the seven inhibitors, and the IC50 values for DNA unwinding were determined for all three helicases. In most cases, these compounds were either more potent or more selective than ciprofloxacin (Figure 10 and Table 2). Based upon their differential inhibition of the three helicases, the inhibitors were classified into one of two groups:

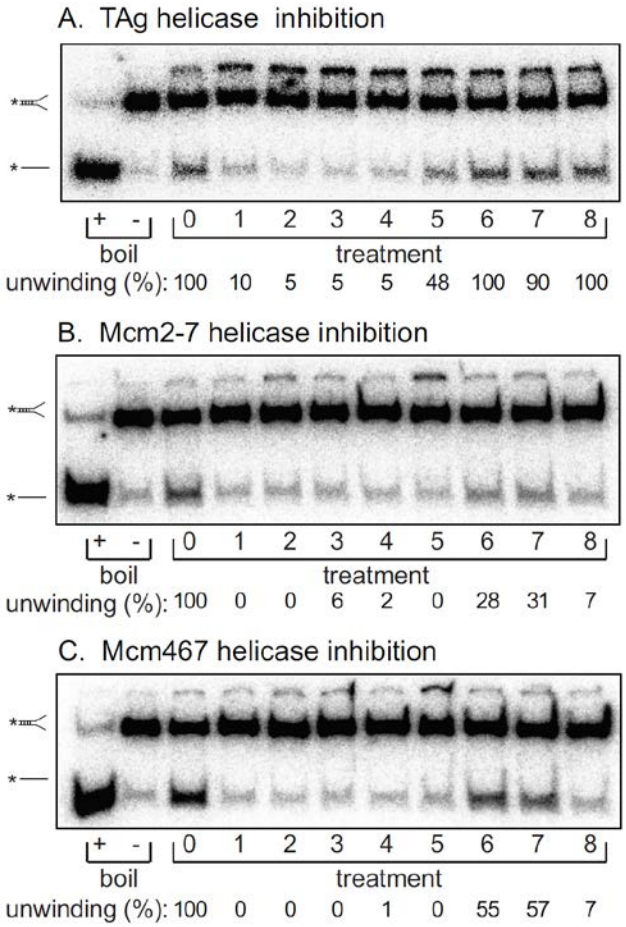

Figure 9: Effects of select (fluoro)quinolone inhibitors on A) TAg helicase, B) Mcm2-7, and C) Mcm467 activity.

For each panel: +, boiled DNA fork; -, intact fork; 0, solvent control; 1, compound 125248; 2, 924384; 3, MAL2-11b; 4, 268973; 5, 388612; 6, 314850; 7, 271327; and 8, ciprofloxacin. Inhibitors were added to a final concentration of 1 mM, as in Figure 7. The values below the gels indicate the percent of DNA unwinding by the indicated helicase normalized to the solvent control (treatment 0).

The first was General inhibitors. These inhibitors that had approximately equal effects on all three helicases include MAL2-11b (Figure 9) and compounds 125248, 924384, 268973, and 388612 (Table 2). Interestingly, unlike any of the (fluoro)quinolones characterized, the triazole 924384 and the structurally related compound 388612 were more effective at inhibiting TAg than either Mcm complex (Table 2). The IC50 values for each of these compounds are similar to one another and ranged from ~50-400 μM.

The second was Mcm-selective inhibitors. Two inhibitors (271327 and 314850) fall into this category. The fluoroquinolone 271327 inhibited both Mcm complexes with an IC50 of ~300-450 μM but had a negligible effect on TAg within the concentration range tested (Figure 10). Although the limited solubility of 271327 prevented us from testing higher concentrations, we can conclude that the IC50 against TAg is at least an order of magnitude greater than that of the Mcm complexes. In contrast, 314850 preferentially inhibited Mcm2-7 relative to Mcm467 but had little effect on TAg.

Table 2 Structures and IC_{50} values of selected inhibitors

			IC_{50} μM*				
Inhibitor	Structure	Source‡ (purity)	Yeast	Human	Mcm2-7	Mcm467	T-antigen
Ciprofloxacin	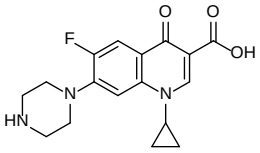	Fluka (>98%, HPLC)	590 (520-670)	240 (160-350)	632 (553-723)	1890 (1240-2870)	4010 (2910-5530)
MAL2-11b	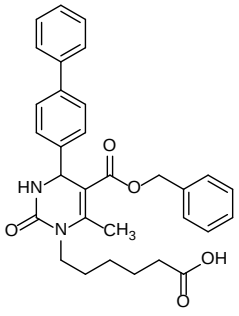	J. Brodsky (>99%, evaporative light scattering and UV spectroscopy (Wright et al. 2008))	ND	ND	96 (47-193)	112 (56-226)	192 (144-256)

125248 (Bouzard et al. 1992)	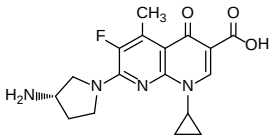	DDC-UC (>90%, HPLC/MS)	460‡	14 (6-30)	72 (52-100)	130 (113 - 151)	190 (180-201)
924384 (Kumar et al. 2008)	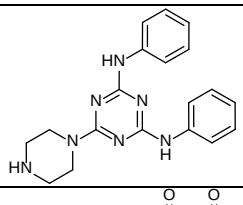	ChemBridge 7473736 (>90%, NMR)	93 (67-130)	10‡	115 (105-127)	246 (226-268)	70 (56-87)
268973	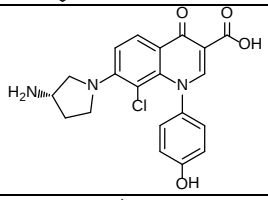	DDC-UC (>90%, HPLC/MS)	160 (37-730)	ND	188 (154-229)	272 (234-316)	476 (364-622)
388612	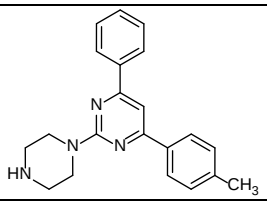	DDC-UC (>90%, HPLC/MS)	<10 nM‡	ND	396 (284-551)	345 (304-391)	126 (84-188)
271327 (Domagala et al. 1991)	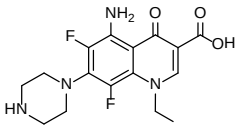	ChemBridge 5281925 (>90%, NMR)	700‡	210 (67-650)	361 (294-444)	460 (394-538)	> 1000
314850	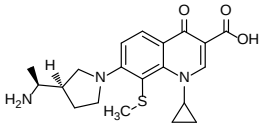	DDC-UC (>90%, HPLC/MS, NMR)	520 (400-690)	340 (150-740)	261 (219-312)	707 (579-865)	> 1000

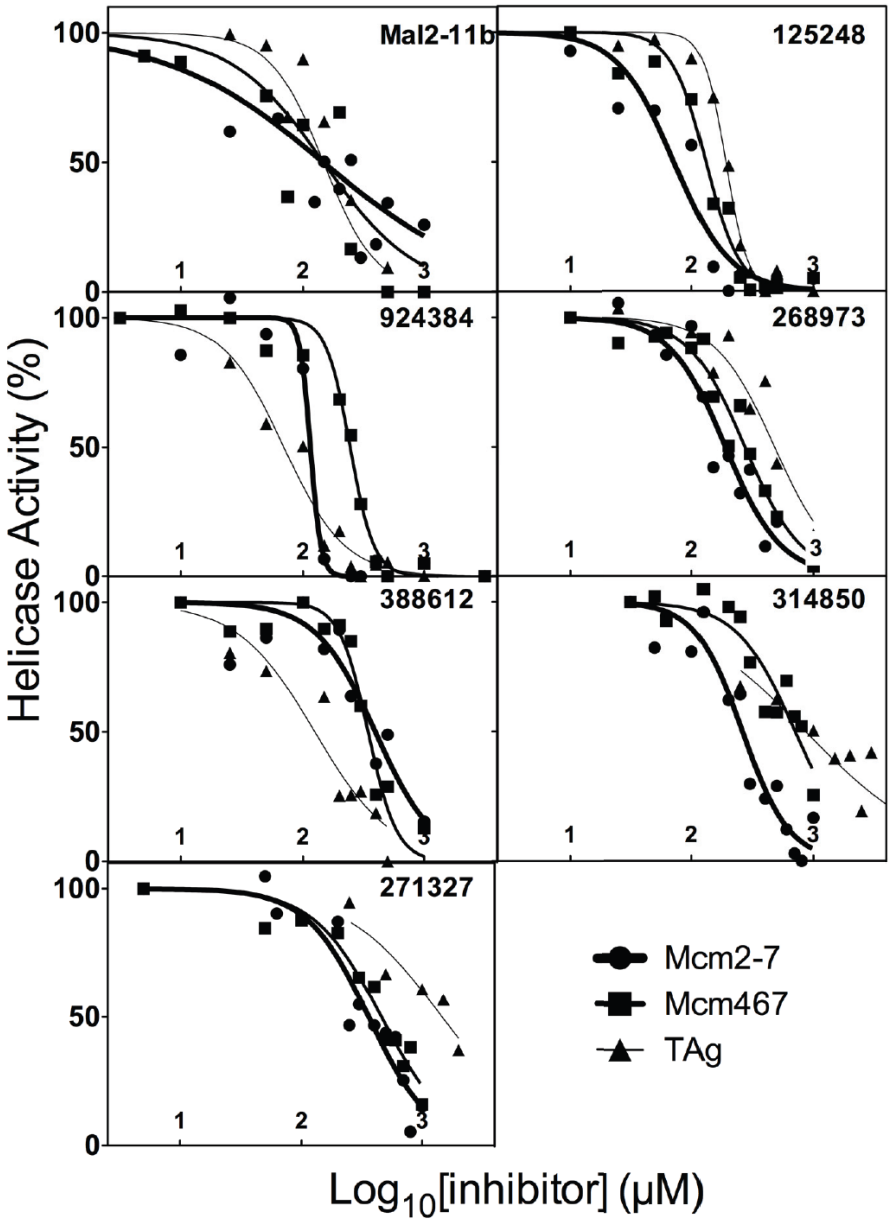

Figure 10: The identified inhibitors exhibit diverse specificities against different helicases

3.7 MECHANISM OF INHIBITION BY CIPROFLOXACIN RELATED COMPOUNDS

As noted above, DNA unwinding is the culmination of a variety of simpler biochemical activities. Thus, the seven representative inhibitors and ciprofloxacin may function by physically interacting with the helicase, the DNA substrate, or the ATP. To understand how all eight inhibitors block helicase activity, their effects on steady-state ATP hydrolysis were measured (Figure 11A). Relative to MAL2-11b, which completely inhibits ATP hydrolysis of Mcm2-7, Mcm467, and TAg (Figure 7C (treatment 7) and 11A (treatment 3)), both the general and Mcm-selective inhibitors demonstrated only a modest inhibition of ATP hydrolysis (*e.g.*, 268973; Figure 11A, treatment 4), while several demonstrated essentially no inhibition of ATP hydrolysis (*e.g.*, 314850 and 271327; Figure 11A, treatment 6 and 7).

These results suggest one of three possible scenarios: First, the inhibitors (with the possible exception of MAL2-11b) might not target the ATPase active sites. Second, the inhibitors may deregulate or uncouple the activity of the enzyme rather than block ATP hydrolysis. Third, at least in the case of the Mcm2-7 complex, the inhibitors could preferentially target the ATPase active sites but are selective for the low-turnover regulatory sites. Although the second and third possibilities are difficult to distinguish, the first explanation can be tested. While we cannot rigorously test for competitive inhibition using our helicase endpoint assay, we can test if increased ATP concentration overcomes the inhibitory effects of these compounds (Figure 11B). Although doubling the ATP concentration in the absence of inhibitor caused a slight increase in helicase activity (1.5 to 2-fold, Figure 11B, treatment 0), in most cases, doubling the ATP concentration in the

presence of the inhibitors caused a much larger increase in activity (3 to 20-fold). These results suggest that the inhibitors disrupt ATPase active sites in the Mcm2-7 complex in some manner. In contrast the inhibitory effects of 924384, MAL2-11b, and 268973 could not be rescued by an increase in ATP concentration (Figure 11B treatments 2-4), suggesting that these inhibitors operate independently of the ATPase active sites.

Because these compounds are also planar double ring molecules, they could conceivably inhibit helicase activity via DNA intercalation. To examine this model, we tested our inhibitors in a standard topoisomerase assay (Jones-Held 1992). The rationale of this assay is that intercalating compounds will introduce supercoils into a fully relaxed plasmid. Topoisomerase I (Topo I) will remove these introduced supercoils, but after quenching and gel electrophoresis the intercalator will diffuse away and produce a detectable compensatory supercoiling increase.

Following plasmid relaxation, each inhibitor was added to 1 mM final concentration in the topoisomerase assay (Figure 11C, treatments 1-8). The general inhibitors 125248 (treatment 1), 924384 (treatment 2), 268973 (treatment 4) and 388612 (treatment 5) cause extensive DNA intercalation, while in contrast, MAL2-11b (treatment 3) and the more Mcm-selective inhibitors (314850, 271327, and ciprofloxacin, treatments 6-8) demonstrated little or no intercalation (Figure 11C). However, lack of apparent intercalation could also be caused by Topo I inhibition. To test this possibility, the assay was repeated under conditions in which Topo I and each inhibitor were added to the reaction at the same time. Under these conditions, Topo I inhibition will only yield supercoiled plasmids (Figure 11D). Under this criterion and comparing the results to Figure 11C, only MAL2-11b (Figure 11D, treatment 3) is a Topo I inhibitor. Although the general inhibitors can intercalate into dsDNA at 1 mM concentration (Figure 11C), *in vitro*

helicase inhibition occurs at much lower inhibitor concentrations. Repeating the intercalation assay at more modest inhibitor concentrations (2-3 fold over calculated IC_{50} for helicase inhibition) only 125248 and 268973 continued to demonstrate significant DNA intercalation (Figure 11E, treatments 1 and 4). Thus, most of the tested inhibitors, including ciprofloxacin, do not appear to function through intercalation, suggesting that they more directly affect the helicase activity.

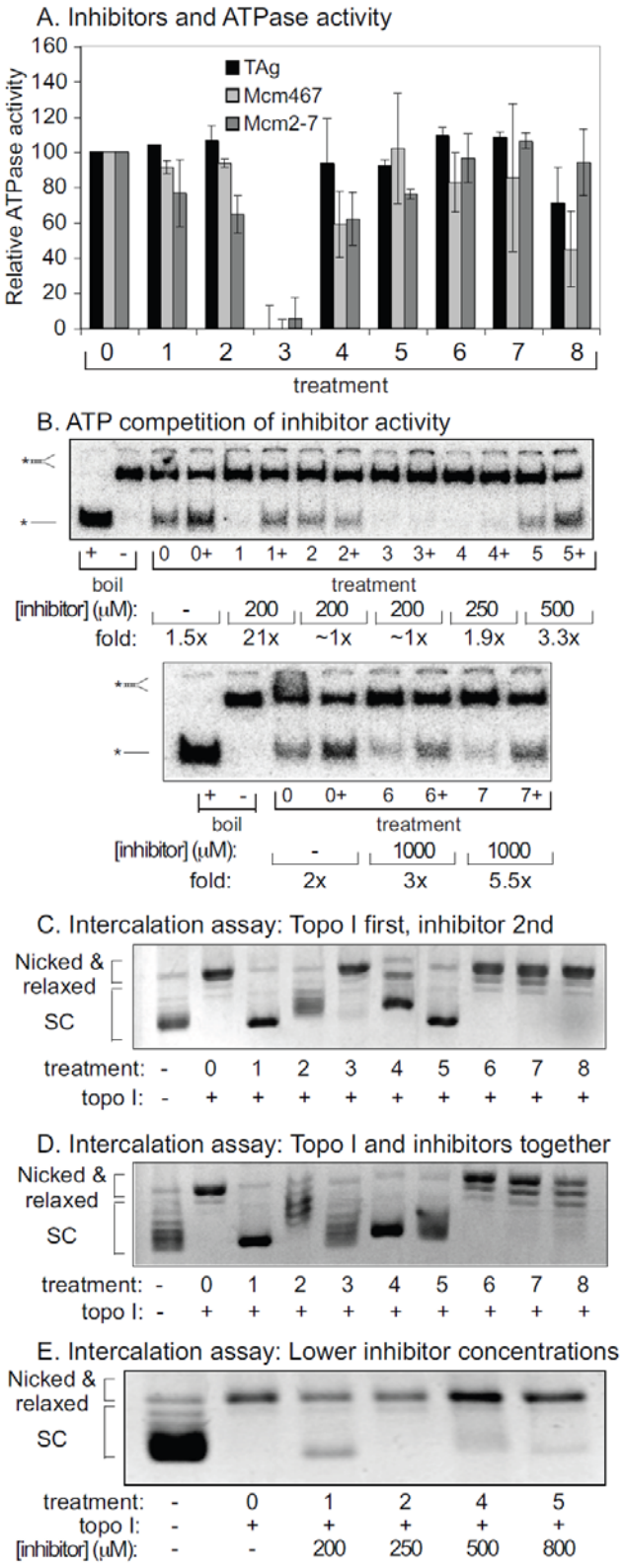
A. Inhibitors and ATPase activity
Relative ATPase activity
160
140
120
100
80
60
40
20
0
TAg
Mcm467
Mcm2-7
0 1 2 3 4 5 6 7 8
treatment
B. ATP competition of inhibitor activity
+ - 0 0+ 1 1+ 2 2+ 3 3+ 4 4+ 5 5+
boil
treatment
[inhibitor] (μM): - 200 200 200 250 500
fold: 1.5x 21x ~1x ~1x 1.9x 3.3x
+ - 0 0+ 6 6+ 7 7+
boil
treatment
[inhibitor] (μM): - 1000 1000
fold: 2x 3x 5.5x
C. Intercalation assay: Topo I first, inhibitor 2nd
Nicked & relaxed
SC
treatment: - 0 1 2 3 4 5 6 7 8
topo I: - + + + + + + + + +
D. Intercalation assay: Topo I and inhibitors together
Nicked & relaxed
SC
treatment: - 0 1 2 3 4 5 6 7 8
topo I: - + + + + + + + + +
E. Intercalation assay: Lower inhibitor concentrations
Nicked & relaxed
SC
treatment: - 0 1 2 4 5
topo I: - + + + + +
[inhibitor] (μM): - - 200 250 500 800

Figure 11: Mode of action of the various small molecule inhibitors

Treatment order for each panel: 0, solvent control; 1, compound 125248; 2, 924384; 3, MAL2-11b; 4, 268973; 5, 388612; 6, 314850; 7, 271327; and 8, ciprofloxacin. A) Effects of each inhibitor on steady state ATP turnover by Mcm2-7, Mcm467, and TAg. This experiment was identical to that shown in Figure 7C with the indicated helicase used at 100 nM concentration, but 1 mM of the indicated inhibitor was added prior to ATP addition. Bar graphs show the levels of ATP hydrolysis observed after 30 min of incubation as a % of the ATP hydrolysis observed in the absence of inhibitor (treatment 0). B) Effect of increased ATP concentration with indicated inhibitor on DNA unwinding activity of Mcm2-7. The standard helicase reaction was supplemented with the indicated inhibitor concentration (numbered 1-8 as in A) in the presence (+) or absence of an additional 5 mM ATP. ATP and the indicated inhibitor were added together to Mcm2-7 without preincubation. "Fold" refers to the ratio of DNA unwinding between the reactions containing 10 mM ATP and containing 5 mM ATP. C) Ability of inhibitors to intercalate into DNA. In the intercalation assay (Materials and Methods), Topo I (4 units) was used to relax 50 ng of monomeric pUC19 (treatment 0; compare supercoiled DNA (left) with relaxed DNA (right)). After 1 h of Topo I treatment, 1mM of the indicated inhibitor was added and samples were incubated for an additional 1 h D) Topo I activity inhibition assay. This experiment was identical to C), except that Topo I and the indicated inhibitor were added at the same time. Topo I inhibition is indicated if addition of both inhibitor and topoisomerase together generates supercoiled DNA, while experiments shown in C) generate relaxed plasmid. E) An intercalation assay performed with the indicated inhibitors at lower concentrations. These assays were similar to C) (Topo I added first, and the inhibitor added second), except the indicated concentration of inhibitor was used.

3.8 CIPROFLOXACIN IS NOT A GENERAL HELICASE INHIBITOR

An ideal Mcm2-7 inhibitor would specifically target this helicase both biochemically and in living cells. To test this hypothesis, these properties were assayed in the following experiments.

To further define inhibitor selectivity, we examined their in vitro effects on representative helicases at 1mM concentration (Figure 12). Inhibitors 125248, 924384, and 268973 (treatments 1-3) were the least specific, causing nearly complete inhibition of DnaB and T4 gp41. Interestingly, only one additional inhibitor (314850, treatment 6) effectively inhibited the SsoMcm complex. This discrepancy may be due to the high assay temperature (65°C) required to assess SsoMcm helicase activity(McGeoch et al. 2005). Inhibitor 271327 (treatment 7) caused substantially less inhibition among the helicases tested than either 125248 or 924384. In contrast, none of the tested helicases were substantially inhibited by ciprofloxacin (Figure 12, treatment 8). Combined with the IC50 data summarized in Table 1, Mcm2-7 is the only helicase tested that is preferentially inhibited by ciprofloxacin.

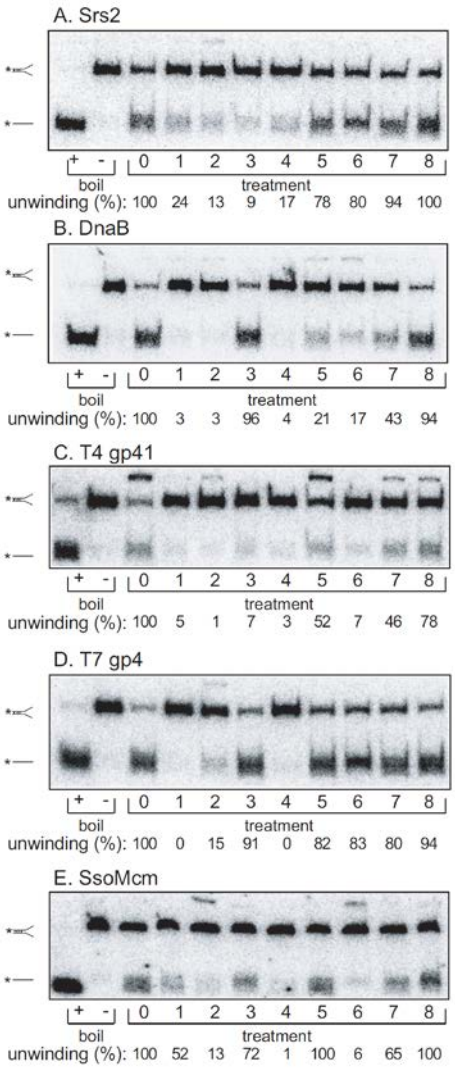

Figure 12: Ciprofloxacin poorly inhibits hexameric helicases unrelated to the Mcms.

All inhibitors were used at 1 mM final concentration. Lane order for each panel: +, boiled DNA fork; -, intact fork; 0, solvent control; 1, compound 125248; 2, 924384; 3, MAL2-11b; 4, 268973; 5, 388612; 6, 314850; 7, 271327; and 8, ciprofloxacin. The helicase tested is listed at the top of each gel, and the percent of helicase activity remaining in the presence of inhibitor is listed below each gel. The reaction conditions used for each helicase are similar to that used for Mcm2-7 and described in the Experimental Procedures. The values below the gels indicate the percent of DNA unwound by the indicated helicase normalized to the solvent control (treatment 0).

3.9 CIPROFLOXACIN AND LIBRARY COMPOUNDS INHIBIT YEAST AND HUMAN CELL GROWTH

To examine the general cellular toxicity of these inhibitors, growth inhibition of micro-cultures by serial dilution of inhibitors was tested in a 96-well format in yeast (Simon et al. 2000). Wild type yeast is resistant to ciprofloxacin (Figure 13A). However, resistance to many compounds in yeast reflects an inability to accumulate sufficient concentrations of such compounds due to the prevalence of multidrug transporters (reviewed in (Balzi and Goffeau 1995)). To circumvent this potential problem, we used a yeast mutant *(Δerg6)* (Welihinda et al. 1994) previously shown to non-specifically decrease drug resistance. As anticipated, this strain had demonstrable growth sensitivity to both ofloxacin and ciprofloxacin (Figure 13A).

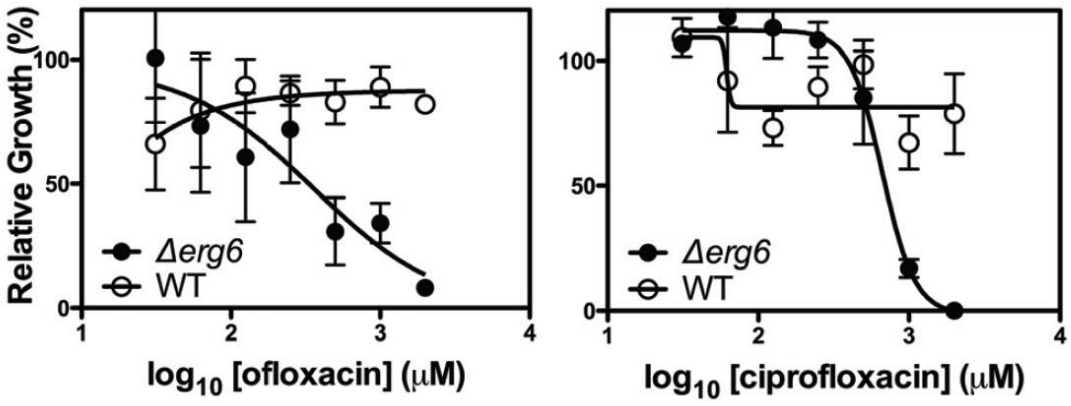

Figure 13: Fluoroquinolone sensitivity: Wild Type VS Δ*erg6*

Δ*erg6* cells show demonstrable sensitivity to fluoroquinolones.

Using the Δ*erg6* strain, the remaining compounds were tested for growth inhibition over a range of concentrations (Figure 14, Table 2). Several compounds inhibited growth at

lower concentrations than they inhibited *in vitro* helicase activity (388612, 268973, and 924284), suggesting that proteins other than Mcm2-7 are more sensitive to inhibition. These data are consistent with their poor helicase selectivity as demonstrated above. In contrast, several compounds were less efficient at inhibiting yeast growth than helicase activity (125248 and 314850). However, two inhibitors (ciprofloxacin and to a lesser extent 271327) have IC_{50} curves that closely match the IC_{50} curves for Mcm2-7 helicase activity (Figure 17, Table 2), consistent with the possibility that the primary cellular target is Mcm2-7.

Inhibitor cytotoxicity was next examined in a non-tumor human cell line (RPE-TERT, Figure 14). In general, these cells were demonstrably more sensitive to the tested inhibitors than yeast. RPE-TERT cells were ~10-fold more sensitive to 125248 and 924384 (IC_{50}s of about 10 μM) than 271327 and 314850 (IC_{50}s ~500-700 μM). The extreme sensitivity of human cells to both 125248 and 924384 suggests that Mcm2-7 is not a major cellular target. In contrast ciprofloxacin kills human cells and inhibits yeast growth at roughly similar concentrations (i.e., human cells are only ~ 2.5 fold more sensitive than yeast).

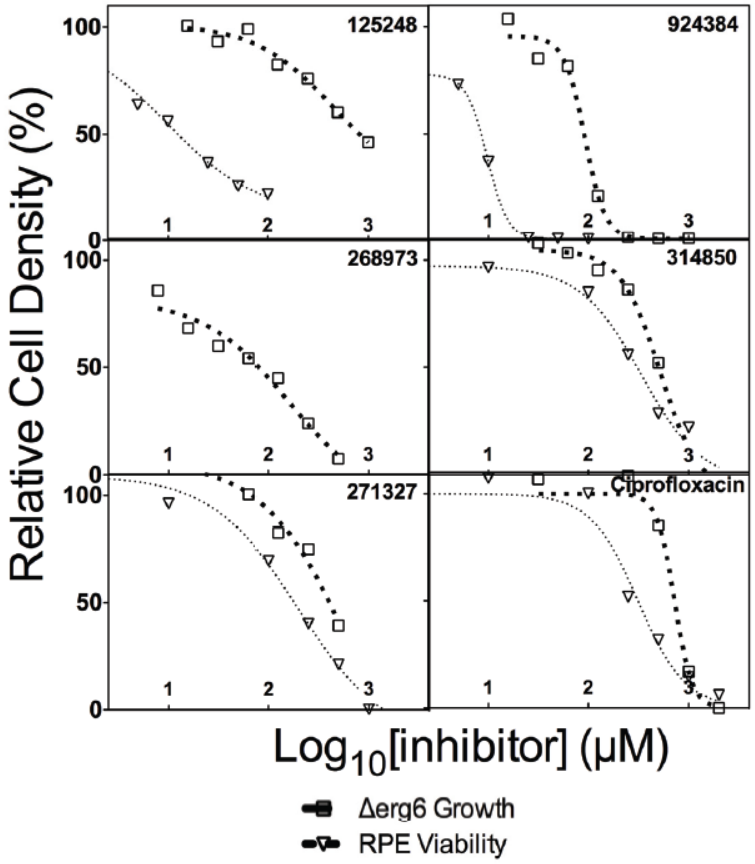

Figure 14: Sensitivity of yeast and human cells to inhibitors

Representative assays are shown, and were performed as described in Chapter 2.4.8. The results are normalized to growth in the presence of 1% DMSO.

3.10 IDENTIFICATION OF AN MCM MUTANT THAT CONFERS CIPROFLOXACIN RESISTANCE

While the above data were consistent with Mcm inhibition in cells, the same could be said for any replication protein. To address if the Mcm complex was the cellular target, we first tested to see if overexpression of the Mcm complex was sufficient to confer ciprofloxacin resistance. Δ*erg6* cells were transformed with three integrating plasmids bearing the six

MCM genes under bidirectional GAL inducible promoters. Although all six MCMs were successfully overexpressed, no difference could be seen between in the IC_{50}s of cells overexpressing the construct and regular Δ*erg6* cells (Figure 15). Similar results were obtained expressing the Mcms individually and in pairs.

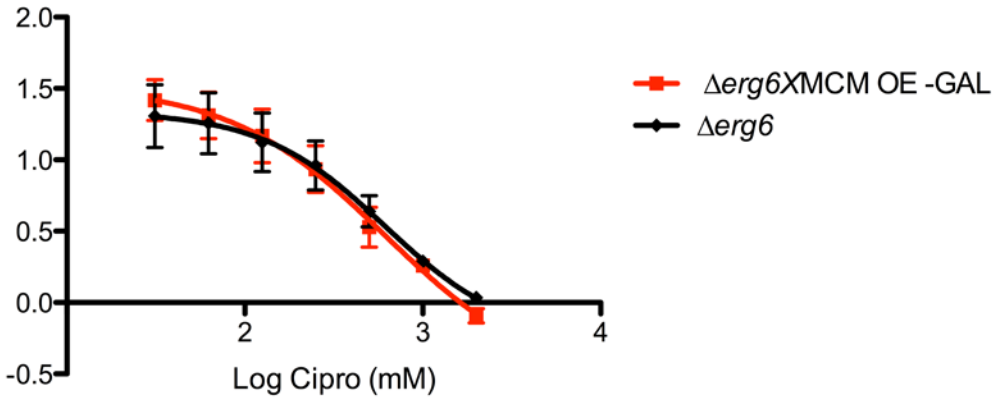

Figure 15: MCM overexpression does not confer ciprofloxacin resistance

All 6 Mcm subunits were overexpressed in the Δ*erg6* background. The IC_{50} levels were indistinguishable from the parent strain.

Given the difficulties of creating Δ*erg6* double mutants, a variety of Mcm and DNA replication mutants were initially screened against W303 yeast utilizing a growth conditions that render the yeast permeable to small molecules. After verifying that we have similar sensitivity to ciprofloxacin under these conditions, we observed that while the viable ATPase active site mutants were indistinguishable from wild type, the checkpoint mutants and Mcm4-Chaos3 showed slight resistance (Figure 16).

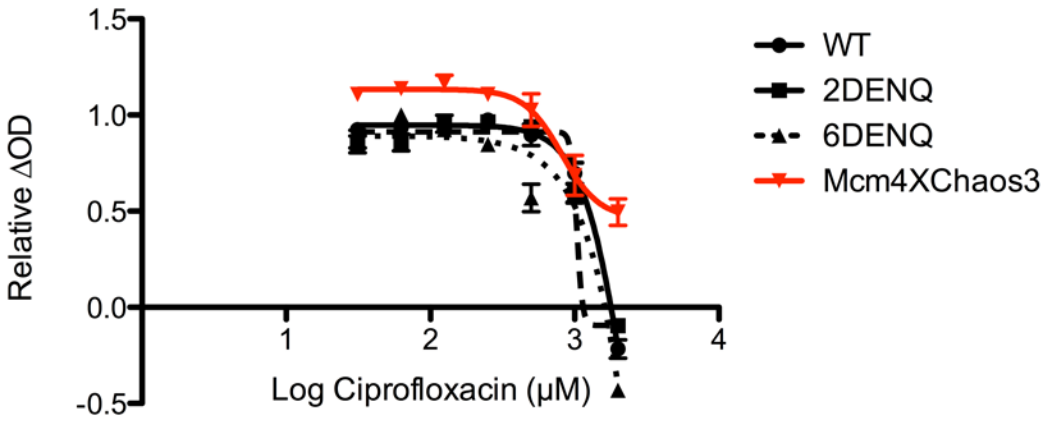

Figure 16: MCM mutants tested in permeabilized yeast

To rule out variability from the assay, we constructed a double mutant Δ*erg6*X*mcm4chaos3* strain, and found that this slight resistance to Ciprofloxacin was retained. (Figure 17) (Δ*erg6* IC_{50}: 590 µM (95% CI=520-670 µM) vs. Δ*erg6 mcm4chaos3*:1300 µM (95% CI=1200-1400 µM). Combined with the data described above, we conclude that Mcm2-7 is a ciprofloxacin target.

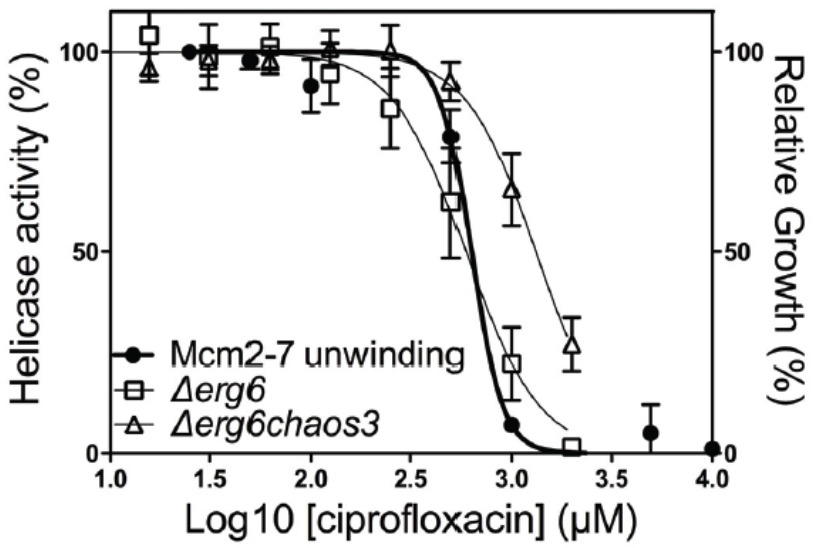

Figure 17: The *Mcm4chaos3* mutation confers ciprofloxacin resistance.

In yeast, cellular growth and in vitro helicase activity is impaired with nearly identical concentration dependence. Mcm4chaos3 mutants demonstrate increased resistance to ciprofloxacin. In all graphs, the data represent the average of ≥3 experiments, and the error bars represent the standard deviations.

3.11 DISCUSSION

We provide evidence that ciprofloxacin (and to a lesser extent compound 271327) inhibits the activity of the budding yeast Mcm2-7 helicase both biochemically and in cell culture. Although our experiments largely focus on yeast, we also demonstrated that ciprofloxacin inhibits the viability of human cells at roughly similar concentrations. As fluoroquinolones have been extensively used in human medicine and their pharmacological properties are established (Collin et al. 2011), the fluoroquinolone scaffold might well serve as a useful platform in the development of Mcm2-7 inhibitors with enhanced therapeutic potential. Although inhibition of Mcm2-7 occurs at ciprofloxacin

concentrations higher than its normal therapeutic range (also see below), our results suggest that some of the side effects seen with this and other fluoroquinolones may be due to inhibition of DNA replication.

3.11.1 Relationship to prior studies

Fluoroquinolones serve as potent antibiotics due to their strong inhibition of the prokaryotic DNA gyrase. Although eukaryotes are relatively resistant to ciprofloxacin at normal therapeutic levels, cytotoxicity is noted at high drug concentrations (reviewed in (Collin et al. 2011)). The eukaryotic topoisomerase II enzyme is a target for fluoroquinolones such as ciprofloxacin, as the drug inhibits topoisomerase II *in vitro* (Barrett et al. 1989), and mutants in topoisomerase II have been isolated with increased *in vitro* fluoroquinolone resistance (Elsea et al. 1995). Moreover, cells exposed to cytotoxic levels of fluoroquinolones arrest in G2 and demonstrate chromosomal breaks consistent with the known role of topoisomerase II in mitosis (Smart et al. 2008), However it should be noted that these are also relatively common phenotypes of various known DNA replication mutants (e.g (Hennessy et al. 1990)).

Both our *in vitro* and cell-based studies strongly support Mcm2-7 as a new eukaryotic target for fluoroquinolones. Our finding that the Mcm *mcm4chaos3* mutant has significantly increased ciprofloxacin resistance provides evidence that at least part of fluoroquinolone cytotoxicity is likely due to defects in DNA replication.

3.11.2 Inhibitory effects of amino acid modifiers

Although chemically reactive amino acid modifying agents are too unstable, non-specific, and irreversible to assist in studies of Mcm2-7 *in vivo*, there is considerable precedence for using modifying reagents *in vitro* to determine a mode of action in complex systems (Vignais and Lunardi 1985). For example, DNA replication requires a large number of nucleotide hydrolases (*e.g.*, ORC, Cdc6, Mcm2-7, RFC, primase, and DNA polymerases (Bell and Dutta 2002)), and knowledge of the inhibitory spectrum of modifiers on individual replication factors will aid future studies that examine functional interactions between these proteins. Because preincubation of TAg with ATP relieved much of the inhibitory effects of these modifiers (Figure 7B), they most likely affect ATP binding and oligomerization of TAg, which is ATP-dependent. One interesting difference between inhibition of the Mcms and TAg is with the guanidyl modifier phenylglyoxal (PG), which inhibits both Mcm2-7 and Mcm467 without affecting TAg. This property could make PG an experimentally useful reagent *in vitro* if Mcm2-7 activity needs to be specifically ablated.

3.11.3 Mode of (fluoro)quinolone inhibition

Our results suggest that most of the studied inhibitors likely interfere with the ATPase active sites of the helicases. Although these molecules only have a modest effect on bulk ATP hydrolysis of Mcm2-7 (Figure 11A), helicase inhibition is largely suppressed by increased ATP concentration (Figure 11B). The relatively high observed IC_{50}

concentrations are consistent with this possibility, as the ATP $Km_{0.5}$ for helicase activity by the yeast Mcm2-7 is ~2 mM (Bochman and Schwacha 2008). However, if (fluoro)quinolones act as inhibitors of ATPase active sites, how can the relatively minor inhibition of ATP hydrolysis be explained?

For Mcm2-7, bulk ATP hydrolysis correlates poorly with DNA unwinding. There are mutations that cause substantial reductions in ATP hydrolysis but have only minor effects on *in vitro* DNA unwinding (*e.g.*, Mcm3KA (Bochman and Schwacha 2008)), while other mutations retain robust steady state ATP hydrolysis but reduce *in vitro* DNA binding or unwinding (*e.g.*, Mcm6DENQ (Bochman and Schwacha 2008; Bochman and Schwacha 2010)). Only two of the Mcm2-7 ATPase active sites are responsible for most of the observed steady state ATP hydrolysis (*i.e.*, the Mcm3/7 and 7/4 active sites (Davey et al. 2003; Bochman et al. 2008)).

The remaining active sites, though clearly essential, hydrolyze ATP poorly. These data suggest that occupancy and turnover at these sites correspond predominately to a regulatory role rather than a direct contribution to helicase function. If the (fluoro)quinolone inhibitors preferentially target the regulatory rather than catalytic sites, only a modest change in ATP hydrolysis might be observed. Alternatively, the inhibitors may function to poison the helicase. By binding to a single active site, the inhibitor might uncouple ATP hydrolysis from DNA unwinding by altering the ability of adjacent active sites to communicate.

This model also explains the effect of these inhibitors on TAg, a homohexameric helicase that contains identical ATPase active sites that coordinately unwind DNA during SV40 replication (Gai et al. 2004). Finally, the fluoroquinolones could inhibit helicase activity by blocking ssDNA binding; however this interpretation is difficult to reconcile

with our observations that elevated levels of ATP restore Mcm2-7 helicase activity in the presence of most of the examined fluoroquinolones (Figure 11B).

3.11.4 Prospects for tailoring fluoroquinolones as effective helicase inhibitors for Mcm2-7

Helicases are abundant in eukaryotes. For example, in yeast, ~2% of open reading frames contain known helicase structural motifs (Shiratori et al. 1999). In addition to Mcm2-7, many human helicases (*e.g.*, the RecQ family members such as the Werner, Bloom, and RecQ4 helicases, (van Brabant et al. 2000)) are also potential therapeutic targets. Given the paucity of available helicase inhibitors and our observations that different fluoroquinolones differentially inhibit a variety of helicases (Figure 12), fluoroquinolones may provide a general and malleable molecular scaffold for the development of efficient helicase inhibitors with tailored specificities.

Further development of fluoroquinolones provides a useful route to develop Mcm2-7-specific inhibitors of therapeutic value, as Mcm over expression correlates with cancer, and multiple studies indicate that the Mcm2-7 subunits are potential targets (Toyokawa et al. 2011; Suzuki et al. 2012). Several of the inhibitors that we examined (ciprofloxacin, 271327 and 314850), demonstrate at least partial selectively for Mcm2-7 over a host of other helicases tested and ciprofloxacin appears to target Mcm2-7 in yeast. As ciprofloxacin and related fluoroquinolones are common and approved human antibiotics (Tanabe et al. 2000), this molecular scaffold has proven pharmaceutical utility. Although our inhibitors only act at concentrations that exceed typical therapeutic use, this situation has precedence. For example, high doses of sodium phenylbutyrate are used in the

treatment of malignant tumors, in which plasma concentrations of the compound are well over 1 mM (Phuphanich et al. 2005). Given the degree of selectivity that we observe with an off-the-shelf pharmaceutical designed for an entirely different application, our limited screen of ciprofloxacin-related compounds has identified several chemicals with improved properties, validating the likelihood that additional structural refinement using ciprofloxacin as a starting point will yield molecules with enhanced potency and specificity.

Our discovery of Mcm2-7 inhibitors has utility in other areas. First, they may function as a useful research tool both *in vitro* and *in vivo*. As each of the six Mcm subunits are individually essential, analysis of the role of the replicative helicase has largely focused on model systems such as *S. cerevisiae* that have especially well developed genetic tools. Such inhibitors also have potential utility for biochemical studies, especially using systems (*e.g.*, *Xenopus* egg extracts (Lebofsky et al. 2009)) that have highly tractable biochemical advantages but are poorly amenable to genetic manipulation. Second, the discovery that fluoroquinolones can inhibit the eukaryotic helicase may explain some of the cytotoxic effects observed with ciprofloxacin and other fluoroquinolones (Olcay et al. 2011). Our finding that the *mcm4chaos3* allele confers resistance to ciprofloxacin supports our hypothesis that the Mcm2-7 complex is a ciprofloxacin target in cells and suggests that it could also be contributing to the deleterious side effects seen with this class of compounds.

4.0 STRUCTURAL ANALYSIS OF MUTANTS AFFECTING THE MCM 2/5 'GATE'

The experiments in this chapter were performed by Nicholas Simon under the supervision of Anthony Schwacha and James Conway.

4.1 SUMMARY

The replicative helicase is the molecular motor that unwinds double stranded DNA to the single stranded DNA substrate required by DNA replication machinery. In eukaryotes, this helicase is the CMG (CDC45, MCM, GINS) complex, which is comprised of 11 different subunits (Moyer et al. 2006). Six of these subunits are AAA+ ATPases, and form the Mcm2-7 complex, the replicative helicase's catalytic core. This molecular motor holds the distinction of being the only hexameric helicase in which each of the six subunits are distinct and essential. Given that other hexameric helicases are oligomers of a single protein, this suggests that the six different Mcm subunits each contribute differently to the complex's function. Numerous lines of evidence have shown that Mcm2 and Mcm5 form an ATP-dependent discontinuity, acting as "gate"(Bochman and Schwacha 2008; Costa et al. 2011) This discontinuity lends itself to the model in which Mcm loading is regulated by altering its topological state, physically opening the complex to load it onto origins of

replication and closing it to begin S-phase. However, there exists discrepancies among the published Mcm2-7 structures and biochemical literature regarding the state of the 2/5 gate in the presence of nucleotides and other binding partners. Furthermore, to date all functions for the Mcm gate have been purely speculatory, as there are no known viable mutants that have been positively shown to be defective for gate function. Toward addressing these questions, we have used single particle averaging from transmission electron micrographs to determine the structure of the *S. cerevisiae* Mcm2-7 complex in the apo state, along with mutants predicted to be open or closed based on our prior biochemical work. This was compared to structures of complexes containing mutations in certain AAA+ active site motifs. We found that the gate in the mutant complex mcm2DENQ, containing a mutation in the walker B motif, has a much narrower gate than the wild type complex, suggesting a structural cause for the mutant's regulatory phenotypes in yeast.

We also determined the structure of Mcm2-7 containing the bypass-of-block mutation in Mcm5, *mcm5bob1*, a proline to leucine mutation that bypasses the necessity of the essential regulatory kinase CDC7/DBF4(DDK), allowing for DDK-independent entry into S-phase (Hardy et al. 1997). Our results indicate that the *mcm5bob1* mutation shifts Mcm5 into the Mcm2/5 gate in the complex's open state. We propose that Mcm complexes containing mcm5bob1 protein is predisposed to a closed position, which is what allows it to bypass the need for DDK phosphorylation. Toward this end, we have used transmission electron microscopy and single particle averaging to compare wild type Mcm complexes with complexes containing mcm5bob1.

4.2 INTRODUCTION

The faithful replication of DNA is a highly coordinated and regulated process. Multiple chromosomes, each bearing multiple origins of replication, must be accurately replicated once, and only once, per cell cycle. A major hub of this regulation is the Mcm2-7 complex (Bochman and Schwacha 2009).

Mcm2-7, along with CDC45 and the four members of the GINS complex, form the eukaryotic replicative helicase (Moyer et al. 2006; Costa et al. 2011). However, unlike CDC45 and GINS, Mcm2-7 is associated with chromatin starting in early G1 phase, and its activity is regulated throughout the cell cycle. Multiple lines of evidence imply that the six different AAA+ active sites in Mcm2-7 play different roles in the regulation and enzymatic activity of the complex throughout the cell cycle. By separating the loading and DNA unwinding activities of the complex in different parts of the cell cycle, the cell is able to prevent replication errors from occurring.

Specifically, Mcm2-7 is loaded onto origins of replication in early G1 phase by the loading factors CDC6 and CTF1. Together with the ORC complex these proteins form the Pre-Replication Complex (PreRC). In the Pre-RC the Mcms remain in a catalytically inactive state until the start of S-phase. Upon DDK and CDK dependent phosphorylation events, the Pre-RC is reorganized, loading factors are removed from the nucleus, GINS and CDC45 bind to the Mcm complex and DNA unwinding begins (reviewed in (Bochman and Schwacha 2009; Boos et al. 2012).

Previous work has implicated that a topological discontinuity exists at the active site between two Mcm subunits, Mcm2 and Mcm5, forming an ATP-dependent “gate” (Bochman and Schwacha 2007; Bochman et al. 2008). Biochemically it appears this gate

must be closed in order for *in vitro* DNA unwinding to occur. We propose that this gate has an *in vivo* relevance, and that it is open during G1 to facilitate loading on to DNA and must be closed at the beginning of S-phase to initiate DNA unwinding.

Several structures of Mcm2-7 with various ligands have recently been determined, each with different implications for the state of the Mcm2/5 gate. Costa et al. demonstrated that the *Drosophila* Mcm complex fluctuates between an open lockwasher and a notched planar ring in the apo state, and only the coordinated binding of ATP and the CMG components CDC45 and GINS are able to close the complex fully (Costa et al. 2011).

A later structure of the Mcm2-7 from a minimalist eukaryote, *E. cuniculi* showed that the complex is in an open state upon nucleotide binding (the apo state was too heterogeneous to converge on a structure). *E cuniculi* is unusual in that while it has homologues of the members of the GINS complex it either lacks CDC45 entirely or it has diverged to the point where homology cannot be detected by sequence analysis, making it unclear if it has a complete CMG complex which could close the ring (Lyubimov et al. 2012).

Sun *et al.* provide the highest resolution structure to date of a eukaryotic Mcm complex in the structure of the higher order ORC/CDC6/CDT1/MCM (OCCM) complex (Sun et al. 2013), an pre-RC intermediate, determined with cryoEM, and is similar to the image averaged structure obtained by Remus *et al.* who observed a closed double hexamer bound around DNA (Remus et al. 2009).

The goal of the study was to assess whether the gate has a physiological role by determining the structure of viable Mcm regulatory mutants we predict to have abnormal gate function. We found that the Mcm mutants *mcm5bob1* and *mcm2denq* result in complexes biased toward a closed state relative to wild type complexes.

4.3 OPTIMIZATION OF STAINING CONDITIONS

Numerous conditions were explored to optimize negative staining of the Mcm 2-7 complex. A wide variety of salt concentrations, buffer compositions, and heavy metal stains, namely uranyl acetate, uranyl formate, ammonium molybdate, and phosphotungstic acid, were tested and we ultimately determined that uranyl acetate provided the best staining conditions in our hands (Figure 18A). However, a large problem was heterogeneity of our protein samples. Some of this could be attributed to the dynamic state of the complex that has been shown previously (Bochman and Schwacha 2008; Costa et al. 2011), however we also saw evidence of protein aggregates and loss of complex integrity.

Initially we tried several strategies to improve the quality of our samples to enrich for functional hexamers. Small scale gel filtration was used to separate hexamers from smaller species, however this approach significantly diluted the sample and failed to remove protein aggregates (Figure 18B).

Since most Mcm subassemblies fail to bind DNA (Bochman and Schwacha 2007), another approach was to use biotin-bound DNA oligonucleotides with a photocleavable linker, and incubate complexes with the DNA and ATPγS to enrich for functional hexamers that could bind DNA. However this approach also had problems with sample concentration (Figure 18C).

To address whether the heterogeneity problem was due to protein instability, we tested mild crosslinking conditions Glutaraldehyde crosslinking showed some promise, and suggested that the problems with complex stability and misfolded proteins may have been arising during the staining process (Figure 18D). With this in mind, we were able to improve staining under non-crosslinking conditions by increasing sample concentration and reducing adsorption time, minimizing the time the complex spent in a dilute solution without the risk of potential artifacts introduced by crosslinking.

18 A)

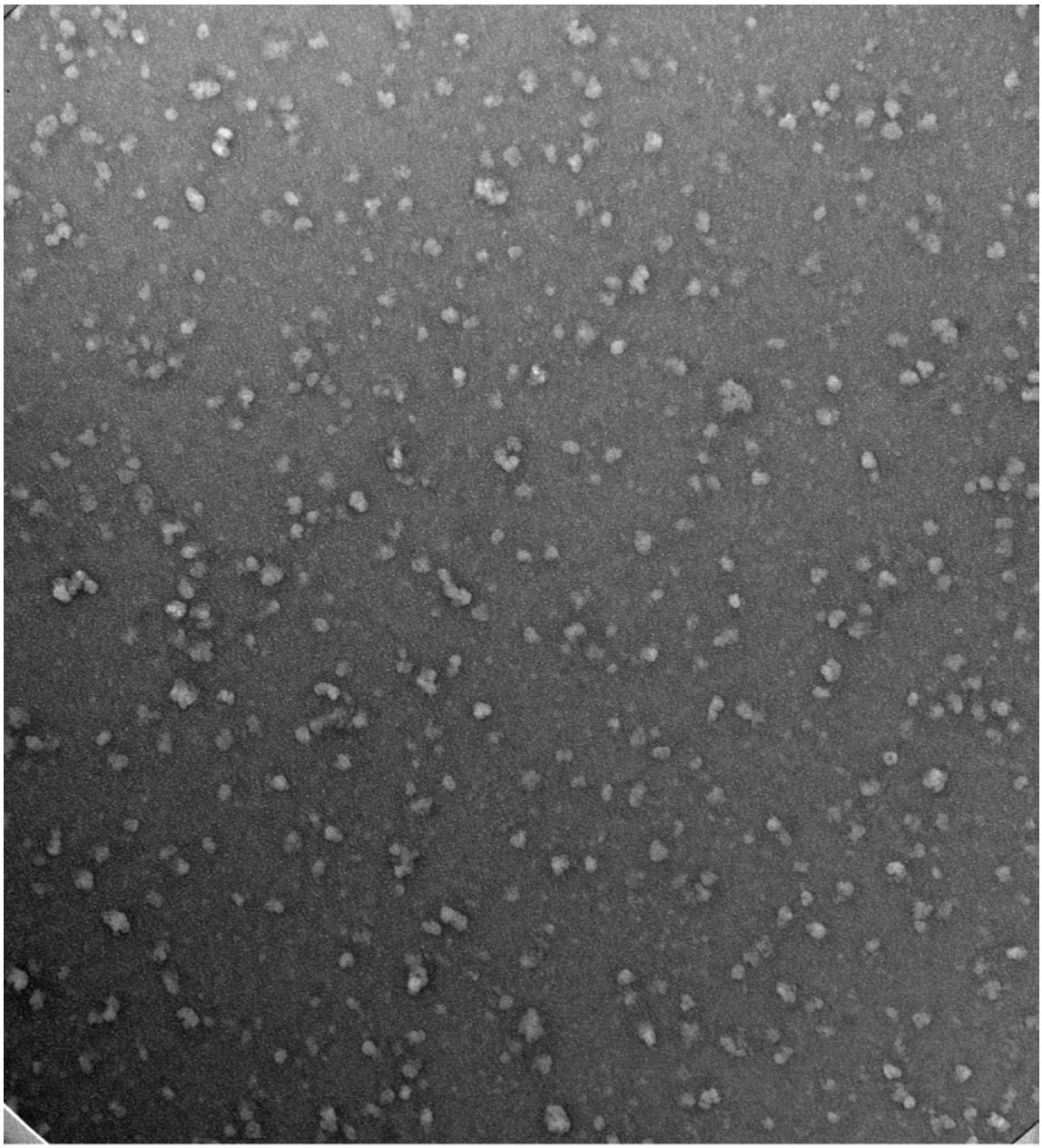
72505bob1e.tif
bob1 2733 1:40
1.5 UA
Cal: 1.286 pix/nm
12:19 07/25/11
100 nm
HV=80kV
Direct Mag: 56000x
Microscopy Facility

18 B)

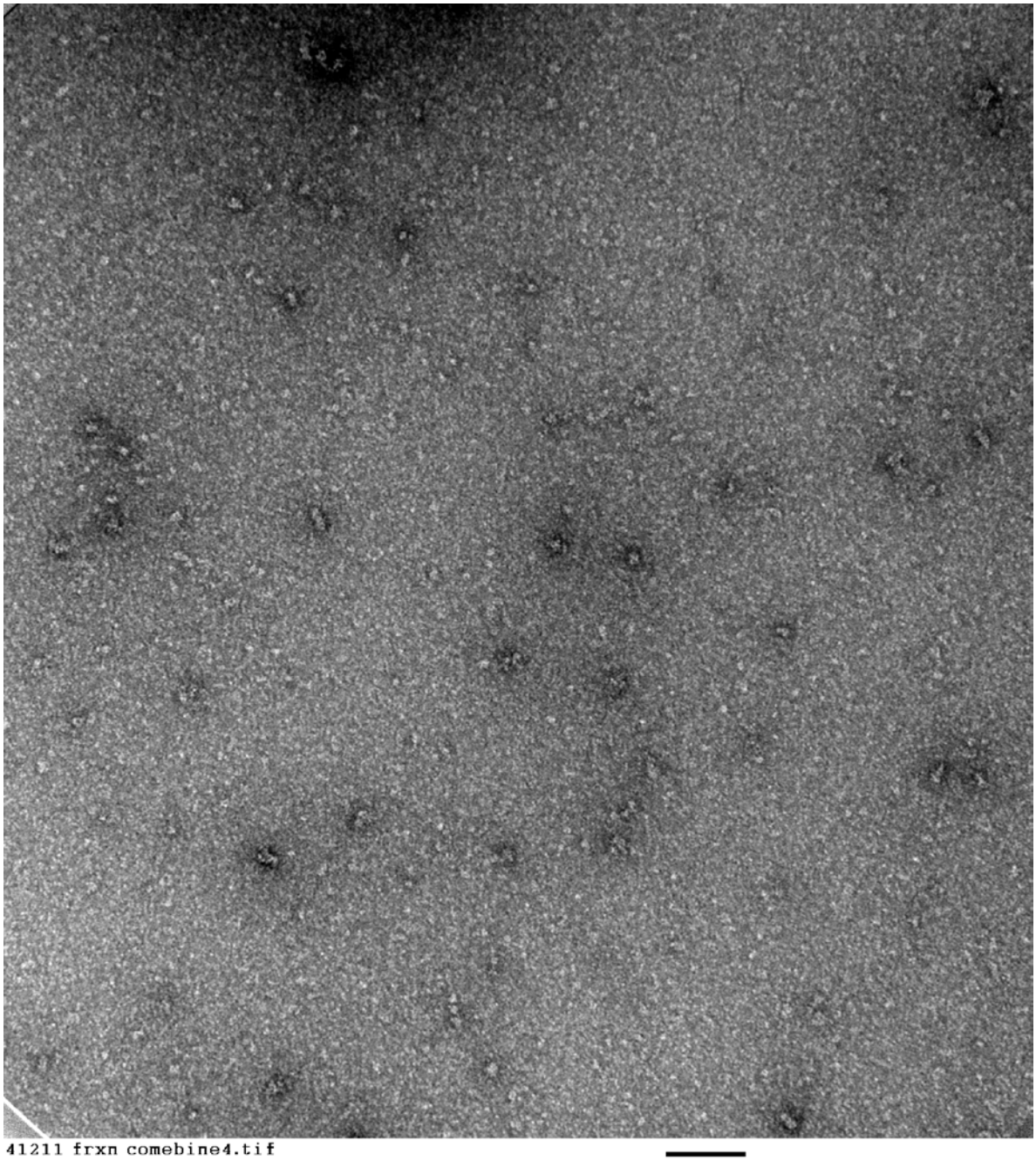
41211 frxn comebine4.tif
4-12 fraction combine
1.5 UA pos
0:09 04/13/11
100 nm
HV=80kV
Direct Mag: 71000x
Microscopy Facility

18 C)

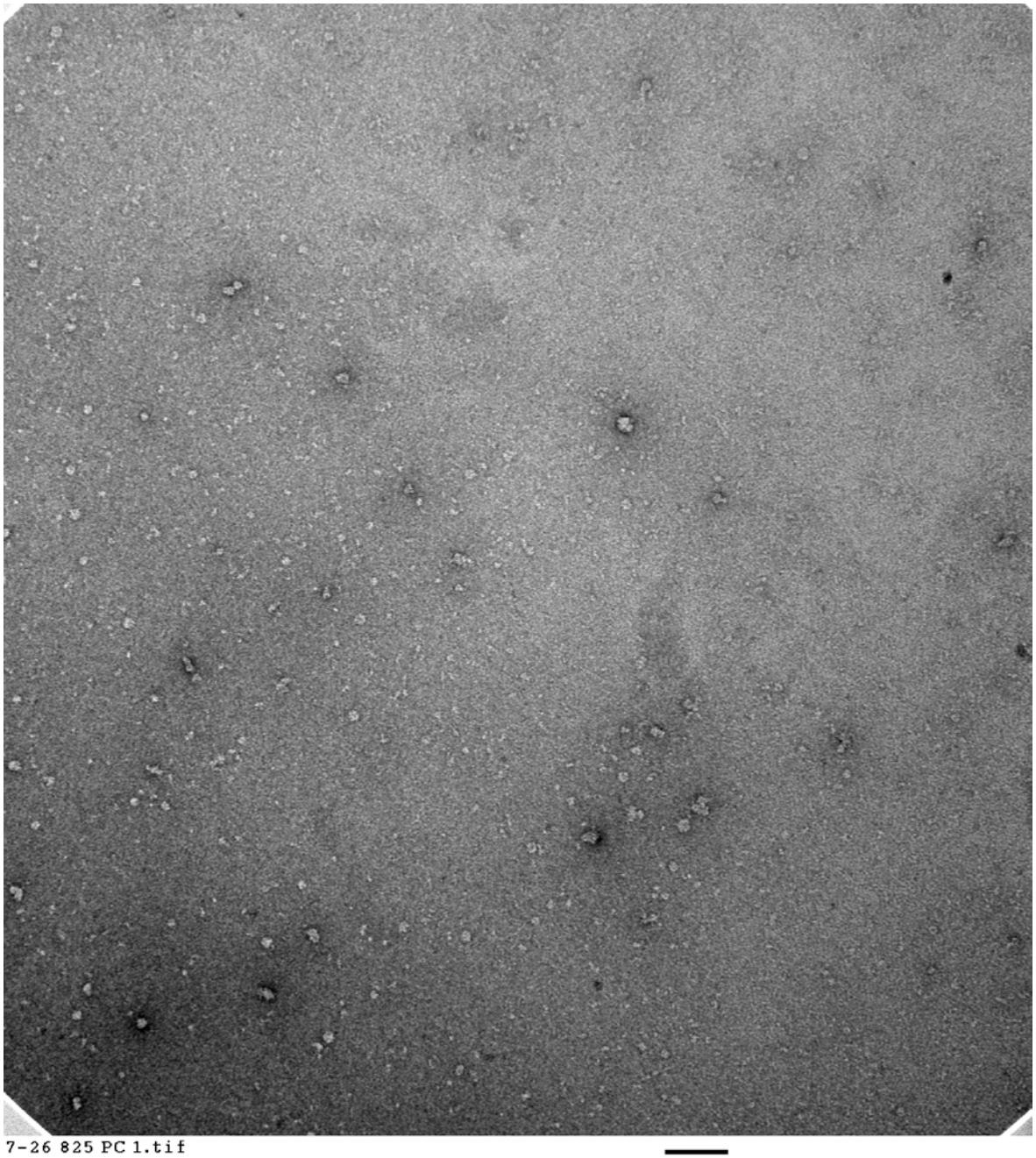
7-26 825 PC 1.tif
from 825
cleaved at 254
Microscopist: NS
100 nm
HV=80kV
Direct Mag: 56000x
Microscopy Facility

18 D)

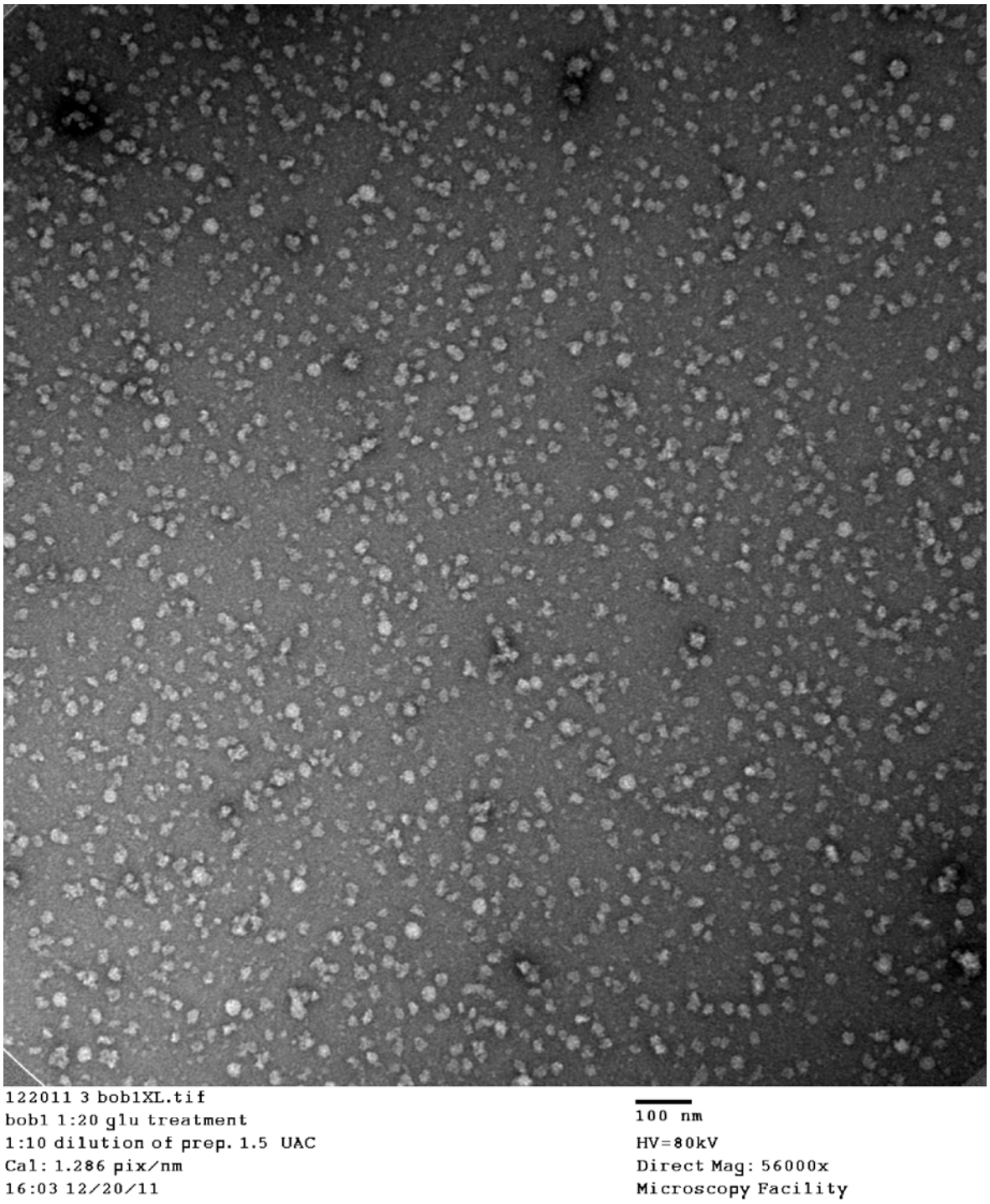

Figure 18 Optimization of protein samples for negative staining

All samples were diluted in binding buffer then stained with 1.5% uranyl acetate. A) Standard staining conditions B) Pooled gel filtration fractions. Mcm2-7bob1 protein preparation was fractionated over a calibrated 1mL gel filtration column. Fractions containing hexamer-sized complexes were pooled and subjected to s standard staining conditions. C) DNA bound Mcms released by photocleaving. Mcms were bound to biotynlated oligonucleotide 825 in a standard binding reaction (See section 2.4.1) After the reaction was complete, 25uL streptavidin magnetic beads suspended in binding buffer were added to the reaction tubes. Tubes were placed on a tube rotator for 30 minutes, then placed into a magnetic rack and the beads allowed to settle, and the liquid drawn off. Beads were washed again in binding buffer, then exposed to UV light (254 nM) for 1 minute by spotting the liquid onto saran wrap placed over a UV light box. Tubes were placed back in the magnetic rack, the liquid drawn off and adsorbed to a copper grid for negative staining D) Mcms treated with mild crosslinking. 1 µL of a 1:20 dilution of fresh glutaraldehyde to 9 µL of a 1:10 dilution of protein preparation 2733 for 1 minute then quenched with 1 µL of a 1M solution of Tris-glycine, the resulting liquid adsorbed to a grid and stained normally.

Ultimately, we decided that instead of trying to optimize the protein sample and sacrifice yield, it would be faster to focus on high contrast, separated particles and rely on diligent pruning and aggressive thresholding during refinements to discard unwanted heterogeneity. Among the various conditions tested, 1.5% percent uranyl acetate resulted in the best contrast. Figure 19 shows a representative micrograph.

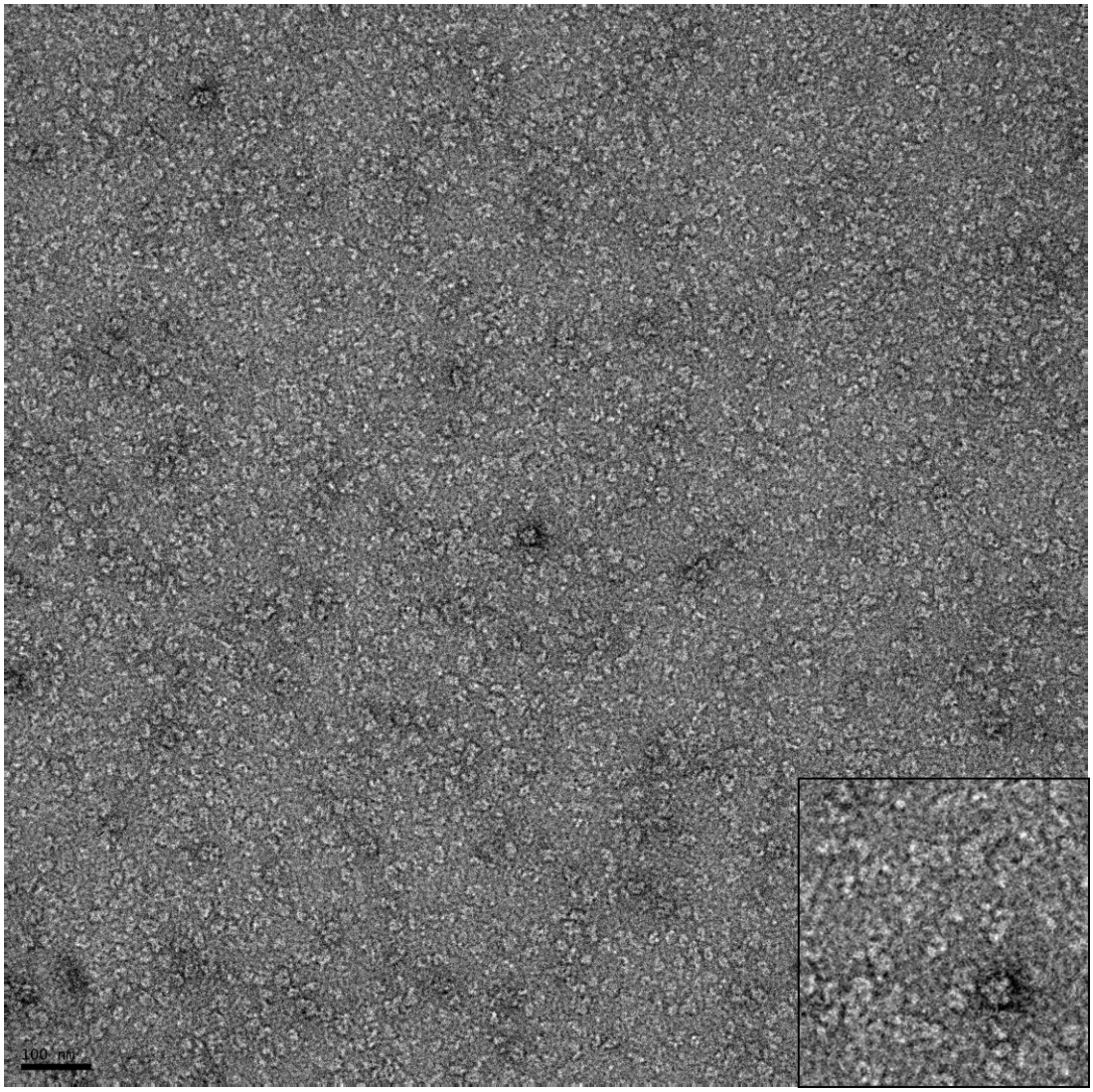

Figure 19 Negative Stain of the Mcm2-7 complex

1.5% uranyl acetate. Images taken at 40000X magnification, 200kV. The black scale bar represents 100 nanometers. Inset is 200x200 nanometers

4.4 SINGLE PARTICLE RECONSTUCTION WITH EMAN2

We chose to use the open source EMAN2 software suite for our single particle analysis (http://blake.bcm.edu/emanwiki/EMAN2) (Tang et al. 2007). The primary reason was for ease of use, as EMAN2's graphical user interface simplifies 3D refinement by providing prompts for building python command strings and arguments. This results in a shallow learning curve, which allows a relative novice to run 3D refinements independently. It also one of the few processing suites that is entirely self-contained, containing modules for boxing particles, CTF tuning, and generating and analyzing 3D models without having to switch between programs.

However, it became clear that particular properties of the Mcm complex (see section 4.8) resulted in unique challenges not generally faced in EMAN2 reconstructions. Our decision to use convergence on classes and models as a way around the heterogeneity problem meant that our data sets needed to be significantly larger than anticipated. This is evidenced in Figure 20, which shows the difference in reference class average quality between a particle set of 1000, typically enough to generate class averages in EMAN2, and a particle set of 40,000 particles

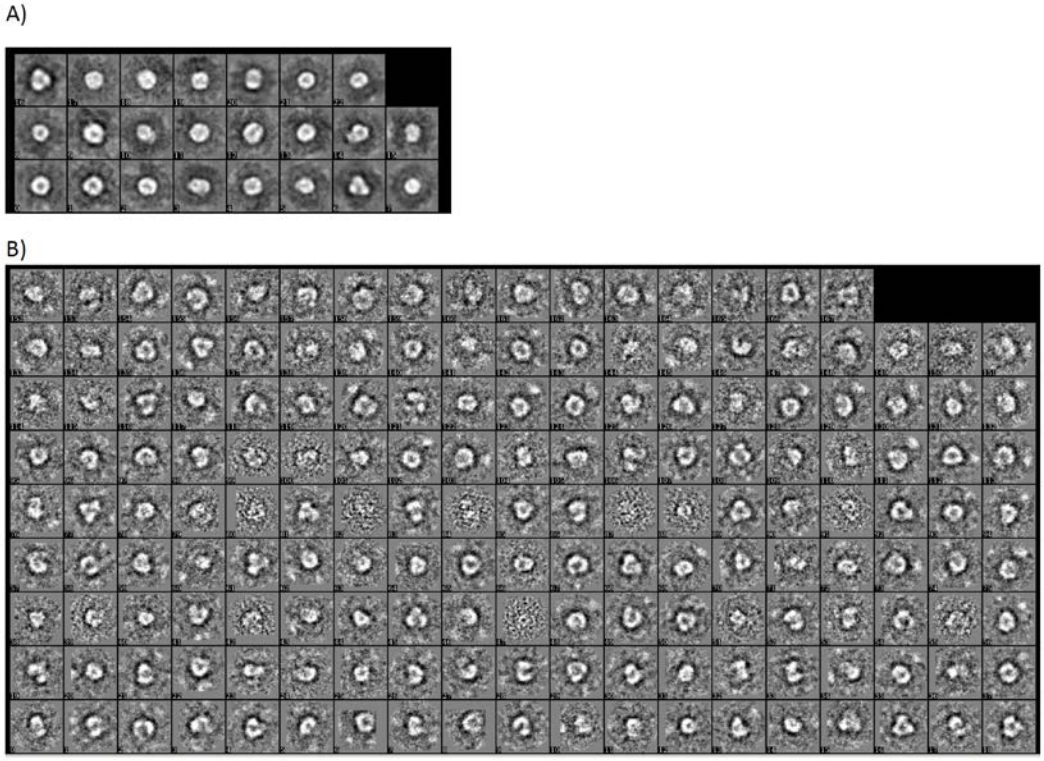

Figure 20: Optimization of reference free class averaging

A) An initial attempt at generating reference free class averages using a particle count of 1000, typically sufficient for generating an initial model in EMAN2, protein preparation 2733

B) Class averages obtained with a particle set containing 40,000 particles and applying a 0.25 threshold, protein preparation 2733

The large scale of the projects required some deviations from the typical EMAN2 refinement parameters, which are detailed in Section 2.4.8

4.5 THE WILD TYPE MCM 2-7 COMPLEX FORMS AN OPEN RING

Having prepared a sample grid with recombinant wild type Mcm2-7 hexamers, we collected several hundred micrographs, resulting in a total of approximately 45,000 picked particles used in the refinement stage. During initial refinement, we found that we had an underrepresentation of side views due to the complex's tendency to land in a limited number of orientations. To increase our orientation sampling, we took ~150 images of Mcm particles adsorbed to a grid in a high glycerol buffer (see methods for recipe), and refined our structure against a smaller set of particles including those from high glycerol conditions, before doing further refinement against the entire data set (Figure 21).

A)

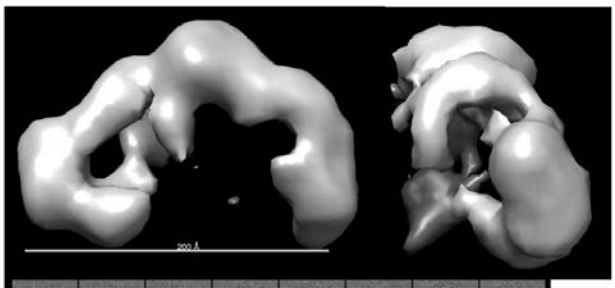

B)

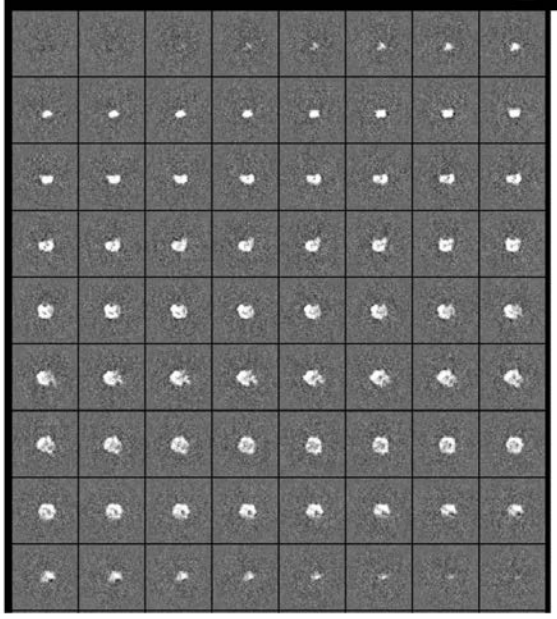

C)

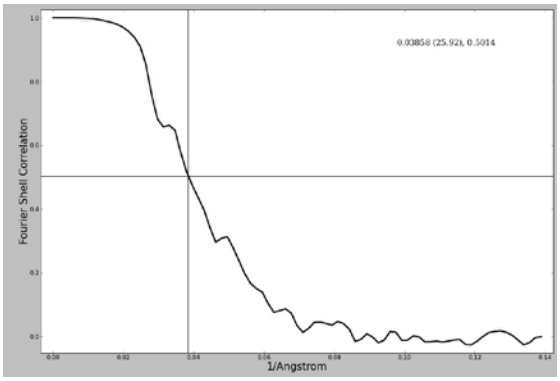

Figure 21: 3D reconstruction of *S. cerevisiae* Mcm2-7

A) EM map showing views of the Mcm2-7 complex down the central channel and from the side. Structure represents 33 thousand particles from protein preparation 2590. B) Z-slices through the 3D volume. C) FSC plot, estimated resolution is 26.3 Å

We estimate a resolution of 26.3 Å from the Fourier shell correlation (FSC) at the 0.5 threshold (Figure 21C), which is comparable to previously determined Mcm structures from negative stain (see Table 1). These curves are plotted by dividing the data set in two and performing two independent refinements, then measuring how well the two independent models match. Like the *D. melanogaster* Mcm2-7, in the absence of nucleotide our complex forms an open lockwasher. Notably different is the large size of the gap in the complex, the significance of which is discussed further below.

4.6 THE MCM5BOB1 MUTATION BIASES THE GATE TOWARD A CLOSED FORMATION

We were interested in regulatory mutants that may have phenotypes attributable to aberrant gate function. One promising candidate is the bypass of block allele, *mcm5bob1* which contains a P83L in Mcm5 (Hardy et al. 1997). This mutant previously has been proposed to cause a conformational change in Mcm2-7 complex (Fletcher et al. 2003), and secondary structure predictions indicate that the mutation may extend the length of a predicted α-helix in Mcm5 (Figure 22).

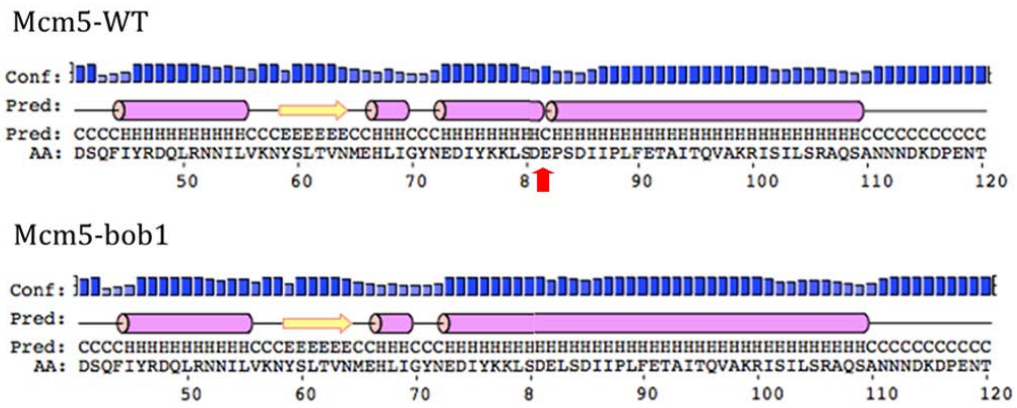

Figure 22: Secondary structure prediction of the *mcm5bob1* mutation

The arrow denotes the break in the α-helix that is removed upon loss of proline 83. Secondary structure predicted with PSIPRED (McGuffin et al. 2000)

Given *mcm5bob1's* ability to bypass the need for DDK and the secondary structure prediction, we hypothesized that this phenotype is due to the mutant's ability to mimic the active (closed) formed of the complex. We tested this by determining the mutant complex's structure (Figure 23 A, B)

A)

B)

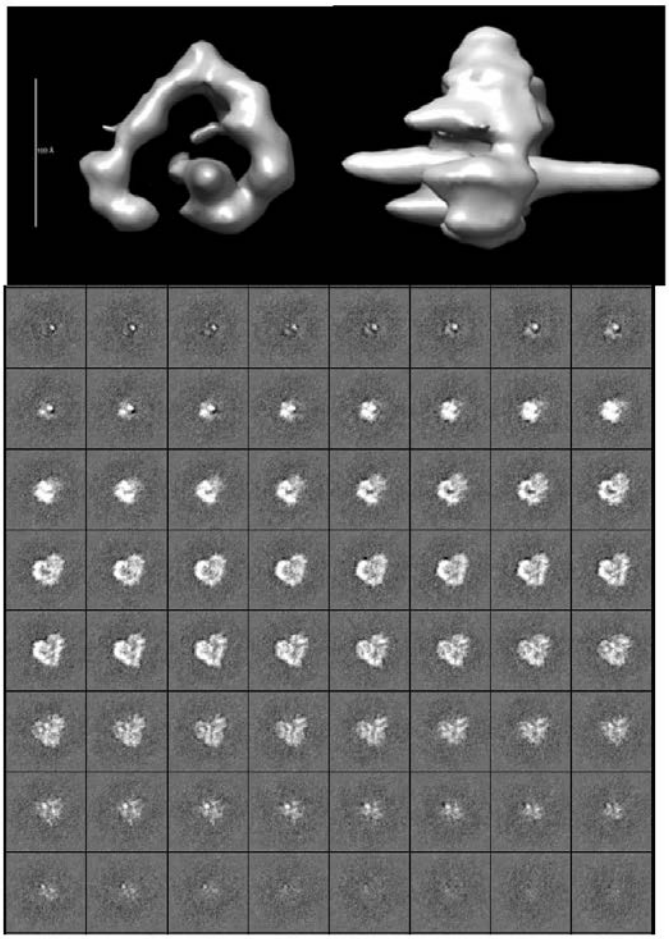

C)

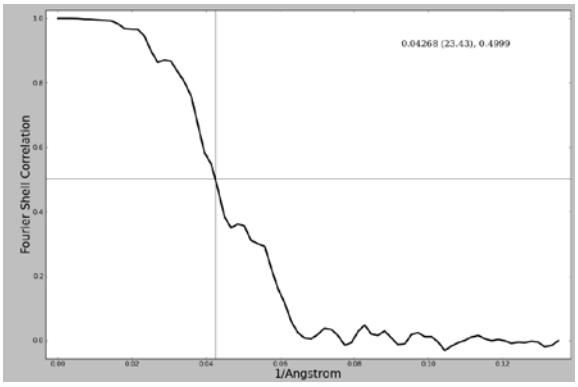

Figure 23: 3D reconstruction of the Mcm2-7 complex containing mcm5bob1p

A) 3D volume facing down the central channel of the complex and from the side. Structure was generated from 35 thousand particles of protein preparation 2733 B) Z-slices through the projected volume. C) FSC plot, estimated resolution of 25 Å.

Resolution of the complex containing mcm5bob1 (mcm5bob1 complex) was estimated to be 24.8 Å from the Fourier shell correlation at 0.5 (Figure 23C). The complex has a noticeably narrower gap than the WT complex. Notably, it also has positive density in the middle. This density extending outward is not an artifact, as it can be seen in individual particles. The width is consistent with DNA, and we suspect that it is DNA that has co-purified with the complex.

4.7 ATPASE ACTIVE SITE MUTATIONS IN THE 2/5 GATE APPEAR TO CONFORM TO BIOCHEMICAL PREDICTIONS

Given the large discrepancy in the gate size of our WT structure compared to those previously published, we wanted to independently verify the state of the gate with ATPase active site mutants that have previously been shown to be biased toward an open or closed state based on circular ssDNA binding assays. Approximately 25000 particles were picked each for complexes containing mutations in the Walker A motif of Mcm5 (5K>A), predicted to be open, the Walker B motif of Mcm2 (2DE>NQ), a viable mutant predicted to be closed, and the Walker B site of Mcm6 (6DE>NQ). For 2DENQ and 6DENQ, this resulted in structures of comparable quality to our WT structure.

6DENQ, which we expected to look like wild type, does indeed form a large open structure (Figure 24A, B). Resolution of this structure was estimated to be 32.6 Å from the FSC (Figure 24C).

A)

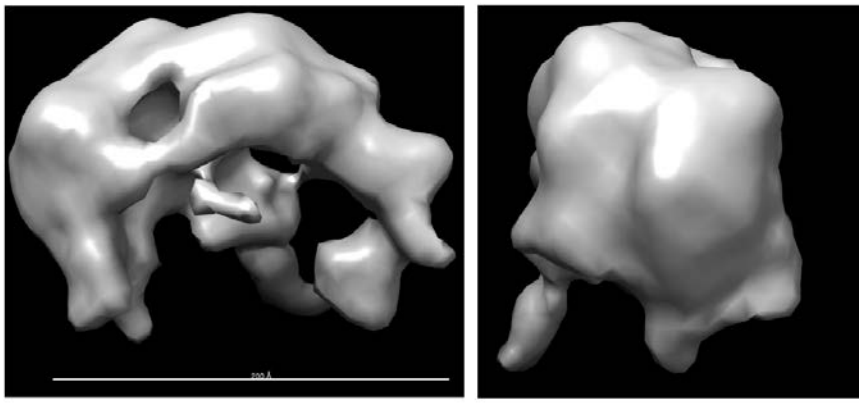

B)

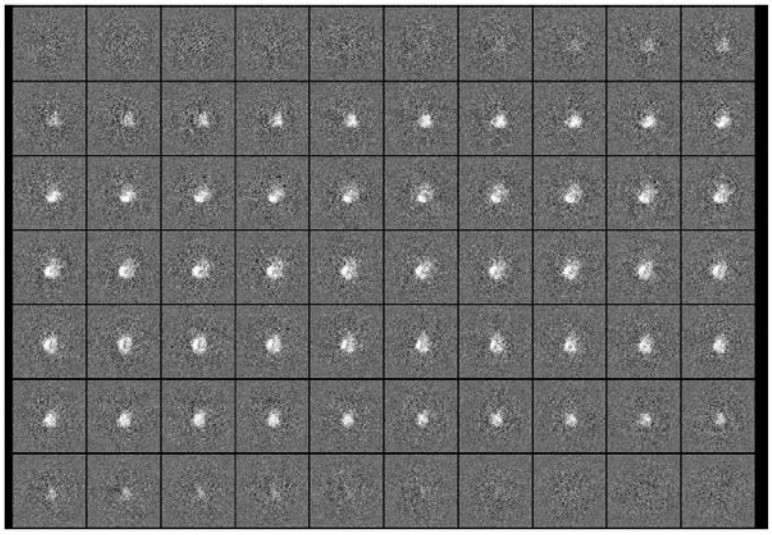

C)

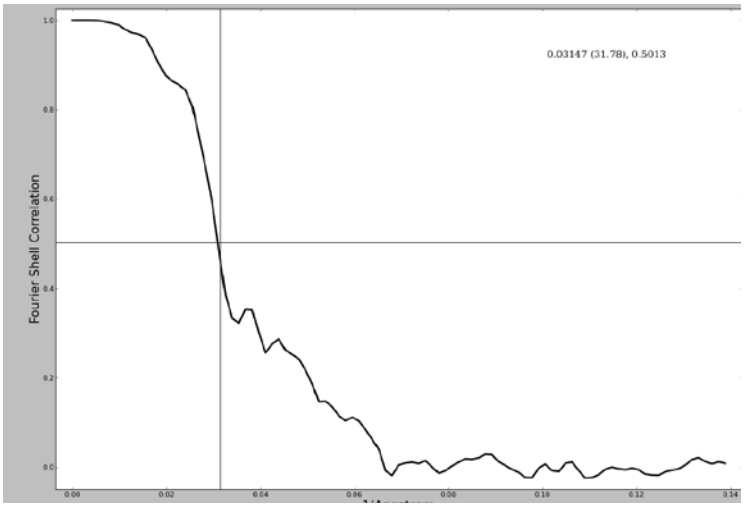

Figure 24: 3D reconstruction of mcm6DENQ

A: 3D volume of the mcm6DENQ open toroid. Structure represents 11 thousand particles from protein preparation 2298 B) Z slices through the 3D volume. C) FSC plot, estimated resolution of 32 Å.

The mcm2DENQ complex structure, in contrast (Figure 25A, B), looks more like the mcm5bob1 structure, however it is not as tightly closed. It is still measurably narrower than either the WT or 6DENQ structures. From the FSC curve we estimate a 26.2 Å resolution (Figure 25C).

Strangely, we were unable to converge on a single solution for the 5KA mutant despite quality staining and sufficient particles. A representative refinement is shown in Figure 26, which largely appears to noise, however one commonality of all mcm5ka refinements is the reduced density in the middle of the 3D volumes, visible in the 2D slices in 26B. This suggests that mcm5ka is a toroid, but the lack of convergence may mean there is no one predominant conformational state. Based on our prior work, we expected to see an open ring. Resolution was not estimated, as a convergent solution was not reached.

A)

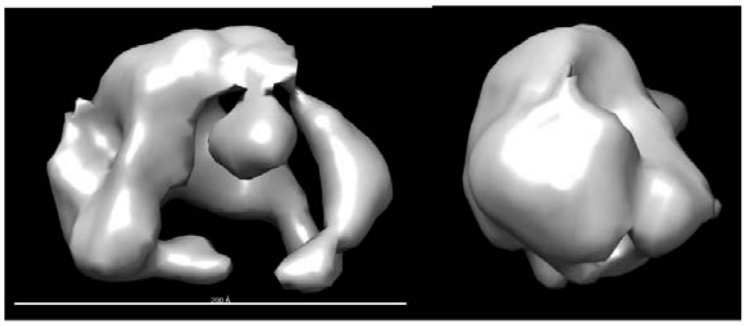

B)

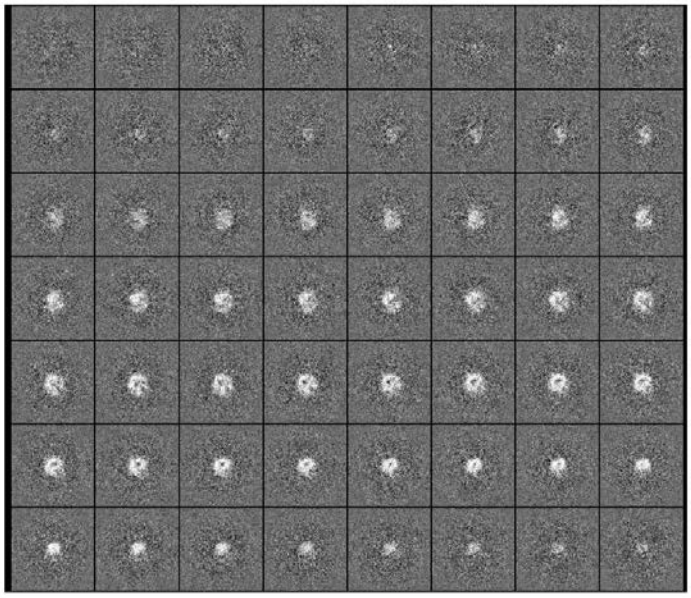

C)

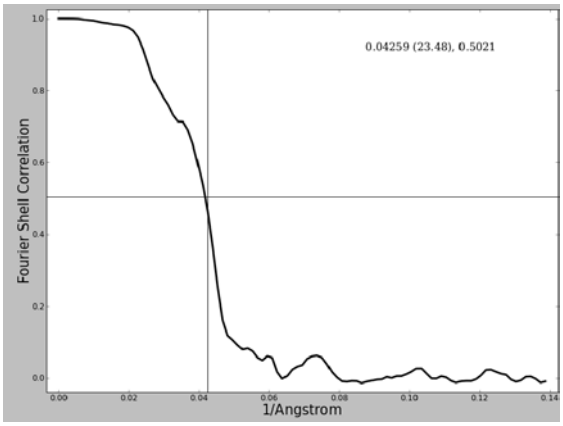

Figure 25: 3D reconstruction of 2DENQ

A) 3D volume of mcm2DENQ. Structure represents 27 thousand particles from protein preparation 2251 B) 2D Z-slices through the 3D volume C) FSC plot, estimated resolution 26 of Å.

A)

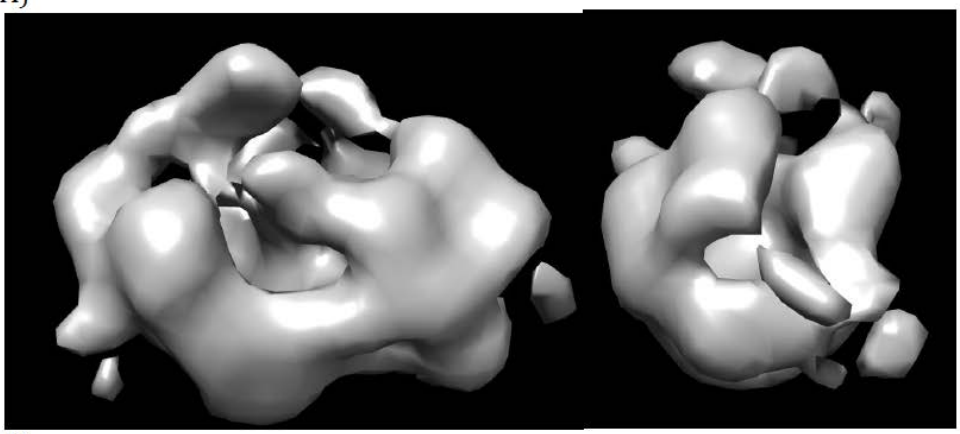

B)

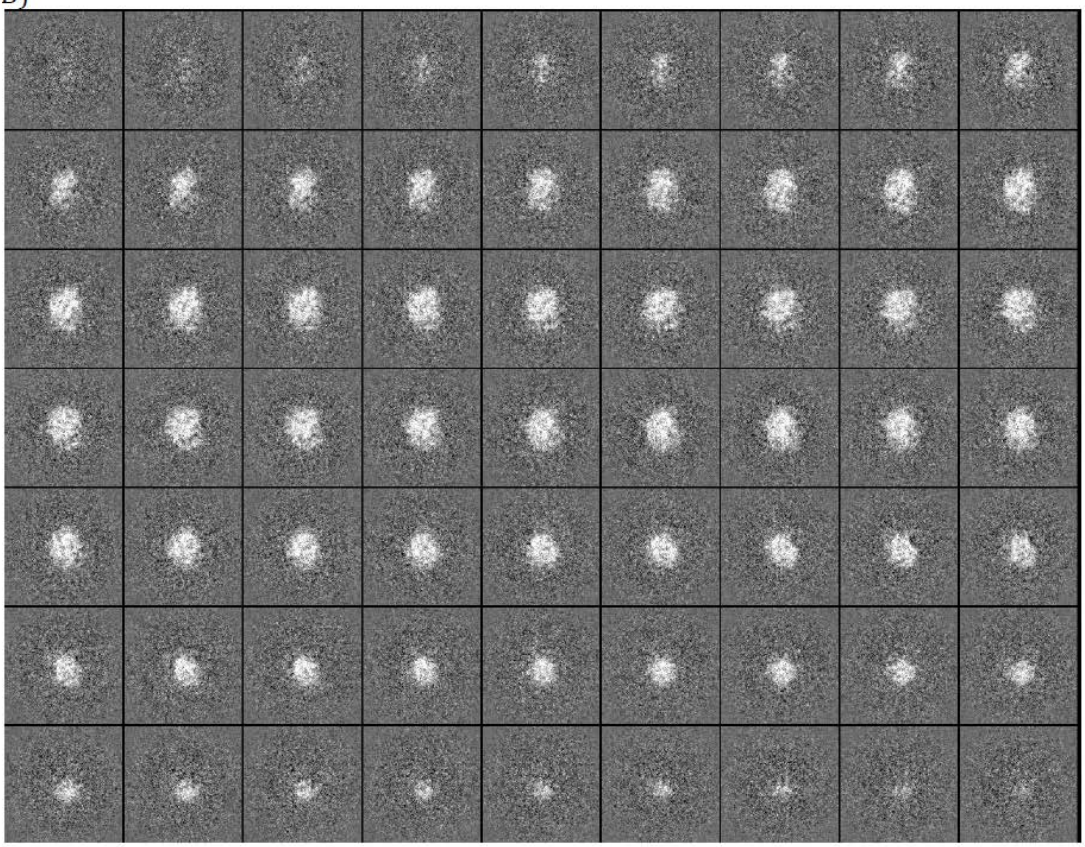

Figure 26: Mcm5KA does not converge on a toroid

A) 3D envelope of the refinement. 26 thousand particles from preparation 2512 were used in the refinement from B) 2D Z-slices through the 3D model

4.8 DISCUSSION

There were considerable challenges to overcome in this project. Despite the precedence of using EMAN2 for single particle reconstruction from negative stain (Tang et al. 2007), we faced some unique challenges. Foremost is fact that Mcm2-7 is able to exist in multiple conformations. Coupled with the complex's relatively small size, this hampers the ability of the software to align like particles. Further exasperating this problem is the fact that the Mcm complex is asymmetric, but is made up of a ring of subunits that are all homologous with each other, giving the complex six-fold 'pseudo-symmetry'

For these reasons, it became apparent that number of particles required, levels of thresholding, and number of iterations of refinements differed significantly from complexes more amenable to single particle reconstruction. We solved these issues, to a degree, by collecting extensive amounts of data and aggressively culling particles during 3D refinement. Therefore, we must temper our conclusions with the knowledge that it is possible we are converging on a state that does not represent the majority of the particles, but merely a state containing a subset of particles conducive to single particle reconstruction. However, the agreement between previously published biochemical and cell data and our structures lends credence to their validity.

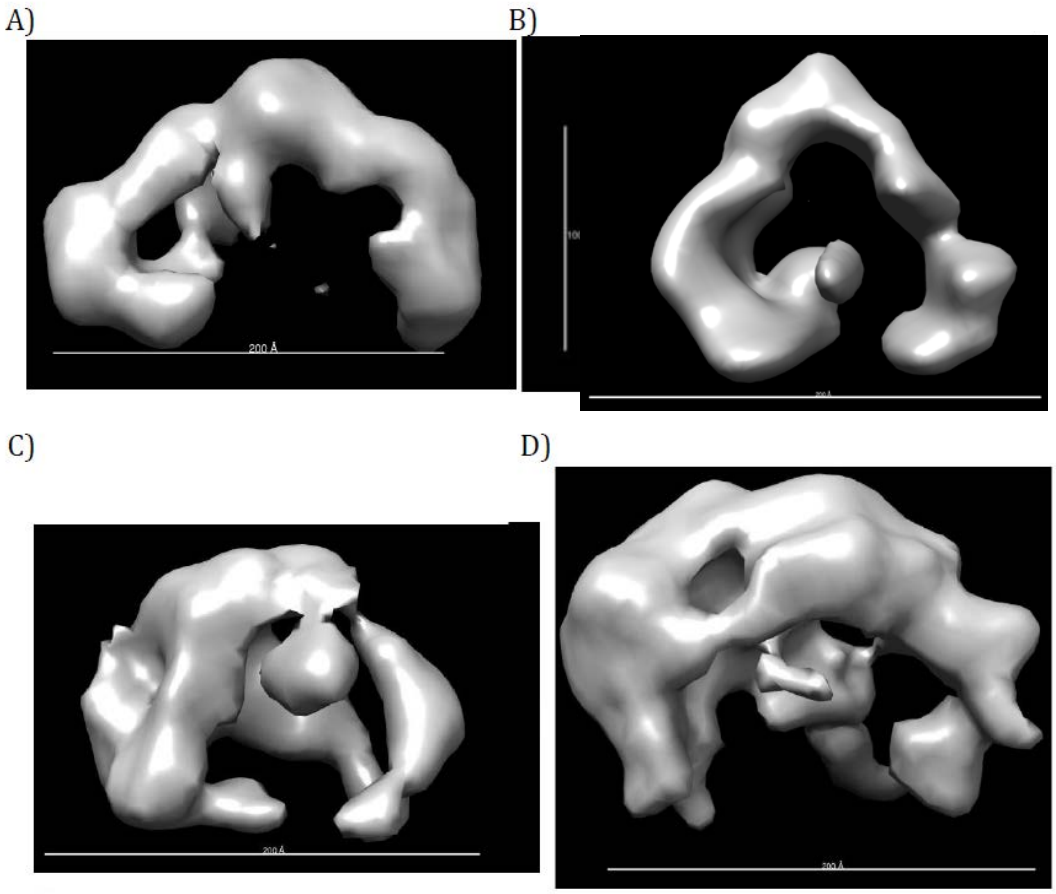

Figure 27: Comparison of WT and the regulatory mutant Mcm2-7 complexes

A) Wild Type B) mcm5bob1 complex C) mcm2DENQ complex D) mcm6DENQ complex

The wild type and mcm6denq complexes have large openings at the 2/5 gate, and consequently the width of these complexes extends beyond 200 Å.

We show evidence that the Mcm2/5 gate has a physiological role in S-phase entry, as evidenced by the fact that the regulatory mutant *mcm5bob1* makes an Mcm complex that is biased toward the closed state. This supports the long standing hypothesis that the DDK phosphorylation causes a conformational change in the complex and switches it to a biochemically active state (Fletcher et al. 2003).

It is unclear why the bob1mutant appears to co-purify with DNA, however there is precedence in the literature, as the OCCM complex also co-purifies with DNA (Sun et al. 2013).

Comparing the wild type structure with the bob1 mutant, it appears that P83L mutation causes Mcm5 to shift inwards toward the gate, close to its position in the CMG complex (Costa et al. 2011). Notably, Mcm5 is the subunit to which CDC45 and the GINS complex bind, and *mcm5bob1* mutants have mis-regulated CDC45 loading at origins of replication (Sclafani et al. 2002). The slight opening we see is consistent with the one seen in the CMG complex lacking ATP. This provides a model in which the bob1 phenotype results in the complex adopting a conformation competent to load CDC45 and GINS without the need for DDK phosphorylation (Figure 28).

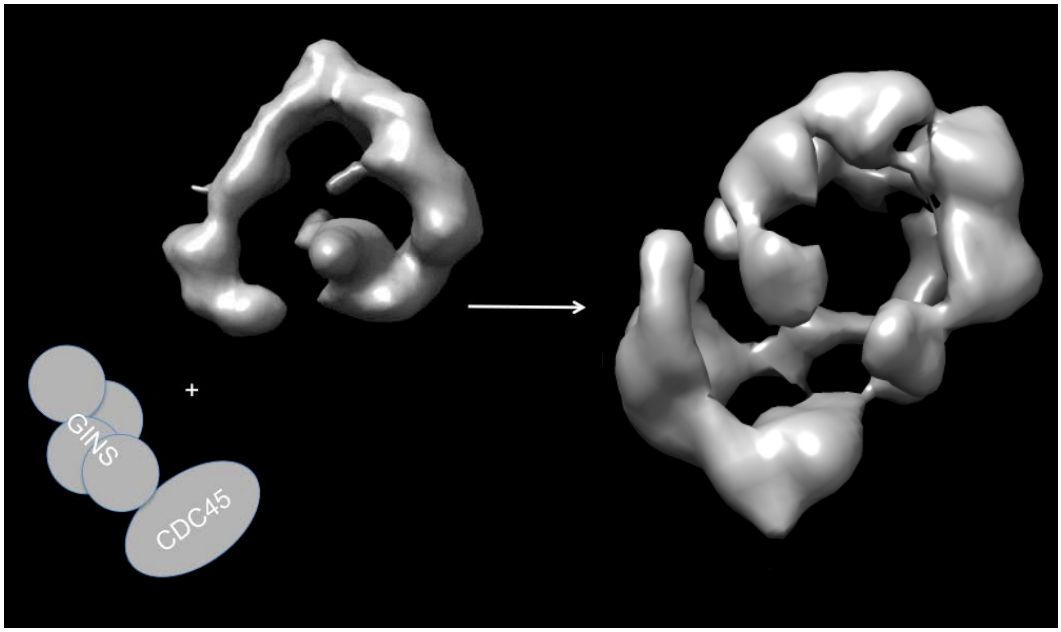

Figure 28: Proposed model for mcm5bob1 bypass

P83L allows Mcm5 to shift into the space it occupies in the CMG complex, prematurely allowing CDC45 and GINS to bind. CMG map from (Costa et al. 2011), EMD-1833 coordinates retrieved from EM database

The models of the viable mutants mcm2DENQ and mcm6DENQ are consistent with previously reported biochemistry data (Bochman and Schwacha 2008; Bochman and Schwacha 2010). Mcm2DENQ behaves as a closed ring in circular DNA binding experiments (Bochman and Schwacha 2010), which is recapitulated in our presented model. In contrast, Mcm6DENQ behaves like wild type *in vitro*, and has less severe phenotypes than Mcm2DENQ in yeast cell culture (E. Tsai, S. Vijayraghavan, A. Schwacha in preparation). In particular, Mcm2DENQ is defective in the DNA replication checkpoint control, a phenotype that could be readily accommodated by a closed ring conformation. The mcm5KA mutant complex was expected to converge on an open form, as predicted from our biochemical data (Bochman and Schwacha 2008), and in our hands the asymmetry of an open toroid seems to aid 3D refinement, yet we were unsuccessful at converging on a solution. One possibility is that mcm5KA is not 'locked' in an open state, but instead is adopting a variety of open states which behave similar in bulk biochemical assays but are diverse enough to hamper 3D refinement.

Notably, all the refinements presented here were performed in the absence of ATP, as our attempts to refine structures in the presence of ATP were unsuccessful. With hypothesize is because total the lack of an opening makes it too difficult for the software to distinguish subunits around the ring.

Altogether these data provide evidence that the Mcm2/5 gate plays an important regulatory role in cell cycle progression, and suggest that the physical closing of the ring is a critical step for S-phase entry. Furthermore, the fact that at a viable ATPase mutant causes a conformational change in the complex indicates that Mcm2-7 uses ATP hydrolysis to affect its own conformational state, rather than it being solely dictated by the

proteins it is bound to (IE as part of the pre-RC or CMG complex). In light of previous work (Remus et al. 2009; Sun et al. 2013) we think it likely that the difference between WT and mcm5bob1 complexes seen here mimics the transition state between the pre-RC and the activated CMG complex.

5.0 DISCUSSION, CONCLUSIONS AND FUTURE DIRECTIONS

5.1 THE MCM2-7 COMPLEX IS INHIBITED BY QUINOLONE COMPOUNDS

The results discussed in Chapter 3 identify Mcm2-7 as a target of the fluoroquinolone ciprofloxacin for both *in vitro* helicase activity and in growth in cell culture. While these compounds are not of sufficient potency for therapeutic use, they do provide starting basis for future, higher throughput screens.

5.1.1 Helicase activity is an effective readout for screening Mcm inhibitors

One concern with any small molecule screen is the choice of assay readout. With any screen, a significant number of false positives will be generated by compounds that disrupt the assay's readout. In this regard, helicase activity may be seen disadvantageous when compared assays that use ATPase activity as a readout, as the inclusion of DNA provides an additional layer of complexity of the assay and provide tested compounds an additional substrate to disrupt. However, given that there are multiple AAA+ sites in Mcm2-7 that contribute unequally to the complex's function (Schwacha and Bell 2001) and mutations in β-hairpins can uncouple ATPase from helicase activity (Jenkinson and Chong 2006), it would appear that ATPase activity is a less sensitive readout, supported by our finding that

compounds that disrupt helicase activity with an IC_{50} below 100 μM have little to no effect on bulk ATP hydrolysis (Figure 10A, treatments 1 and 2).

The effectiveness of measuring helicase activity while counter-screening a related helicase is demonstrated by the fact that we identified multiple compounds that appear to only inhibit the Mcm complex and not other tested helicases. Furthermore, while we were ultimately unsuccessful in identifying an inhibitor that was specific for Mcm2-7 over Mcm467, two compounds, ciprofloxacin and 271327, had higher potency against Mcm2-7, suggesting that such discrimination is possible and could be attained in a more comprehensive, iterative screen.

5.1.2 The quinolone backbone is an effective scaffold for designing novel Mcm2-7 inhibitors

The quinolone scaffold has been used extensively in the development of novel antibiotics, and here we demonstrate its utility for use with the eukaryotic replicative helicase. Though our screen was small in scale, we nonetheless observed that changes in functional groups decorating the quinolone ring modulated selectivity and potency of the helicase inhibitors.

In particular we observe that substitutions at the C7 position on the quinolone ring seem to have the greatest effect on modulating potency, however the small scale of our screen means we have not exhaustively tested this possibility.

5.1.3 Ciprofloxacin and other compounds are effective in cellular culture

One surprising result was that the IC_{50} values for Mcm2-7 helicase activity inhibition and Δ*erg6* growth inhibition by ciprofloxacin were nearly identical. It is unclear if this is merely coincidental, but regardless, the fact that even though our compounds are of limited potency *in vitro* they are still able to cause a biological effect at concentrations roughly equivalent to stop the enzyme *in vitro*. While the inhibitors we have described here are not nearly potent enough for therapeutic use, they do have sufficient potency for research applications, similar to what is used for hydroxyurea (Amberg et al. 2006).

5.1.4 Possible Mechanisms of fluoroquinolone inhibition

We were not able to determine a precise mode of action for our inhibitors, however we were able to rule out interference with assay substrates and provide some clues as to what is being disrupted. The observation that ATPase activity was unaffected by most of our compounds was somewhat disappointing at face value, however it did confirm that the structural integrity of the Mcm2-7 complexes was unaffected, with the possible exception of the compound Mal2-11b. Having ruled out interference with DNA and ATP substrates alone (Figures 10c and 10b), three likely scenarios remain.

The first is that the compounds do disrupt ATP hydrolysis, but only at low turnover sites. The fact that increasing ATP concentration can overcome the inhibitory effects of some of these compounds does lend credence to this hypothesis, however it's contradicted by the observation that we don't see the strong selectivity of Mcm2-7 over Mcm467 suggested by that mechanism. Attempts were made to measure the activity of these low

turnover sites in mutant complexes containing Walker A mutations in the 7/3 and 4/7 active sites, but they had little to no activity above background in the linear range of the assay even in the absence of inhibitors.

The second possibility is that inhibitors disrupt the protein/DNA interface. Ciprofloxacin does show a slight defect in ssDNA binding activity, roughly 50% of that seen in solvent controls. We attempted to measure the ssDNA binding activity of the library compounds, however the chemical properties of the inhibitors interfere with our double filter binding assay. The mechanism remains plausible, and the apparent ATP rescue we see in Figure 10b may be indicative of the increased ssDNA binding kinetics seen in Mcm2-7 upon ATP pre-incubation (Bochman and Schwacha 2007).

The third possibility is that the inhibitors are allosterically inhibiting DNA unwinding. One possibility is that they are uncoupling ATP hydrolysis and helicase activity. There is precedence for this in the archaeal literature, as mutations in the helix-2-insert hairpin abolish helicase activity and actually slightly increase ATPase activity (Jenkinson and Chong 2006). Alternatively, coordination between subunits could be lost, similar to what is seen when the allosteric control loop (Figure 3) is disrupted (Barry et al. 2009).

5.1.5 Future directions

Our observation that *mcm4chaos*3 confers ciprofloxacin resistance was insightful for two reasons. First, it provided evidence that the Mcm2-7 is an intracellular target of ciprofloxacin. Second, by demonstrating that Mcm mutants exist that are resistant to helicase inhibitors, we validated the use of a cell-based assay utilizing the high throughput technologies available in yeast.

Purifying 6 Mcm proteins (or 11, in the case of CMG) is likely not feasible in the quantities needed to screen hundreds of thousands of compounds. Rather than using a biochemical assay as the primary screen, recent advances in yeast screening technology provide a cheaper and simpler alternative. Given that we have identified one resistant Mcm mutant already, it is reasonable to assume that other Mcm mutants to other potential inhibitors exist as well. Therefore, one could screen thousands of compounds for their ability to arrest growth of drug sensitive yeast strains such as Δ*erg6* or Δ*pdr5,* then counter screen with a Mcm mutant library and look for compounds that permit the growth of specific Mcm mutants. This can be done efficiently with DNA barcoded mutant libraries, which allow for several strains to grow within the same well of a 96 well plate, and qPCR can be used to quickly identify and quantify which specific mutants show increased growth in the presence of inhibitory compounds (Ho et al. 2009).

However, while they might not be feasible as a high throughput assay, helicase assays and other biochemical assays will remain a necessary step in validating any potential helicase inhibitors. Furthermore, it would also be prudent to test these compounds against the CMG complex as well. It has been observed that CDC45 and GINS stimulate

the ATPase activity of Mcm2-7(Ilves et al. 2010), so effects we see on helicase activity may be decreased or exaggerated in the context of the fully activated form of the complex.

5.2 PHYSIOLOGICAL RELEVANCE OF THE MCM2/5 GATE

Chapter 4 describes our efforts to determine the relevance of the Mcm2/5 gate by examining the structure of predicted 'gate mutants.'

5.2.1 Differences between the currently determined structures of Mcm2-7

Our work joins a growing body of structural data available for Mcm2-7, and we observe key differences between our structures and those determined previously. The most obvious is the large conformational difference seen in our WT structure and those seen by other groups (Costa et al. 2011; Lyubimov et al. 2012; Sun et al. 2013)(Figure 29).

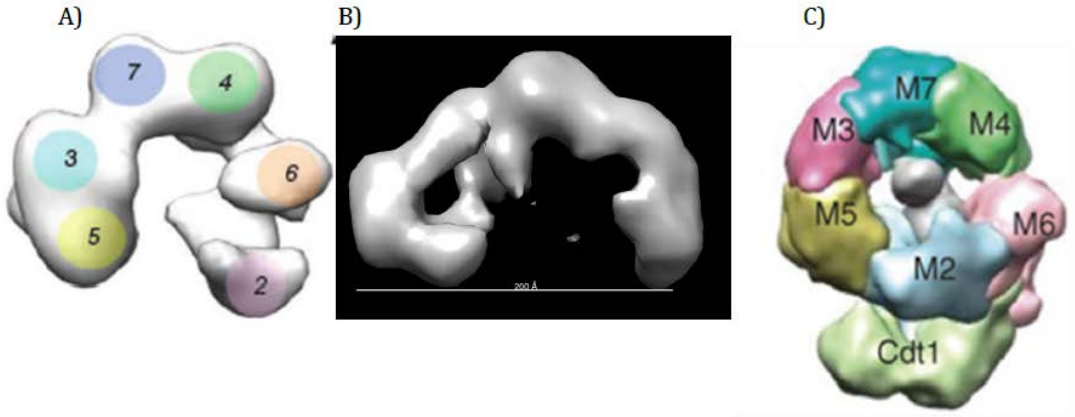

Figure 29: Comparison of solved Mcm structures

A) *Drosophila* Mcm 2-7 from (Costa et al. 2011) B) *S. cerevisiae*, this study. C) OCCM complex from (Sun et al. 2013) Adapted with the permission of Nature Publishing Group

Are these simply species specific differences? Given the high degree of sequence conservation of the Mcms among eukaryotes (Bochman and Schwacha 2009), it seems unlikely that there are fundamental differences in the way the complex works. However, it should be noted that *D. melanogaster* Mcm2-7 has not yet been shown to possess helicase activity outside the context of the CMG complex (Moyer et al. 2006; Ilves et al. 2010).

One should also remember that the Mcm complex does not exist in a vacuum: throughout every stage of the cell cycle it is constant contact with other proteins. It's conceivable that the Mcms of some species are more dependent on those intracellular interactions than others. Perhaps *D. melanogaster's* Mcm complex does look like the complex from yeast, but only when bound to loading factor such as Cdt1.

Finally, this could be due differences in purification strategies. To date, all structures of Mcms containing an "open" structure have been obtained from complexes purified from baculovirus ((Costa et al. 2011; Lyubimov et al. 2012) and this study). Since the phosphorylation state of baculovirus produced proteins is unknown, and given the importance phosphorylation plays in activating the complex, it possible differences in the phosphorylation state of these complex are responsible for the observed structural differences.

5.2.2 Phenotype of the *mcm5bob1* mutation

For several years the Sclafani lab has championed the cause of the **b**ypass **o**f **b**lock mutant, bob1, which bypasses the need for the essential regulatory kinase DDK. Modeling based

on the crystal structure of the N-terminal fragment of the *M. thermautotrophicus* Mcm suggested a "domain push" model as the mechanism for the mutant's ability to dispense with DDK by allowing stochastic binding of CDC45 (Fletcher et al. 2003; Hoang et al. 2007)

Analysis of the structure of the Mcm5bob1 complex supports this hypothesis. Contrasting it with the wild type structure, it appears that the P83L causes Mcm5 to tuck into the position it occupies as a member of the CMG complex. This suggests that the primary consequence of CDC7/DBF4 (DDK) phosphorylation results in a conformational change in the Mcm complex, allowing GINS and CDC45 to bind. This also explains why we and other groups have failed to make an equivalent mutation in Mcm2 that mimics the bob1 phenotype, as Mcm2 does not mediate contacts between GINS, CDC45, and the rest of the complex as Mcm5 does.

5.2.3 ATPase active site mutants and their relationship to the gate

The observation that mcm2DENQ is also preferentially closed lends credence to the model that the 6/2 active site is regulating the 2/5 gate (Bochman and Schwacha 2010). However, given that the structure was determined in the absence of ATP, why is an ATPase active site mutant causing this effect on the complex's conformation?

We have long posited that 2DENQ plays a regulatory role (see Figure 1). Given that the 6/2 active site has extremely low turnover (Schwacha and Bell 2001), it would seem that the active site's function doesn't depend on several rounds of ATP binding and hydrolysis like those required for helicase activity, but instead uses ATP as a molecular switch. Although canonically Walker B motifs are associated with the coordination of

magnesium and water during ATP hydrolysis, there is evidence to suggest that in the Mcm complex mutations in this motif may also have an effect on ATP binding (Gomez et al. 2002). Therefore it's possible that the difference we are observing is due to a lack of ATP or ADP that normally co-purifies in that subunit in wild type complexes.

Another possibility is that the ATPase activity at the 6/2 site is required to transmit the state of the 2/5 gate to neighboring subunits. Our wild type Mcm2-7 structure has a ring opening large enough that subunits besides Mcm2 and Mcm5 likely have a role in its opening. Mcm2DENQ still has a small opening, but if it is deficient in communicating the state of the 2/5 active site to Mcm6, this may explain why the opening is much smaller than the wild type complex. It's conceivable that the other proteins involved in the G1 to S-phase condition are sufficient to compensate for this defect, which is why *mcm2DENQ* mutations in yeast are viable (Schwacha and Bell 2001). Unlike *mcm5bob1* mutants (Hoang et al. 2007), *mcm2DENQ* does not have origins which prematurely fire even though both mutants are predisposed to a closed position. It does, however, have late origin firing defects, as well as defects in the DNA replication checkpoint and sister chromatid cohesion defects. These regulatory defects may be symptomatic of a lack of communication between regulatory elements and structural states in Mcm2-7 normally communicated by the Mcm 6/2 active sites.

5.2.4 Future directions

Several questions arise now that now that we have identified a mutation that disrupts the Mcm gate. How does mcm5bob1 get loaded onto DNA? Does it bind origin DNA more tightly than WT? It would be desirable to collect data on the mutation as part of the

different higher order complexes the Mcm complex becomes part of as it progresses through the cell cycle. Mcm5bob1 in conjunction with Cdt1/Cdc6, are part of the OCCM complex, the pre-RC, or the CMG complex would shed light on many of these questions.

We also have evidence that at least one Mcm active site mutation causes a conformational change in the ring. Curiously, mutations in the Walker A and arginine finger motifs in the 6/2 active site are lethal (Schwacha and Bell 2001; Bochman et al. 2008). Why is this the case? Do these mutations cause a conformational change greater in severity? Structure determination of these mutants may give us answers we cannot achieve genetically.

Alternatively, we could take advantage of the variety of synthetic DNA substrates available. A complex that is preferentially closed may interact differently with DNA than one that is open, perhaps by binding tighter, or lacking an ability to bind DNA origin-like bubbles.

Finally, labelled subunits with MBP fusions would allow us to make definitive subunit assignments. The presence of an open gate narrows down the possibilities to two orientations, but in a fully closed complex that landmark is lost. These tags may also provide enough asymmetry to aid in 3D refinements of closed complexes, which have been unsuccessful in our hands.

APPENDIX A

APPENDIX: INHIBITION OF MCM2-7, MCM467, AND SV40 LARGE T ANTIGEN BY LIBRARY COMPOUNDS

The following compounds were added to helicase reactions at a final concentration of 1mM. Numbers indicate percent DNA unwinding relative to solvent control and represent ≥2 repetitions.

Structures	Name	Mcm2-7	Mcm467	TAg
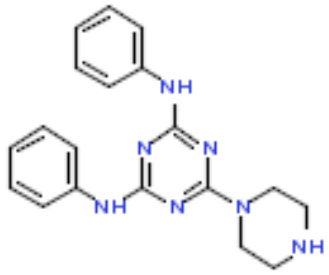	924384	0±0	1.3±1.3	10.6±5
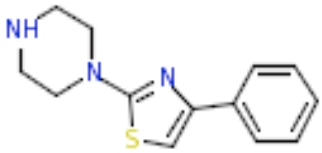	981780	54±25	106±6	104±18
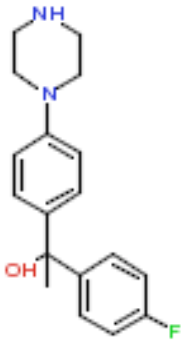	155971	54±6	32±6	90±16
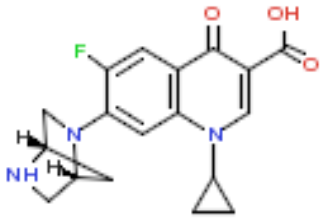	102362	40±10	40±2	92±5
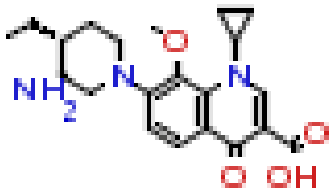	454789	71±5	41±16	101±16

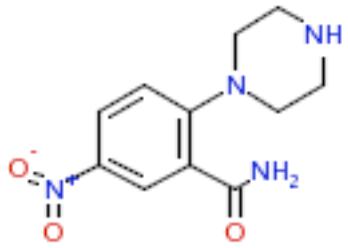	939001	53±2	49±20	81±2
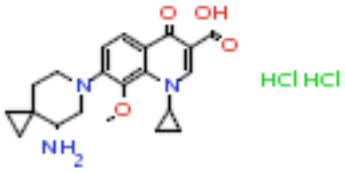	441520	47±14	36±9	79±0.3
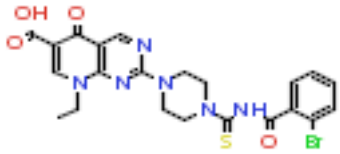	780771	79±14	55±2	89±8
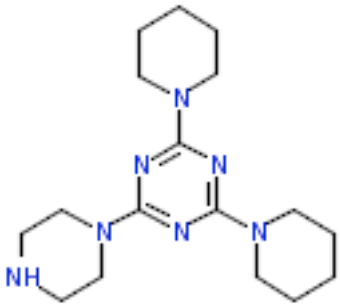	921213	47±13	79±17	100±13
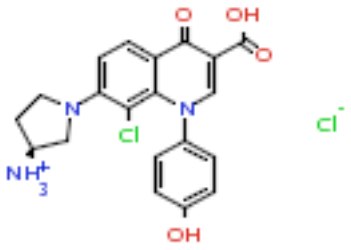	268973	0±0	11±5	26±5

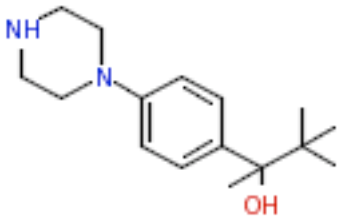	155968	13±8	8±8	71±4
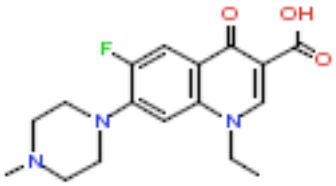	99564	22±4	34±1	74±15
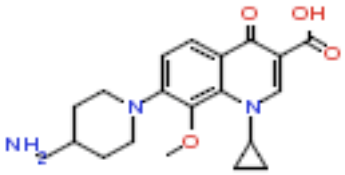 Chiral	469514	40±17	24±3	91±16
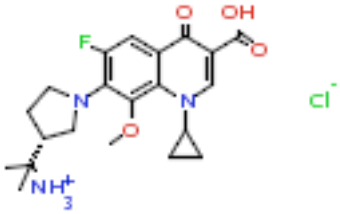	358088	50±0.5	14±4	79±6
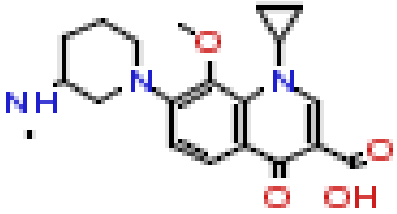	311135	31±9	3±3	29±2

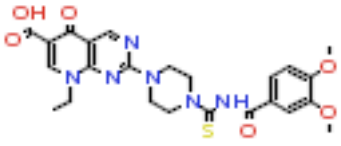	780938	40±18	29±16	97±13
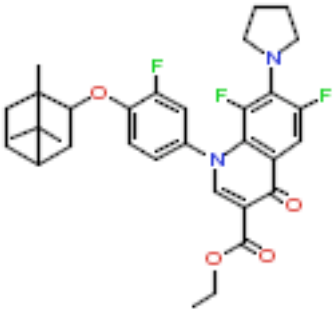	414145	37±11	46±6	106±8
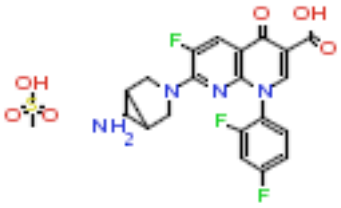	177528	33±9	7±1	86±3
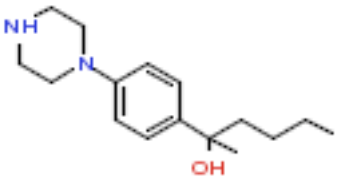	155975	44±5	42±19	95±6
	787796	36±8	29±29	117±14

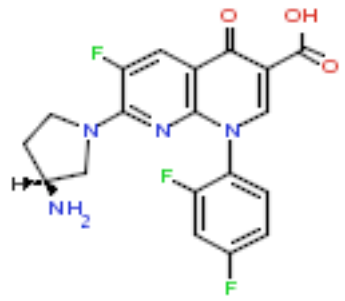	102328	28±17	32±17	111±7	
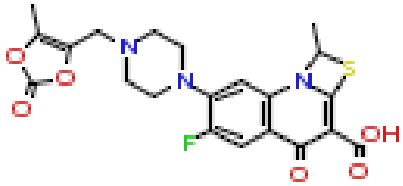	694829	40±9	20±1	100±6	
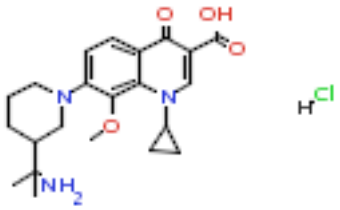	354880	0±0	4±4	28±9	
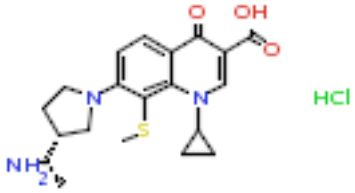	314850	0±0	18±18	84±13	
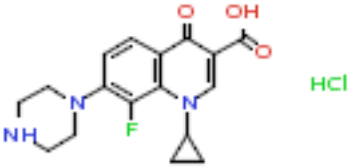	117756	52±19	53±30	94±1	

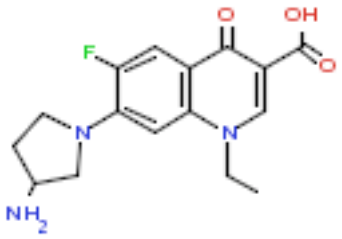	101683	22±8	58±1	75±7
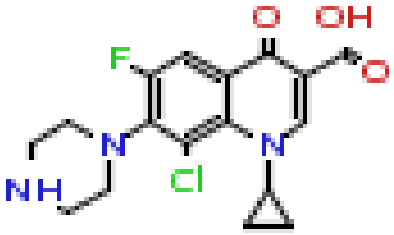	252474	43±14	57±29	96±1
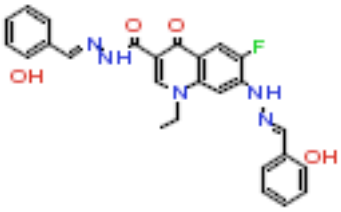	407174	0±0	0±0	57±12
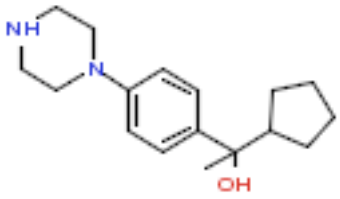	155969	40±14	48±18	78±18
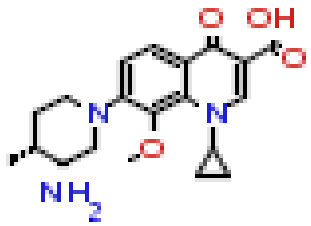	437813	71±6	65±26	97±6

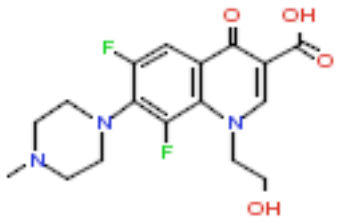	102619	42±7	64±1	99±1
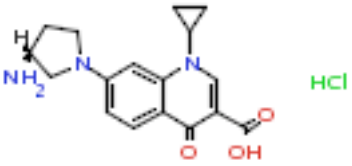	191465	33±16	39±7	56±2
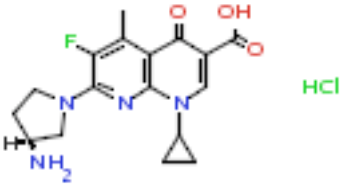	125248	0*	5±5	13±4
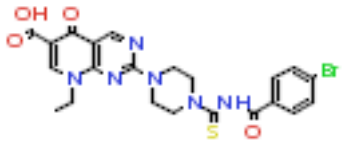	776386	68±19	79±1	71±24
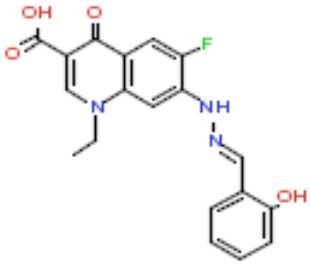	407895	88±4	51±16	86±18

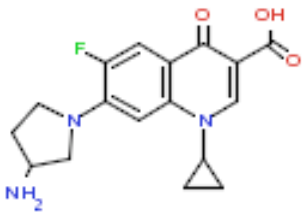 Chiral	101684	34±5	63±22	84±19
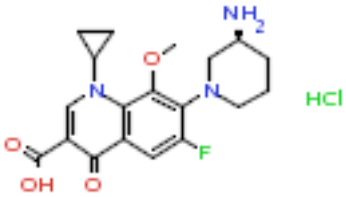	441478	27±12	49±19	87±6
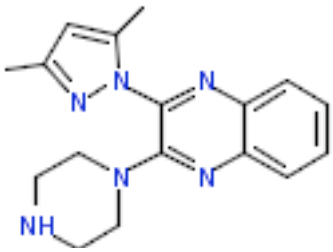	952880	21±3	52±8	79±15
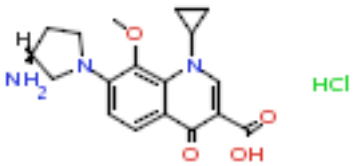	169049	10±6	29±7	66±4
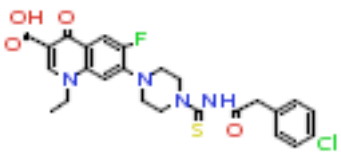	776390	54±31	71±16	94±11

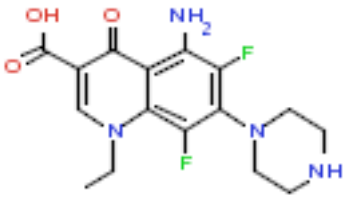	271327	7±3	75±13	89±8
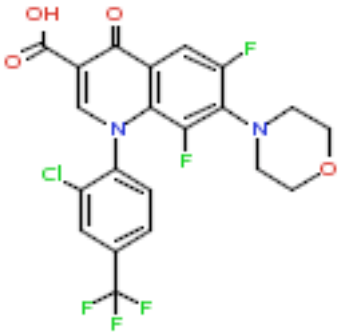	412617	46±6	72±23	83±18
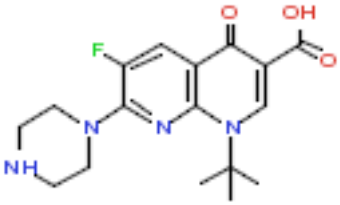	102530	30±3	52±8	83±27
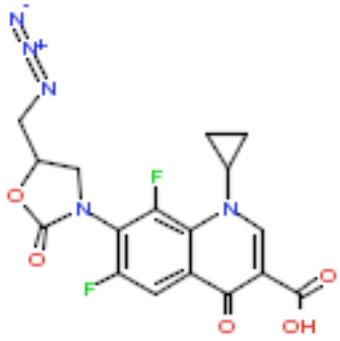	102494	42±10	28±7	83±8

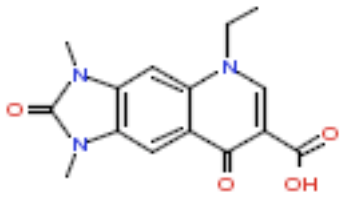	99547	38±25	31±2	99±1
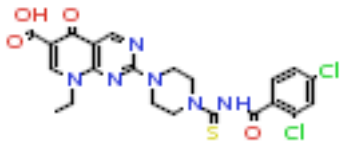	776387	36±10	78±1	96±7
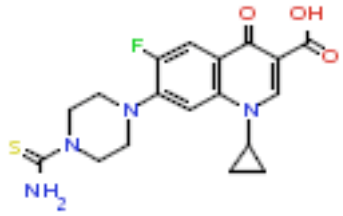	102288	8±8	48±5	93±5
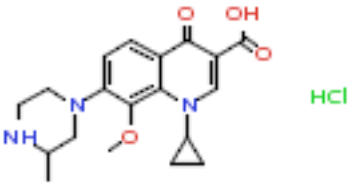	299587	74±48	56±24	87±10
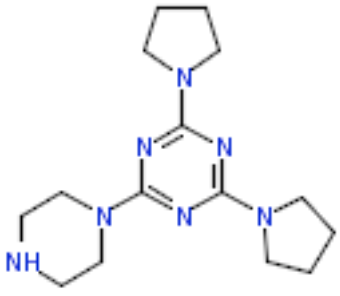	1002635	41±27	75±3	94±2

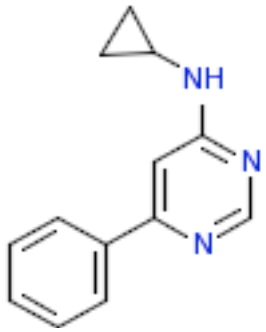	749948	51±35	38±12	82±10
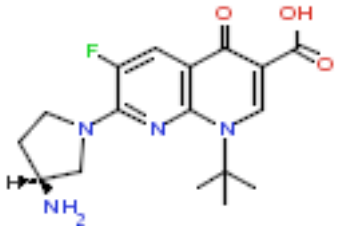	102519	25±4	25±10	95±4
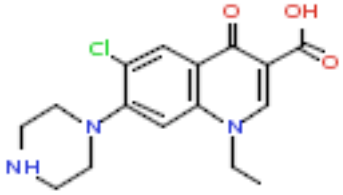	100236	27±7	37±3	95±5
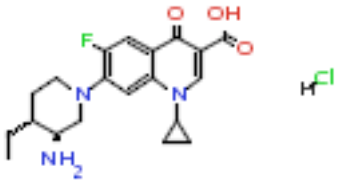	481427	14±7	31±13	102±13
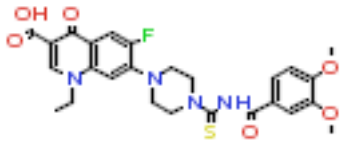	776388	23±11	42±3	101±4

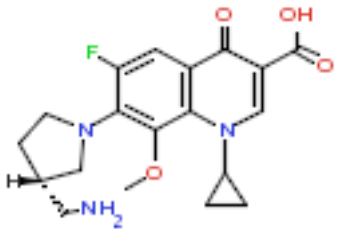	117757	23±1	53±25	95±7
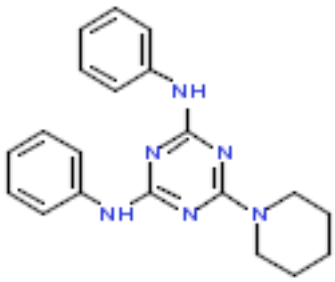	390077	9±1	29±9	40±28
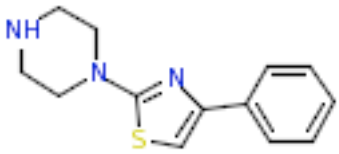	981780	23±6	63±37	101±10
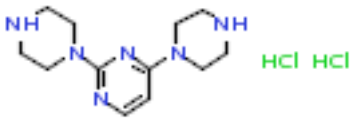	130040	0±0	13±13	92±5
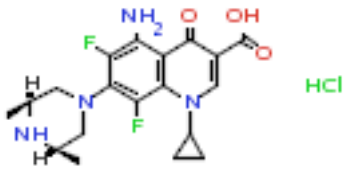	102522	40±12	37±1	82±15

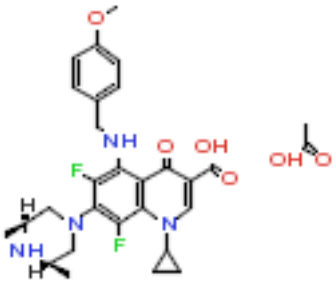	102467	67±38	65±26	99±8
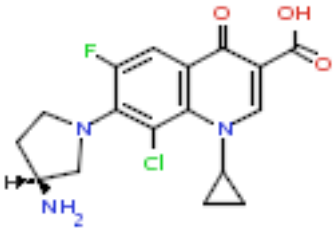	114703	60±40	49±7	108±13
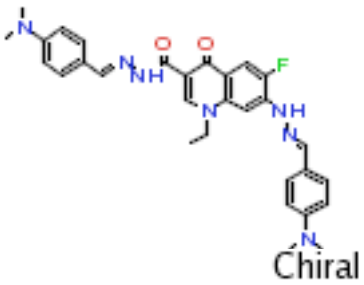	401677	49±23	56±11	104±8
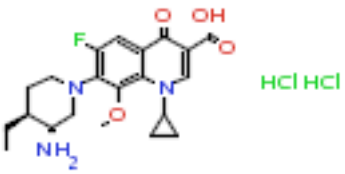	486364	75±41	28±13	54±23
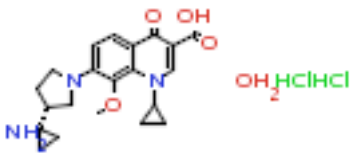	787793	60±11	80±20	102±8

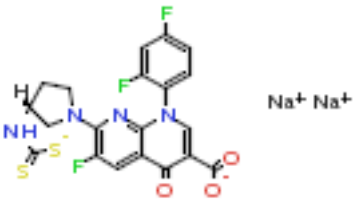	102451	50±18	22±18	85±2
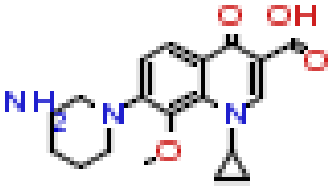	301696	40±25	39±7	110±13
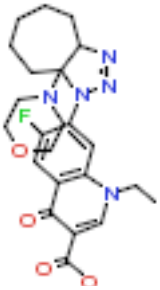	502404	35±9	32±3	94±6
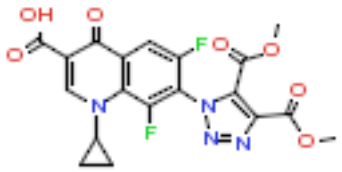	502395	46±22	27±15	88±12
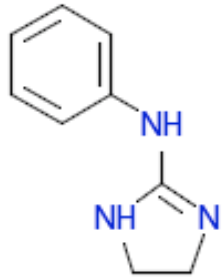	180340	35±7	34±17	100±1

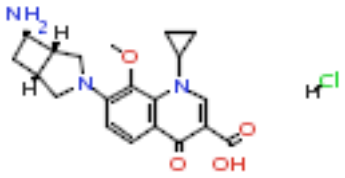	422271	42±26	29±18	83±5
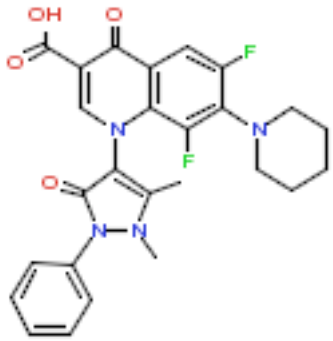	383399	62±14	31±19	97±6
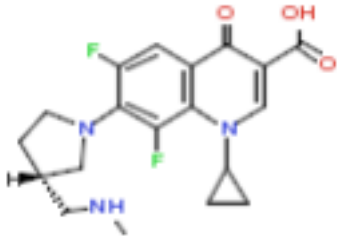	116029	30±2	28±9	119±9
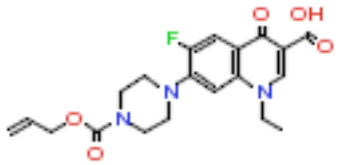	101551	30±1	22±0.5	109±10
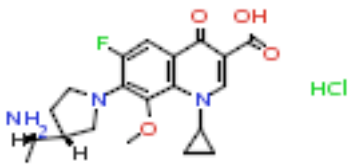	118606	49±22	54±20	100±4

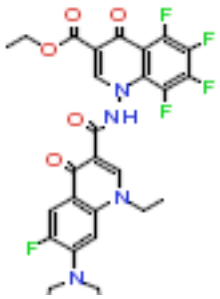	502394	48±32	22±4	85±9
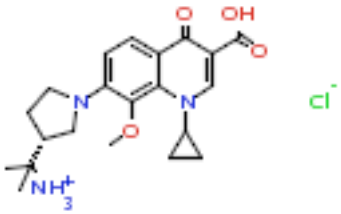	269710	22±8	26±9	107±20
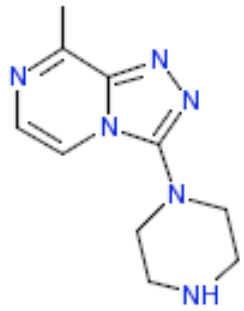	612335	33±19	32±14	108±4
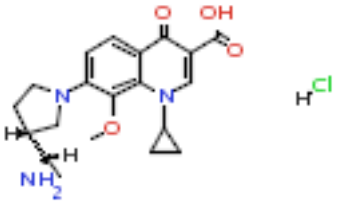	142744	48±23	24±1	108±20
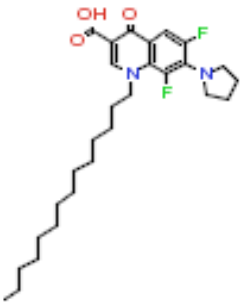	413586	34±10	26±8	97±2

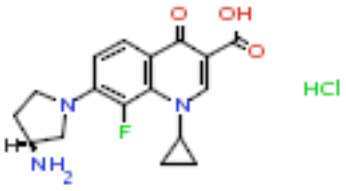	125251				
		38±15	35±11	101±13	
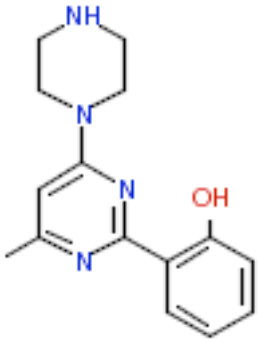	388520				
		35±6	24±7	97±4	
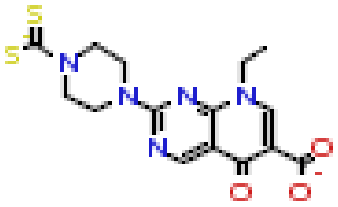	101609				
		46±11	16±4	100±10	
Chiral					
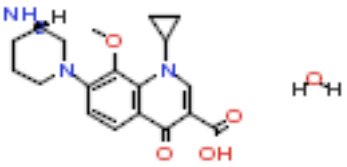	532969				
		83±45	18±3	82±19	
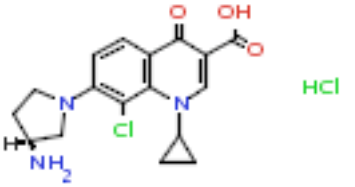	116997				
		35±9	26±15	78±16	

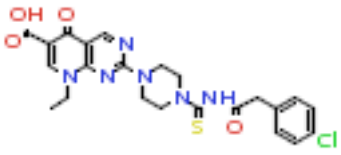	773537	28±17	36±6	72±4
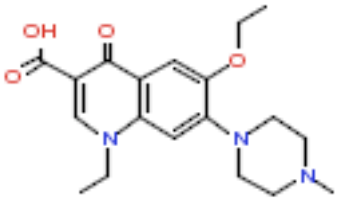	502424	78±52	28±7	54±15
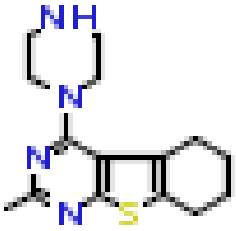	935699	43±33	58±11	56±15
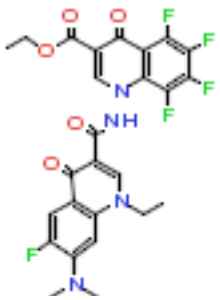	537947	72±4	20±19	79±1
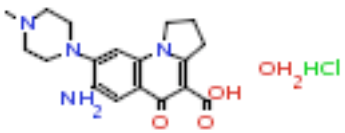	394299	9±9	3±3	93±1

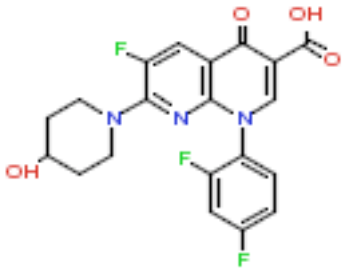	102554	60±9	60±31	95±8
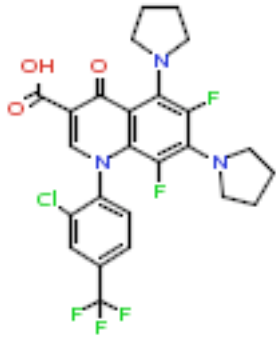	412160	0±0	38±5	75±16
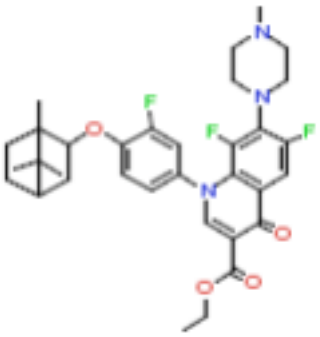	804270	25±2	19±8	82±20
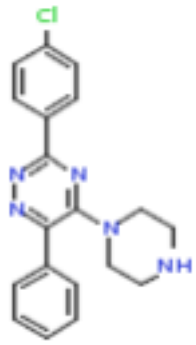	587706	10±7	54±6	64±22

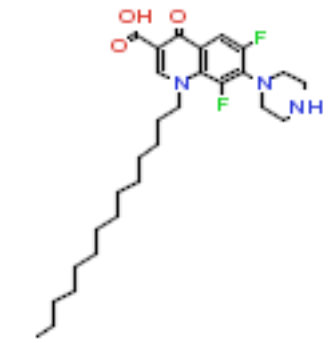	414908	25±3	39±9	62±26	
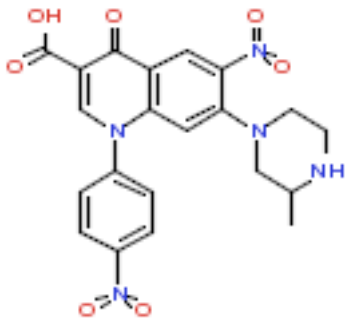	408743	66±1	13±5	77±22	
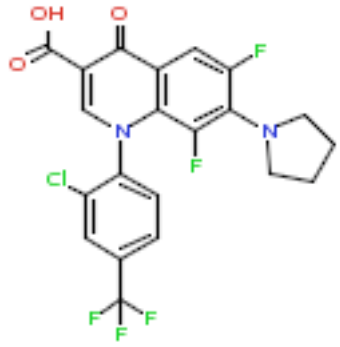	412152	10±10	24±5	54±1	
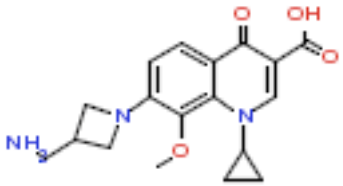	299588	25±5	67±29	82±10	

Chiral 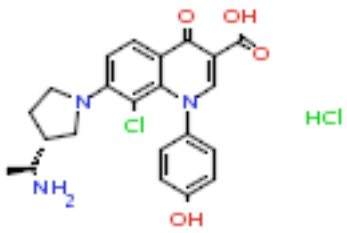	486369	0±0	0±0	3±3	
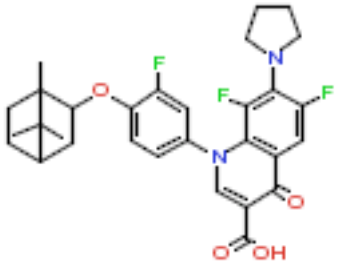	502423	41±25	6±6	93±8	
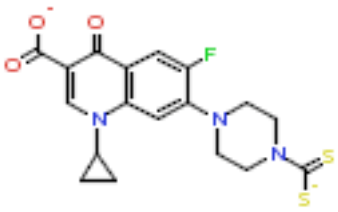	779984	53±36	29±2	89±7	
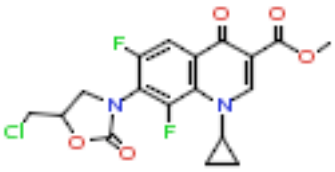	102443	28±15	25±4	72±27	
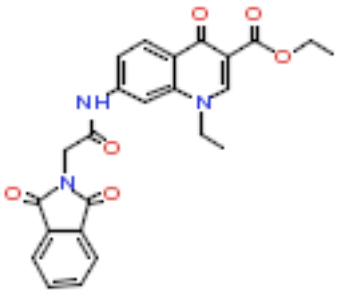	99540	2±0.5	18±1	87±1	

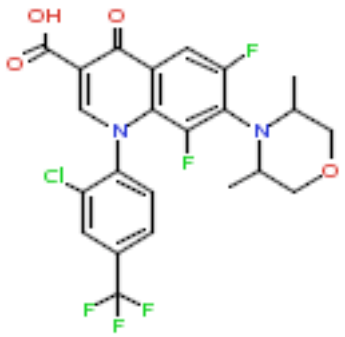	412153	65±34	21±8	88±8	
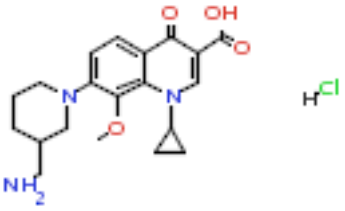	323801	16±0.5	36±3	87±5	
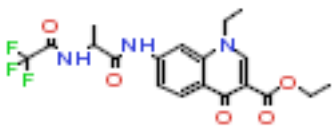	99539	19±18	27±7	74±5	
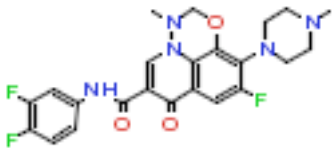	502433	12±17	21±7	88±6	

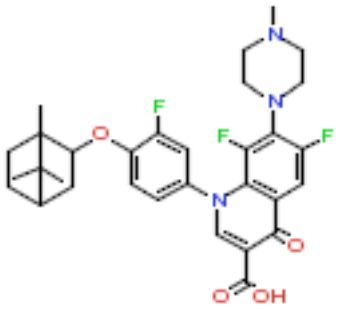	502430	71±42	35±4	85±11
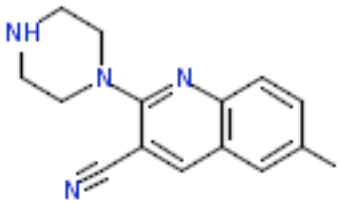	406185	101±40	31±17	95±5
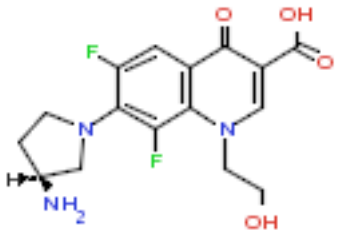	102592	67±31	19±12	81±6
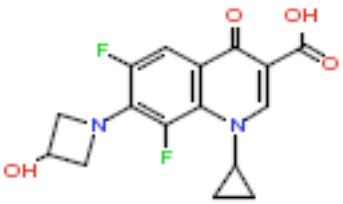	102582	40±40	58±35	94±3
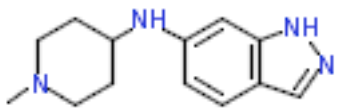	384191	0±0	22±8	48±14

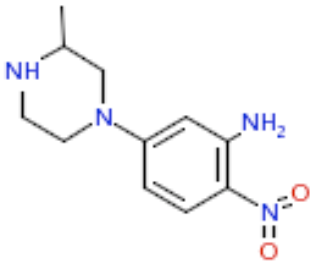	388867	48±8	59±17	94±9
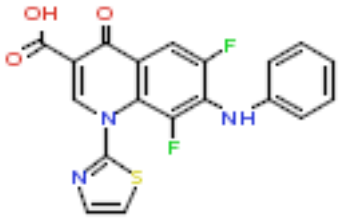	502400	50±20	28±1	99±3
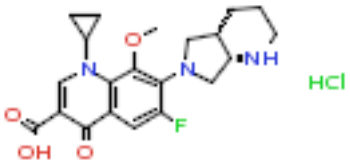	700762	33±13	63±1	92±10
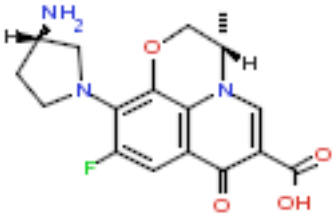	102650	3±3	33±0.5	74±2
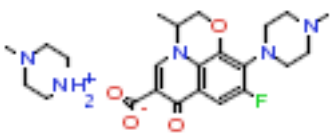	125070	35±16	51±30	84±18

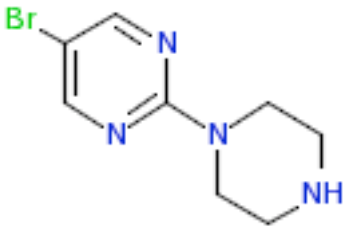	943410	41±15	71±8	95±8	
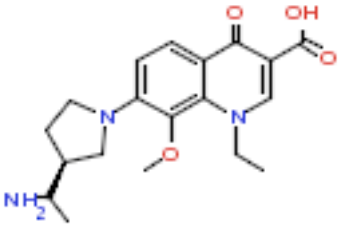	363957	46±27	50±12	104±5	
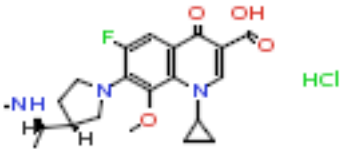	125261	124±47	66±18	100±6	
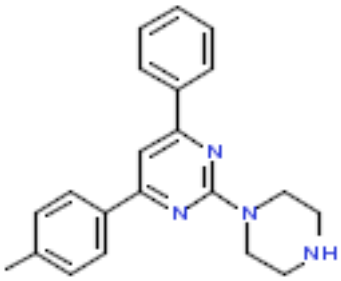	388612	0*		25±18	39±11

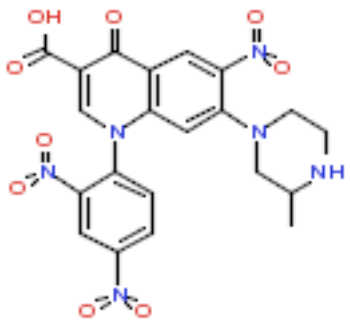	415275	17±22	11±9	45±12
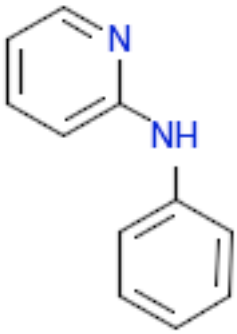	114186	88±28	65±11	92±8

BIBLIOGRAPHY

Adachi Y, Usukura J, Yanagida M. 1997. A globular complex formation by Nda1 and the other five members of the MCM protein family in fission yeast. *Genes Cells* **2**: 467-479.

Aiello D, Barnes MH, Biswas EE, Biswas SB, Gu S, Williams JD, Bowlin TL, Moir DT. 2009. Discovery, characterization and comparison of inhibitors of Bacillus anthracis and Staphylococcus aureus replicative DNA helicases. *Bioorganic & medicinal chemistry* **17**: 4466-4476.

Ali SH, Chandraker A, DeCaprio JA. 2007. Inhibition of Simian virus 40 large T antigen helicase activity by fluoroquinolones. *Antivir Ther* **12**: 1-6.

Amberg DC, Burke DJ, Strathern JN. 2006. Inducing yeast cell synchrony: hydroxyurea arrest. *CSH protocols* **2006**.

Bae B, Chen YH, Costa A, Onesti S, Brunzelle JS, Lin Y, Cann IK, Nair SK. 2009. Insights into the architecture of the replicative helicase from the structure of an archaeal MCM homolog. *Structure* **17**: 211-222.

Balzi E, Goffeau A. 1995. Yeast multidrug resistance: the PDR network. *J Bioenerg Biomembr* **27**: 71-76.

Barrett JF, Gootz TD, McGuirk PR, Farrell CA, Sokolowski SA. 1989. Use of in vitro topoisomerase II assays for studying quinolone antibacterial agents. *Antimicrob Agents Chemother* **33**: 1697-1703.

Barry ER, Lovett JE, Costa A, Lea SM, Bell SD. 2009. Intersubunit allosteric communication mediated by a conserved loop in the MCM helicase. *Proc Natl Acad Sci U S A* **106**: 1051-1056.

Bell SP, Dutta A. 2002. DNA replication in eukaryotic cells. *Annu Rev Biochem* **71**: 333-374.

Bell SP, Stillman B. 1992. ATP-dependent recognition of eukaryotic origins of DNA replication by a multiprotein complex. *Nature* **357**: 128-134.

Bochman ML, Bell SP, Schwacha A. 2008. Subunit organization of Mcm2-7 and the unequal role of active sites in ATP hydrolysis and viability. *Mol Cell Biol* **28**: 5865-5873.

Bochman ML, Schwacha A. 2007. Differences in the single-stranded DNA binding activities of MCM2-7 and MCM467: MCM2 and MCM5 define a slow ATP-dependent step. *J Biol Chem* **282**: 33795-33804.

-. 2008. The Mcm2-7 complex has in vitro helicase activity. *Mol Cell* **31**: 287-293.

-. 2009. The Mcm complex: unwinding the mechanism of a replicative helicase. *Microbiol Mol Biol Rev* **73**: 652-683.

-. 2010. The Saccharomyces cerevisiae Mcm6/2 and Mcm5/3 ATPase active sites contribute to the function of the putative Mcm2-7 'gate'. *Nucleic acids research* **38**: 6078-6088.

Boos D, Frigola J, Diffley JF. 2012. Activation of the replicative DNA helicase: breaking up is hard to do. *Current opinion in cell biology* **24**: 423-430.

Bouzard D, Di Cesare P, Essiz M, Jacquet JP, Ledoussal B, Remuzon P, Kessler RE, Fung-Tomc J. 1992. Fluoronaphthyridines as antibacterial agents. 4. Synthesis and structure-activity relationships of 5-substituted-6-fluoro-7-(cycloalkylamino)-1,4-dihydro-4-oxo-1,8-naphthyridine-3-carboxylic acids. *J Med Chem* **35**: 518-525.

Brewster AS, Chen XS. 2010. Insights into the MCM functional mechanism: lessons learned from the archaeal MCM complex. *Critical reviews in biochemistry and molecular biology* **45**: 243-256.

Brewster AS, Wang G, Yu X, Greenleaf WB, Carazo JM, Tjajadia M, Klein MG, Chen XS. 2008. Crystal structure of a near-full-length archaeal MCM: functional insights for an AAA+ hexameric helicase. *Proc Natl Acad Sci U S A* **105**: 20191-20196.

Bruck I, Kanter DM, Kaplan DL. 2011. Enabling association of the GINS protein tetramer with the mini chromosome maintenance (Mcm)2-7 protein complex by phosphorylated Sld2 protein and single-stranded origin DNA. *J Biol Chem* **286**: 36414-36426.

Bruck I, Kaplan DL. 2011a. GINS and Sld3 compete with one another for Mcm2-7 and Cdc45 binding. *J Biol Chem* **286**: 14157-14167.

-. 2011b. Origin single-stranded DNA releases Sld3 protein from the Mcm2-7 complex, allowing the GINS tetramer to bind the Mcm2-7 complex. *J Biol Chem* **286**: 18602-18613.

-. 2013. Cdc45 protein-single-stranded DNA interaction is important for stalling the helicase during replication stress. *J Biol Chem* **288**: 7550-7563.

Cantalupo P, Saenz-Robles MT, Pipas JM. 1999. Expression of SV40 large T antigen in baculovirus systems and purification by immunoaffinity chromatography. *Methods Enzymol* **306**: 297-307.

Chino M, Nishikawa K, Umekita M, Hayashi C, Yamazaki T, Tsuchida T, Sawa T, Hamada M, Takeuchi T. 1996. Heliquinomycin, a new inhibitor of DNA helicase, produced by Streptomyces sp. MJ929-SF2 I. Taxonomy, production, isolation, physico-chemical properties and biological activities. *The Journal of antibiotics* **49**: 752-757.

Chong JP, Thommes P, Blow JJ. 1996. The role of MCM/P1 proteins in the licensing of DNA replication. *Trends Biochem Sci* **21**: 102-106.

Collin F, Karkare S, Maxwell A. 2011. Exploiting bacterial DNA gyrase as a drug target: current state and perspectives. *Appl Microbiol Biotechnol* **92**: 479-497.

Costa A, Ilves I, Tamberg N, Petojevic T, Nogales E, Botchan MR, Berger JM. 2011. The structural basis for MCM2-7 helicase activation by GINS and Cdc45. *Nat Struct Mol Biol* **18**: 471-477.

Costa A, Pape T, van Heel M, Brick P, Patwardhan A, Onesti S. 2006a. Structural basis of the Methanothermobacter thermautotrophicus MCM helicase activity. *Nucleic acids research* **34**: 5829-5838.

-. 2006b. Structural studies of the archaeal MCM complex in different functional states. *J Struct Biol* **156**: 210-219.

Costa A, van Duinen G, Medagli B, Chong J, Sakakibara N, Kelman Z, Nair SK, Patwardhan A, Onesti S. 2008. Cryo-electron microscopy reveals a novel DNA-binding site on the MCM helicase. *Embo J* **27**: 2250-2258.

Crute JJ, Grygon CA, Hargrave KD, Simoneau B, Faucher AM, Bolger G, Kibler P, Liuzzi M, Cordingley MG. 2002. Herpes simplex virus helicase-primase inhibitors are active in animal models of human disease. *Nat Med* **8**: 386-391.

Davey MJ, Indiani C, O'Donnell M. 2003. Reconstitution of the Mcm2-7p heterohexamer, subunit arrangement, and ATP site architecture. *J Biol Chem* **278**: 4491-4499.

Domagala JM, Bridges AJ, Culbertson TP, Gambino L, Hagen SE, Karrick G, Porter K, Sanchez JP, Sesnie JA, Spense FG et al. 1991. Synthesis and biological activity of 5-amino- and 5-hydroxyquinolones, and the overwhelming influence of the remote N1-substituent in determining the structure-activity relationship. *J Med Chem* **34**: 1142-1154.

Earnshaw DL, Moore KJ, Greenwood CJ, Djaballah H, Jurewicz AJ, Murray KJ, Pope AJ. 1999. Time-Resolved Fluorescence Energy Transfer DNA Helicase Assays for High Throughput Screening. *Journal of biomolecular screening* **4**: 239-248.

Earnshaw DL, Pope AJ. 2001. FlashPlate scintillation proximity assays for characterization and screening of DNA polymerase, primase, and helicase activities. *Journal of biomolecular screening* **6**: 39-46.

Elsea SH, Hsiung Y, Nitiss JL, Osheroff N. 1995. A yeast type II topoisomerase selected for resistance to quinolones. Mutation of histidine 1012 to tyrosine confers resistance to nonintercalative drugs but hypersensitivity to ellipticine. *J Biol Chem* **270**: 1913-1920.

Erzberger JP, Berger JM. 2006. Evolutionary relationships and structural mechanisms of AAA+ proteins. *Annu Rev Biophys Biomol Struct* **35**: 93-114.

Evrin C, Clarke P, Zech J, Lurz R, Sun J, Uhle S, Li H, Stillman B, Speck C. 2009. A double-hexameric MCM2-7 complex is loaded onto origin DNA during licensing of eukaryotic DNA replication. *Proc Natl Acad Sci U S A* **106**: 20240-20245.

Fernandez-Cid A, Riera A, Tognetti S, Herrera MC, Samel S, Evrin C, Winkler C, Gardenal E, Uhle S, Speck C. 2013. An ORC/Cdc6/MCM2-7 complex is formed in a multistep reaction to serve as a platform for MCM double-hexamer assembly. *Mol Cell* **50**: 577-588.

Fletcher RJ, Bishop BE, Leon RP, Sclafani RA, Ogata CM, Chen XS. 2003. The structure and function of MCM from archaeal M. Thermoautotrophicum. *Nat Struct Biol* **10**: 160-167.

Fu YV, Yardimci H, Long DT, Ho TV, Guainazzi A, Bermudez VP, Hurwitz J, van Oijen A, Scharer OD, Walter JC. 2011. Selective bypass of a lagging strand roadblock by the eukaryotic replicative DNA helicase. *Cell* **146**: 931-941.

Gai D, Zhao R, Li D, Finkielstein CV, Chen XS. 2004. Mechanisms of conformational change for a replicative hexameric helicase of SV40 large tumor antigen. *Cell* **119**: 47-60.

Gambus A, Khoudoli GA, Jones RC, Blow JJ. 2011. MCM2-7 form double hexamers at licensed origins in Xenopus egg extract. *J Biol Chem* **286**: 11855-11864.

Gomez-Llorente Y, Fletcher RJ, Chen XS, Carazo JM, San Martin C. 2005. Polymorphism and double hexamer structure in the archaeal minichromosome maintenance (MCM) helicase from Methanobacterium thermoautotrophicum. *J Biol Chem* **280**: 40909-40915.

Gomez EB, Catlett MG, Forsburg SL. 2002. Different phenotypes in vivo are associated with ATPase motif mutations in Schizosaccharomyces pombe minichromosome maintenance proteins. *Genetics* **160**: 1305-1318.

Griep MA, Blood S, Larson MA, Koepsell SA, Hinrichs SH. 2007. Myricetin inhibits Escherichia coli DnaB helicase but not primase. *Bioorganic & medicinal chemistry* **15**: 7203-7208.

Guenther B, Onrust R, Sali A, O'Donnell M, Kuriyan J. 1997. Crystal structure of the delta' subunit of the clamp-loader complex of E. coli DNA polymerase III. *Cell* **91**: 335-345.

Hardy CF, Dryga O, Seematter S, Pahl PM, Sclafani RA. 1997. mcm5/cdc46-bob1 bypasses the requirement for the S phase activator Cdc7p. *Proc Natl Acad Sci U S A* **94**: 3151-3155.

Hennessy KM, Clark CD, Botstein D. 1990. Subcellular localization of yeast CDC46 varies with the cell cycle. *Genes Dev* **4**: 2252-2263.

Ho CH, Magtanong L, Barker SL, Gresham D, Nishimura S, Natarajan P, Koh JL, Porter J, Gray CA, Andersen RJ et al. 2009. A molecular barcoded yeast ORF library enables mode-of-action analysis of bioactive compounds. *Nature biotechnology* **27**: 369-377.

Hoang ML, Leon RP, Pessoa-Brandao L, Hunt S, Raghuraman MK, Fangman WL, Brewer BJ, Sclafani RA. 2007. Structural changes in Mcm5 protein bypass Cdc7-Dbf4 function and reduce replication origin efficiency in Saccharomyces cerevisiae. *Mol Cell Biol* **27**: 7594-7602.

Honeycutt KA, Chen Z, Koster MI, Miers M, Nuchtern J, Hicks J, Roop DR, Shohet JM. 2006. Deregulated minichromosomal maintenance protein MCM7 contributes to oncogene driven tumorigenesis. *Oncogene* **25**: 4027-4032.

Hook SS, Lin JJ, Dutta A. 2007. Mechanisms to control rereplication and implications for cancer. *Current opinion in cell biology* **19**: 663-671.

Hurley LH. 2002. DNA and its associated processes as targets for cancer therapy. *Nat Rev Cancer* **2**: 188-200.

Ilves I, Petojevic T, Pesavento JJ, Botchan MR. 2010. Activation of the MCM2-7 helicase by association with Cdc45 and GINS proteins. *Mol Cell* **37**: 247-258.

Ishimi Y. 1997. A DNA helicase activity is associated with an MCM4, -6, and -7 protein complex. *J Biol Chem* **272**: 24508-24513.

Ishimi Y, Sugiyama T, Nakaya R, Kanamori M, Kohno T, Enomoto T, Chino M. 2009. Effect of heliquinomycin on the activity of human minichromosome maintenance 4/6/7 helicase. *FEBS J* **276**: 3382-3391.

Jarvis EE, Clark KL, Sprague GF, Jr. 1989. The yeast transcription activator PRTF, a homolog of the mammalian serum response factor, is encoded by the MCM1 gene. *Genes Dev* **3**: 936-945.

Jenkinson ER, Chong JP. 2006. Minichromosome maintenance helicase activity is controlled by N- and C-terminal motifs and requires the ATPase domain helix-2 insert. *Proc Natl Acad Sci U S A* **103**: 7613-7618.

Jones-Held S, Held, M. E. 1992. The use of toposisomerase I as a teaching tool for understanding cellular DNA structure & activity. *The American Biology Teacher* **54**: 368-370.

Kanter DM, Bruck I, Kaplan DL. 2008. Mcm subunits can assemble into two different active unwinding complexes. *J Biol Chem* **283**: 31172-31182.

Kaplan DL, Davey MJ, O'Donnell M. 2003. Mcm4,6,7 uses a "pump in ring" mechanism to unwind DNA by steric exclusion and actively translocate along a duplex. *J Biol Chem* **278**: 49171-49182.

Kawabata T, Luebben SW, Yamaguchi S, Ilves I, Matise I, Buske T, Botchan MR, Shima N. 2011. Stalled fork rescue via dormant replication origins in unchallenged S phase promotes proper chromosome segregation and tumor suppression. *Mol Cell* **41**: 543-553.

Kumar A, Srivastava K, Raja Kumar S, Puri SK, Chauhan PM. 2008. Synthesis and bioevaluation of hybrid 4-aminoquinoline triazines as a new class of antimalarial agents. *Bioorg Med Chem Lett* **18**: 6530-6533.

Kwon HJ, Hong YK, Park C, Choi YH, Yun HJ, Lee EW, Kim BW. 2010. Widdrol induces cell cycle arrest, associated with MCM down-regulation, in human colon adenocarcinoma cells. *Cancer letters* **290**: 96-103.

Labib K. 2010. How do Cdc7 and cyclin-dependent kinases trigger the initiation of chromosome replication in eukaryotic cells? *Genes Dev* **24**: 1208-1219.

Labib K, Tercero JA, Diffley JF. 2000. Uninterrupted MCM2-7 function required for DNA replication fork progression. *Science* **288**: 1643-1647.

Lam SK, Ma X, Sing TL, Shilton BH, Brandl CJ, Davey MJ. 2013. The PS1 Hairpin of Mcm3 Is Essential for Viability and for DNA Unwinding In Vitro. *PloS one* **8**: e82177.

Lebofsky R, Takahashi T, Walter JC. 2009. DNA replication in nucleus-free Xenopus egg extracts. *Methods Mol Biol* **521**: 229-252.

Lee JK, Hurwitz J. 2000. Isolation and characterization of various complexes of the minichromosome maintenance proteins of Schizosaccharomyces pombe. *J Biol Chem* **275**: 18871-18878.

Li B, Pai R, Aiello D, Di M, Barnes MH, Peet NP, Bowlin TL, Moir DT. 2013. Optimization of a novel potent and selective bacterial DNA helicase inhibitor scaffold from a high throughput screening hit. *Bioorg Med Chem Lett* **23**: 3481-3486.

Liu C, Wu R, Zhou B, Wang J, Wei Z, Tye BK, Liang C, Zhu G. 2012. Structural insights into the Cdt1-mediated MCM2-7 chromatin loading. *Nucleic acids research* **40**: 3208-3217.

Liu W, Pucci B, Rossi M, Pisani FM, Ladenstein R. 2008. Structural analysis of the Sulfolobus solfataricus MCM protein N-terminal domain. *Nucleic acids research* **36**: 3235-3243.

Lyubimov AY, Costa A, Bleichert F, Botchan MR, Berger JM. 2012. ATP-dependent conformational dynamics underlie the functional asymmetry of the replicative helicase from a minimalist eukaryote. *Proc Natl Acad Sci U S A* **109**: 11999-12004.

Maine GT, Sinha P, Tye BK. 1984. Mutants of S. cerevisiae defective in the maintenance of minichromosomes. *Genetics* **106**: 365-385.

McGeoch AT, Trakselis MA, Laskey RA, Bell SD. 2005. Organization of the archaeal MCM complex on DNA and implications for the helicase mechanism. *Nat Struct Mol Biol* **12**: 756-762.

McGuffin LJ, Bryson K, Jones DT. 2000. The PSIPRED protein structure prediction server. *Bioinformatics* **16**: 404-405.

McKay GA, Reddy R, Arhin F, Belley A, Lehoux D, Moeck G, Sarmiento I, Parr TR, Gros P, Pelletier J et al. 2006. Triaminotriazine DNA helicase inhibitors with antibacterial activity. *Bioorg Med Chem Lett* **16**: 1286-1290.

Merchant AM, Kawasaki Y, Chen Y, Lei M, Tye BK. 1997. A lesion in the DNA replication initiation factor Mcm10 induces pausing of elongation forks through chromosomal replication origins in Saccharomyces cerevisiae. *Mol Cell Biol* **17**: 3261-3271.

Moir D, Stewart SE, Osmond BC, Botstein D. 1982. Cold-sensitive cell-division-cycle mutants of yeast: isolation, properties, and pseudoreversion studies. *Genetics* **100**: 547-563.

Moyer SE, Lewis PW, Botchan MR. 2006. Isolation of the Cdc45/Mcm2-7/GINS (CMG) complex, a candidate for the eukaryotic DNA replication fork helicase. *Proc Natl Acad Sci U S A* **103**: 10236-10241.

Nguyen VQ, Co C, Irie K, Li JJ. 2000. Clb/Cdc28 kinases promote nuclear export of the replication initiator proteins Mcm2-7. *Curr Biol* **10**: 195-205.

Nitiss JL. 2009. Targeting DNA topoisomerase II in cancer chemotherapy. *Nat Rev Cancer* **9**: 338-350.

Olcay E, Beytemur O, Kaleagasioglu F, Gulmez T, Mutlu Z, Olgac V. 2011. Oral toxicity of pefloxacin, norfloxacin, ofloxacin and ciprofloxacin: comparison of biomechanical and histopathological effects on Achilles tendon in rats. *J Toxicol Sci* **36**: 339-345.

Pannunzio VG, Burgos HI, Alonso M, Mattoon JR, Ramos EH, Stella CA. 2004. A Simple Chemical Method for Rendering Wild-Type Yeast Permeable to Brefeldin A That Does Not Require the Presence of an erg6 Mutation. *J Biomed Biotechnol* **2004**: 150-155.

Passmore S, Elble R, Tye BK. 1989. A protein involved in minichromosome maintenance in yeast binds a transcriptional enhancer conserved in eukaryotes. *Genes Dev* **3**: 921-935.

Patel SS, Picha KM. 2000. Structure and function of hexameric helicases. *Annu Rev Biochem* **69**: 651-697.

Pettersen EF, Goddard TD, Huang CC, Couch GS, Greenblatt DM, Meng EC, Ferrin TE. 2004. UCSF Chimera--a visualization system for exploratory research and analysis. *Journal of computational chemistry* **25**: 1605-1612.

Phuphanich S, Baker SD, Grossman SA, Carson KA, Gilbert MR, Fisher JD, Carducci MA. 2005. Oral sodium phenylbutyrate in patients with recurrent malignant gliomas: a dose escalation and pharmacologic study. *Neuro Oncol* **7**: 177-182.

Pogorelcnik B, Perdih A, Solmajer T. 2013. Recent developments of DNA poisons--human DNA topoisomerase IIalpha inhibitors--as anticancer agents. *Current pharmaceutical design* **19**: 2474-2488.

Remus D, Beuron F, Tolun G, Griffith JD, Morris EP, Diffley JF. 2009. Concerted loading of Mcm2-7 double hexamers around DNA during DNA replication origin licensing. *Cell* **139**: 719-730.

Sato M, Gotow T, You Z, Komamura-Kohno Y, Uchiyama Y, Yabuta N, Nojima H, Ishimi Y. 2000. Electron microscopic observation and single-stranded DNA binding activity of the Mcm4,6,7 complex. *J Mol Biol* **300**: 421-431.

Schwacha A, Bell SP. 2001. Interactions between two catalytically distinct MCM subgroups are essential for coordinated ATP hydrolysis and DNA replication. *Mol Cell* **8**: 1093-1104.

Sclafani RA, Tecklenburg M, Pierce A. 2002. The mcm5-bob1 bypass of Cdc7p/Dbf4p in DNA replication depends on both Cdk1-independent and Cdk1-dependent steps in Saccharomyces cerevisiae. *Genetics* **161**: 47-57.

Seguin SP, Evans CW, Nebane-Akah M, McKellip S, Ananthan S, Tower NA, Sosa M, Rasmussen L, White EL, Maki BE et al. 2012. High-throughput screening identifies a bisphenol inhibitor of SV40 large T antigen ATPase activity. *Journal of biomolecular screening* **17**: 194-203.

Shadrick WR, Ndjomou J, Kolli R, Mukherjee S, Hanson AM, Frick DN. 2013. Discovering new medicines targeting helicases: challenges and recent progress. *Journal of biomolecular screening* **18**: 761-781.

Shima N, Alcaraz A, Liachko I, Buske TR, Andrews CA, Munroe RJ, Hartford SA, Tye BK, Schimenti JC. 2007. A viable allele of Mcm4 causes chromosome instability and mammary adenocarcinomas in mice. *Nat Genet* **39**: 93-98.

Shiratori A, Shibata T, Arisawa M, Hanaoka F, Murakami Y, Eki T. 1999. Systematic identification, classification, and characterization of the open reading frames which encode novel helicase-related proteins in Saccharomyces cerevisiae by gene disruption and Northern analysis. *Yeast* **15**: 219-253.

Simon JA, Szankasi P, Nguyen DK, Ludlow C, Dunstan HM, Roberts CJ, Jensen EL, Hartwell LH, Friend SH. 2000. Differential toxicities of anticancer agents among DNA repair and checkpoint mutants of Saccharomyces cerevisiae. *Cancer Res* **60**: 328-333.

Simon N, Bochman ML, Seguin S, Brodsky JL, Seibel WL, Schwacha A. 2013. Ciprofloxacin is an inhibitor of the Mcm2-7 replicative helicase. *Bioscience reports* **33**.

Smart DJ, Halicka HD, Traganos F, Darzynkiewicz Z, Williams GM. 2008. Ciprofloxacin-induced G2 arrest and apoptosis in TK6 lymphoblastoid cells is not dependent on DNA double-strand break formation. *Cancer Biol Ther* **7**: 113-119.

Speck C, Chen Z, Li H, Stillman B. 2005. ATPase-dependent cooperative binding of ORC and Cdc6 to origin DNA. *Nat Struct Mol Biol* **12**: 965-971.

Sun J, Evrin C, Samel SA, Fernandez-Cid A, Riera A, Kawakami H, Stillman B, Speck C, Li H. 2013. Cryo-EM structure of a helicase loading intermediate containing ORC-Cdc6-Cdt1-MCM2-7 bound to DNA. *Nat Struct Mol Biol* **20**: 944-951.

Suzuki S, Kurata M, Abe S, Miyazawa R, Murayama T, Hidaka M, Yamamoto K, Kitagawa M. 2012. Overexpression of MCM2 in myelodysplastic syndromes: association with bone marrow cell apoptosis and peripheral cytopenia. *Exp Mol Pathol* **92**: 160-166.

Takahashi K, Yamada H, Yanagida M. 1994. Fission yeast minichromosome loss mutants mis cause lethal aneuploidy and replication abnormality. *Mol Biol Cell* **5**: 1145-1158.

Takayama Y, Kamimura Y, Okawa M, Muramatsu S, Sugino A, Araki H. 2003. GINS, a novel multiprotein complex required for chromosomal DNA replication in budding yeast. *Genes Dev* **17**: 1153-1165.

Tanabe K, Tokumoto T, Ishikawa N, Shimizu T, Okuda H, Ito S, Shimmura H, Inui M, Harano M, Ohtsubo S et al. 2000. Effect of Deoxyspergualin on the long-term outcome of renal transplantation. *Transplant Proc* **32**: 1745-1746.

Tang G, Peng L, Baldwin PR, Mann DS, Jiang W, Rees I, Ludtke SJ. 2007. EMAN2: an extensible image processing suite for electron microscopy. *J Struct Biol* **157**: 38-46.

Tani H, Akimitsu N, Fujita O, Matsuda Y, Miyata R, Tsuneda S, Igarashi M, Sekiguchi Y, Noda N. 2009. High-throughput screening assay of hepatitis C virus helicase inhibitors using fluorescence-quenching phenomenon. *Biochem Biophys Res Commun* **379**: 1054-1059.

Toyokawa G, Masuda K, Daigo Y, Cho HS, Yoshimatsu M, Takawa M, Hayami S, Maejima K, Chino M, Field HI et al. 2011. Minichromosome Maintenance Protein 7 is a potential therapeutic target in human cancer and a novel prognostic marker of non-small cell lung cancer. *Mol Cancer* **10**: 65.

Tran NQ, Dang HQ, Tuteja R, Tuteja N. 2010. A single subunit MCM6 from pea forms homohexamer and functions as DNA helicase. *Plant molecular biology* **74**: 327-336.

van Brabant AJ, Stan R, Ellis NA. 2000. DNA helicases, genomic instability, and human genetic disease. *Annu Rev Genomics Hum Genet* **1**: 409-459.

Vignais PV, Lunardi J. 1985. Chemical probes of the mitochondrial ATP synthesis and translocation. *Annu Rev Biochem* **54**: 977-1014.

Walker JE, Saraste M, Runswick MJ, Gay NJ. 1982. Distantly related sequences in the alpha- and beta-subunits of ATP synthase, myosin, kinases and other ATP-requiring enzymes and a common nucleotide binding fold. *Embo J* **1**: 945-951.

Welihinda AA, Beavis AD, Trumbly RJ. 1994. Mutations in LIS1 (ERG6) gene confer increased sodium and lithium uptake in Saccharomyces cerevisiae. *Biochim Biophys Acta* **1193**: 107-117.

Wittinghofer A, Scheffzek K, Ahmadian MR. 1997. The interaction of Ras with GTPase-activating proteins. *FEBS letters* **410**: 63-67.

Wong I, Lohman TM. 1993. A double-filter method for nitrocellulose-filter binding: application to protein-nucleic acid interactions. *Proc Natl Acad Sci U S A* **90**: 5428-5432.

Wright CM, Chovatiya RJ, Jameson NE, Turner DM, Zhu G, Werner S, Huryn DM, Pipas JM, Day BW, Wipf P et al. 2008. Pyrimidinone-peptoid hybrid molecules with distinct effects on molecular chaperone function and cell proliferation. *Bioorganic & medicinal chemistry* **16**: 3291-3301.

Wright CM, Seguin SP, Fewell SW, Zhang H, Ishwad C, Vats A, Lingwood CA, Wipf P, Fanning E, Pipas JM et al. 2009. Inhibition of Simian Virus 40 replication by targeting the molecular chaperone function and ATPase activity of T antigen. *Virus Res* **141**: 71-80.

Yardimci H, Loveland AB, Habuchi S, van Oijen AM, Walter JC. 2010. Uncoupling of sister replisomes during eukaryotic DNA replication. *Mol Cell* **40**: 834-840.

Yardimci H, Loveland AB, van Oijen AM, Walter JC. 2012. Single-molecule analysis of DNA replication in Xenopus egg extracts. *Methods* **57**: 179-186.

Zegerman P, Diffley JF. 2007. Phosphorylation of Sld2 and Sld3 by cyclin-dependent kinases promotes DNA replication in budding yeast. *Nature* **445**: 281-285.

Zhang Y, Yang F, Kao YC, Kurilla MG, Pompliano DL, Dicker IB. 2002. Homogenous assays for Escherichia coli DnaB-stimulated DnaG primase and DnaB helicase and their use in screening for chemical inhibitors. *Analytical biochemistry* **304**: 174-179.

Zhou BB, Bartek J. 2004. Targeting the checkpoint kinases: chemosensitization versus chemoprotection. *Nat Rev Cancer* **4**: 216-225.